Draft Research Report
Research Project T1803, Task 12
Stormwater Facilities

INFILTRATION CHARACTERISTICS, PERFORMANCE, AND DESIGN OF STORMWATER FACILITIES

by

Joel W. Massmann
Associate Professor

Carolyn Butchart
Research Assistant

Stephanie Stolar
Research Assistant

Department of Civil and Environmental Engineering
University of Washington, Bx 352700
Seattle, Washington 98105

Washington State Transportation Center
University of Washington, Bx 354802
1107 NE 45th Street, Suite 535
Seattle, Washington 98105

Washington State Department of Transportation
Technical Monitor
Tony Allen
State Geotechnical Engineer

Prepared for

Washington State Transportation Commission
Department of Transportation
and in cooperation with
U.S. Department of Transportation
Federal Highway Administration

January 2002

TECHNICAL REPORT STANDARD TITLE PAGE

1. REPORT NO.	2. GOVERNMENT ACCESSION NO.	3. RECIPIENT'S CATALOG NO.
WA-RD 533.1		

4. TITLE AND SUBTITLE	5. REPORT DATE
INFILTRATION CHARACTERISTICS, PERFORMANCE AND DESIGNS OF STORM WATER FACILITIES	January 2002
	6. PERFORMING ORGANIZATION CODE
7. AUTHOR(S)	8. PERFORMING ORGANIZATION REPORT NO.
Joel Massmann, Carolyn Butchart, Stephanie Stolar	
9. PERFORMING ORGANIZATION NAME AND ADDRESS	10. WORK UNIT NO.
Washington State Transportation Center (TRAC) University of Washington, Box 354802 University District Building; 1107 NE 45th Street, Suite 535 Seattle, Washington 98105-4631	11. CONTRACT OR GRANT NO. Agreement T1803, Task 12
12. SPONSORING AGENCY NAME AND ADDRESS	13. TYPE OF REPORT AND PERIOD COVERED
Research Office Washington State Department of Transportation Transportation Building, MS 47370 Olympia, Washington 98504-7370 Keith Anderson, Project Manager, 360-709-5405	Draft Research Report
	14. SPONSORING AGENCY CODE

15. SUPPLEMENTARY NOTES

This study was conducted in cooperation with the U.S. Department of Transportation, Federal Highway Administration.

16. ABSTRACT

Storm water infiltration facilities help reduce the hydrologic impacts of residential and commercial development. The design of these facilities is particularly challenging because of large uncertainties associated with predictions of both short-term and long-term infiltration rates.

Full-scale "flood tests" conducted at four infiltration facilities in western Washington suggest that lateral flow along the sides of the ponds may be significant. This is similar to "bank storage" that occurs in stream channels. More efficient designs may require a larger ratio of side area to bottom area and that maintenance activities should be considered for the sides as well as the bottom of the pond.

Saturated hydraulic conductivity values estimated from measuring air conductivity and from regression equations derived from grain size parameters were compared to full-scale infiltration rates for 15 sites in western Washington. The estimated values for saturated hydraulic conductivity were up to two orders-of-magnitude larger than the full-scale infiltration rates for some sites and were two orders-of-magnitude smaller at others. These results show that infiltration rates cannot be reliably estimated on the basis of soil properties alone; information related to the hydraulic gradient is also important.

Computer models were compared to identify the flow systems for which saturated models provide reasonable approximations. The difference between saturated and unsaturated flow models was lowest in highly permeable soils and increased as the hydraulic conductivity of the soil decreased. The simulations suggest that steady-state infiltration rates calculated with a saturated model will be 20 to 40% smaller than rates calculated with an unsaturated model for the range of hydraulic conductivities typically found beneath Western Washington infiltration ponds. A comparison of steady-state and transient simulations showed that the steady-state assumption may significantly under-estimate infiltration rates.

17. KEY WORDS	18. DISTRIBUTION STATEMENT
Stormwater infiltration facilities, infiltration rates, hydraulic conductivity estimates, full-scale infiltration tests, numerical simulations.	No restrictions. This document is available to the public through the National Technical Information Service, Springfield, VA 22616

19. SECURITY CLASSIF. (of this report)	20. SECURITY CLASSIF. (of this page)	21. NO. OF PAGES	22. PRICE
None	None		

DISCLAIMER

The contents of this report reflect the views of the authors, who are responsible for the facts and the accuracy of the data presented herein. The contents do not necessarily reflect the official views or policies of the Washington State Transportation Commission, Department of Transportation, or the Federal Highway Administration. This report does not constitute a standard, specification, or regulation.

TABLE OF CONTENTS

EXECUTIVE SUMMARY xi

I INTRODUCTION 1
1.1 Quantitative Descriptions of Infiltration Processes 3
1.2 Infiltration Rates from Design Manuals for Storm Water Infiltration Facilities 8
1.3 Other Criteria and Considerations for Infiltration Ponds 12
1.3.1 Siting Criteria and Considerations 12
1.3.2 Clogging 13
1.3.3 Water Table Elevation 13
1.3.4 Lateral Flow 14

2 ESTIMATING HYDRAULIC CONDUCTIVITY FROM AIR FLOW EXPERIMENTS 20
2.1 Relationship between Air Conductivity and Hydraulic Conductivity 20
2.2 Measuring Air Conductivity 23
2.3 Sensitivity to Permeameter Scale 24
2.4 Measuring Air Conductivity for Synthetic Soils 26
2.5 Measuring Air Conductivity for Natural Soils 27
2.6 Limitations of the Approach 28

3 ESTIMATING SATURATED HYDRAULIC CONDUCTIVITY FROM GRAIN SIZE CURVES 32
3.1 Approaches for Estimating Saturated Hydraulic Conductivity Using Soil Texture Data 32
3.2 Regression Equations for Synthetic Soils 34
3.3 Estimating Saturated Hydraulic Conductivity for Natural Soils by Using the Regression Equation from Synthetic Soils 37
3.4 Regression Equations from Natural Soil Samples 38
3.5 Regression Equation from Both Synthetic and Natural Soil Samples 38

4 FULL-SCALE INFILTRATION TESTS 49
4.1 Field Methods for the Full-Scale Tests 49
4.2 Data Analysis for the Full-Scale Tests 51
4.3 Description of Sites Used for the Full-Scale Tests 52
4.3.1 Clark County Pond 53
4.3.2 Balsam 7-11 Pond, Kitsap County 54
4.3.3 Krista Firs Pond, Kitsap County 54
4.3.4 Cimarron Pond, King County 55
4.4 Estimates of Infiltration Rates Based on the Full-Scale Tests 56
4.4.1 Clark County Pond 56
4.4.2 Balsam 7-11 Pond, Kitsap County 59

4.4.3 Krista Firs Pond, Kitsap County 60
4.4.4 Cimarron Pond, King County 62
4.5 Implications of the Data 63

5 COMPARISON OF FIELD-SCALE INFILTRATION RATES WITH SMALL-SCALE, SATURATED HYDRAULIC CONDUCTIVITY VALUES 79
5.1 Analyses of Estimated Saturated Hydraulic Conductivity and Measured Full-Scale Infiltration Rates 79
5.2 Limitations to Each Approach 80

6 VALIDATION OF BASE MODEL ASSUMPTIONS 84
6.1 Description of Saturated and Unsaturated Flow Models 84
6.1.1 Saturated Flow Model 84
6.1.2 Unsaturated Flow Model 85
6.2 Comparison of Infiltration Rates 86
6.2.1 Steady-State vs. Transient 86
6.2.2 Saturated vs. Unsaturated 88
6.3 Validity of the Steady-State Saturated Flow Assumption 89

7 EVALUATION OF INFILTRATION POND PERFORMANCE 97
7.1 Thurston County Base Model Description 97
7.1.1 Boundary-Conditions 98
7.1.2 Grid 98
7.2 Factors in Pond Performance 99
7.2.1 Water Table Elevation and Lateral Flow 99
7.2.2 Confining Unit 100
7.2.3 Pond Geometry 100
7.2.4 Water Level in the Pond 100
7.2.5 Anisotropy 101
7.2.6 Design Alternatives 101
7.3 Evaluations of Hydraulic Gradients Beneath Infiltration Ponds 102
7.3.1 Importance of Hydraulic Gradients in Infiltration Pond Performance 102
7.3.2 Gradient Changes in Transient Unsaturated Flow Model 103
7.3.3 Gradient Variations Caused by Differences in Hydraulic Conductivity and Water Table Elevation 104

8 CONCLUSIONS AND DESIGN RECOMMENDATIONS 116
8.1 Effects of Hydraulic Gradient 116
8.2 Regressions for Saturated Hydraulic Conductivity 117
8.3 Full-Scale Infiltration Tests 117
8.4 Comparisons of Modeling Approaches 118
8.5 Design Alternatives from Computer Simulations 119

ACKNOWLEDGMENTS 121

REFERENCES 122

FIGURES

Figure		Page
1.1	Moisture zones during infiltration	18
1.2	Estimated infiltration rate for loamy sand using the Green and Ampt equation	18
1.3	Flow system for a wetting front that has reached the water table	19
2.1	Stand-alone air permeameter	31
3.1	A comparison of measured hydraulic conductivity of synthetic soils with predictions made with the Hazen equation	42
3.2	A comparison of measured hydraulic conductivity of synthetic soils with predictions made with regression equation 1.6a	42
3.3	A comparison of measured hydraulic conductivity of synthetic soils with predictions made with regression equation A.8	43
3.4	Hazen equation A.1 derived from synthetic soil and applied to natural soil parameters	43
3.5	Regression equation A.6 derived from synthetic soil and applied to natural soil parameters	44
3.6	Regression equation A.8 derived from synthetic soil and applied to natural soil parameters	44
3.7	A comparison of measured hydraulic conductivity of natural soils with predictions made with the Hazen equation	45
3.8	A comparison of measured hydraulic conductivity of natural soils with predictions made with regression equation B.6	45
3.9	A comparison of measured hydraulic conductivity of natural soils with predictions made with regression equation B.8	46
3.10	A comparison of measured hydraulic conductivity of natural soils and synthetic soils with predictions made with the Hazen equation	46
3.11	A comparison of measured hydraulic conductivity of natural soils and synthetic soils with predictions made with regression equation C.6	47
3.12	A comparison of measured hydraulic conductivity of natural soils and synthetic soils with predictions made with regression equation C.8	47
3.13	Comparison of regressions for natural and synthetic soils	48
4.1	Pressure transducer installed at Krista Firs, Kitsap County	66
4.2	Clark County pond, Clark County, 9616 NE 59th Ave, Vancouver, Wash., 98686	67
4.3	Balsam 7-11, Kitsap County, Lund Ave., SE and Jackson Ave., Port Orchard, Wash., 98366	68
4.4	Krista Firs, Kitsap County, K.C. Place and Cedar Rd E., Port Orchard, Wash., 98366	69
4.5	Cimarron, King County, NE 12th Place and 230th Ave. NE, Sammamish, Wash., 98074	70
4.6	Water levels during the full-scale test at the Clark County pond	71
4.7	Infiltration rate for Clark County averaged over 30-minute intervals	71
4.8	Fraction of total inflow that had infiltrated as a function of time at the Clark County pond	72

4.9	Infiltration rate versus water level for Clark County pond	72
4.10	Horizontal and vertical infiltration during the filling and draining stages	73
4.11	Water levels during the full-scale test at the Balsam 7-11 pond	73
4.12	Infiltration rate for Balsam 7-11 averaged over 30-minute intervals	74
4.13	Fraction of the total flow that had infiltrated as a function of time at the Balsam 7-11 pond	74
4.14	Infiltration rate versus water level for Balsam 7-11 pond	75
4.15	Water levels during the full-scale test at the Krista Firs pond	75
4.16	Infiltration rate for Krista Firs averaged over 30-minute intervals	76
4.17	Fraction of total inflow that had infiltrated as a function of time at the Krista Firs pond	76
4.18	Infiltration rate versus water level for Krista Firs pond	77
4.19	Water levels during the full-scale test at the Cimarron pond	77
4.20	Infiltration rate for Cimarron averaged over 30-minute intervals	78
4.21	Infiltration rate versus water level for Cimarron pond	78
6.1	Cross-section view of steady-state saturated flow model used in comparison study	91
6.2	Cross-section view of transient unsaturated flow model used in comparison study	91
6.3	Pressure head contour map showing the advance of the wetting front at t = 0.024, 0.4, and 2.3 hours	92
6.4	Infiltration rate versus time for K = 0.024 cm/s in Scenario 1	93
6.5	Infiltration rate versus time for K = 0.024 cm/s in Scenario 2	93
6.6	Infiltration rate versus time for K = 0.0024 cm/s in Scenario 1	94
6.7	Infiltration rate versus time for K = 0.0024 cm/s in Scenario 2	94
6.8	Infiltration rate versus time for K = 0.00081 cm/s in Scenario 1	95
6.9	Infiltration rate versus time for K = 0.00081 cm/s in Scenario 2	95
6.10	Infiltration rate versus time for K = 0.0024 in small model	96
6.11	Infiltration rate versus time for K = 0.00081 cm/s in small model	96
7.1	Lacy-Lid infiltration pond in Thurston, County, Wash.	108
7.2	Cross-section view of modeled domain showing locations of five fields	109
7.3	Plan view of row and column spacing	110
7.4	Cross-section view of flow from Lacey-Lid infiltration pond	111
7.5	Infiltration rate versus hydraulic conductivity in field 1	112
7.6	Infiltration rate versus hydraulic conductivity in field 2	112
7.7	Infiltration rate versus pond perimeter	113
7.8	Hydraulic gradient versus time for $K = 2.4 \times 10^{-2}$ cm/s	113
7.9	Hydraulic gradient versus time for $K = 2.4 \times 10^{-3}$ cm/s	114
7.10	Hydraulic gradient versus time for $K = 8.1 \times 10^{-4}$ cm/s	114
7.11	Flow exiting Lacey-Lid pond for different groundwater depths and hydraulic conductivities	115
7.12	Hydraulic gradient values for different groundwater depths and hydraulic conductivities	115

TABLES

Table		Page
1.1	Wetting front suction head for different soil textures	15
1.2	Parameters used to estimate infiltration rates shown in Figure 1.2	15
1.3	Recommended infiltration rates based on USDA soil textural classification	16
1.4	Recommended infiltration rates based on ASTM gradation testing	16
1.5	Correction factors to be used with in-situ infiltration measurements to estimate long-term design infiltration rates	17
1.6	Correction factors from the King County Surface Water Design Manual	17
2.1	Density and viscosity of water and air at different temperatures	30
2.2	Comparison of measured air conductivity values for different size permeameters	30
3.1	Coefficients for the Hazen Equation where d_{10} is in mm and K_s is in cm/s	40
3.2	Sum of mean square error for synthetic and natural soil samples	40
3.3	Sum of mean square error of synthetic and natural soils for selected equations	41
4.1	Summary of data for full-scale infiltration tests	65
4.2	Summary of calculated infiltration rates	65
5.1	Comparison of estimated saturated hydraulic conductivity and long-term full-scale infiltration rates	82
5.2	Ratio of estimated *s* versus long-term infiltration rates (*I*)	83
6.1	Modeling parameters	90
7.1	Descriptions and hydraulic parameters for each field	105
7.2	Infiltration rates for different water table elevations	105
7.3	Effect of confining unit on infiltration rate	106
7.4	Infiltration rates for different pond perimeters	106
7.5	Changes in infiltration rates caused by varying water depths in pond	107
7.6	Changes in infiltration rates caused by anisotropy	107
7.7	Infiltration rate changes due to addition of gravel base	107
8.1	Sum of mean square error of synthetic and natural soils for selected equations	120
8.2	Summary of calculated infiltration rates	120

EXECUTIVE SUMMARY

E.1 Introduction

Storm water infiltration facilities are used to reduce the hydrologic impacts of residential and commercial development. These infiltration facilities—which may include ponds, dry wells, infiltration galleries, and swales—are designed to capture and retain runoff and allow it to infiltrate rather than to discharge directly to surface water. Important benefits of groundwater infiltration facilities include reducing surface-runoff volume, reducing pollutant discharge, reducing thermal impacts on fisheries, increasing groundwater recharge, and augmenting low-flow stream conditions (Duchene et. al, 1992).

The design of infiltration facilities is particularly challenging because of the large uncertainties associated with predictions of both short-term and long-term infiltration rates. These uncertainties in infiltration rates translate into uncertainties in the area and volume that are required for infiltration ponds. The overall objective of the studies described in this report was to provide recommendations for improving approaches used to design infiltration facilities, with particular emphasis on infiltration ponds. These studies involved two main components: a data-collection component and a numerical-modeling component.

E.1.1 Data-collection component

The primary objective of the data-collection component was to investigate the relationship between field-measured infiltration rates and estimates of saturated hydraulic conductivity. The data-collection component involved compiling existing data on field-

scale infiltration rates from previous studies. Field-scale infiltration rates were also measured at selected ponds in western Washington. These field-measured infiltration rates were then compared to estimates of hydraulic conductivity obtained from soil samples collected in the field. The hydraulic conductivity estimates were based on soil gradation analyses and air conductivity tests. The goal was to evaluate how the hydraulic conductivity of near-surface soils compares to field-scale values of infiltration rates. The description of the data collection component is derived from Butchart (2001) and is included in sections 2, 3, and 4.

E.1.2 Numerical-modeling component

The primary objectives of the numerical-modeling component were to compare different modeling approaches, to quantify the sensitivity in the overall function of infiltration ponds to different input parameters, and to develop recommendations for site characterization of and design alternatives for these facilities. Models that simulate both saturated and unsaturated flow were compared with models that consider only saturated flow to identify those flow systems for which saturated models provide reasonable approximations. Both steady-state and transient simulations were developed and compared. The models were used to evaluate the sensitivity of infiltration rates to subsurface stratigraphy, depth to water table, and pond geometry. The models were also used to illustrate the importance of hydraulic gradient in estimating infiltration rates from these facilities. The description of the numerical-modeling component is derived from Stolar (2001) and is included in sections 5 and 6.

E.2 Quantitative Descriptions of Infiltration Processes

Designing infiltration facilities requires quantitative estimates of infiltration rates. Two equations that are commonly used to describe infiltration are Darcy's Law and the Green-Ampt equation. Darcy's law illustrates that two factors control infiltration: hydraulic conductivity and hydraulic gradient. The hydraulic conductivity is a particularly challenging parameter to estimate because it varies by orders-of-magnitude, depending on the geologic media or soil type (Freeze and Cherry, 1979). The hydraulic gradient is the driving force or energy that causes water to move through the soil. This force has two components; one component is due to gravity and the second component is due to pressure. An important and often overlooked implication of Darcy's law is that the infiltration rate is not equal to the hydraulic conductivity unless the gradient equals 1.0.

Darcy's Law is often used to describe infiltration in unsaturated soils through an approximation that is termed the Green-Ampt equation (e.g., Chin, 2000). The Green-Ampt equation was developed by using Darcy's Law in conjunction with a set of assumptions regarding the geometry and material properties of the flow system. This approach assumes ponded water at the ground surface and a wetting front that moves downward as a sharp interface. The Green-Ampt equation shows that initial infiltration rates are higher than the saturated hydraulic conductivity because of relatively high hydraulic gradients when the wetting front is shallow. As the depth of the wetting front increases, the gradient decreases and the infiltration rate approaches the saturated hydraulic conductivity.

The Green-Ampt representation has important implications for the design of infiltration facilities. These results show that short-term infiltration tests will tend to over-estimate long-term infiltration rates. These results also illustrate the importance of the hydraulic gradient term in controlling infiltration rates. The initial infiltration rate is significantly larger than the saturated hydraulic conductivity because the gradient term is larger than 1.0. As more water infiltrates, the gradient decreases and approaches a value of 1.0.

Note that once the wetting front reaches a regional or perched water table, the Green-Ampt approximation is no longer valid. Under these conditions, the hydraulic gradient may drop to a value significantly less than 1.0, and the infiltration rate may be much less than the saturated hydraulic conductivity. This is a very important concept and one that is overlooked in design approaches in which infiltration rates are estimated solely on the basis of soil types or saturated hydraulic conductivity estimates. Once the wetting front has reached the water table, the infiltration rate is still described with Darcy's Law, but the gradient term is more difficult to quantify or predict. This gradient, which is related to the slope of the water table near the pond, will depend upon the soil type, the depth to the water table, the geometry of the pond, and the depth of water in the pond. Under most conditions this gradient will be significantly less than 1.0, and the infiltration rate will be smaller than the saturated hydraulic conductivity, as shown in Darcy's Law.

E.3 Infiltration Rates from Design Manuals for Storm water Infiltration Facilities

Two widely recognized references are used to design storm water infiltration facilities in Washington State. One is the Washington Department of Ecology's

Stormwater Management Manual for Western Washington: Volume III—Hydrologic Analysis and Flow Control Design/BMPs WDOE, 2001), and the second is the *King County Surface Water Design Manual* (King County, 1998).

The Department of Ecology manual recommends three methods for estimating long-term infiltration rates. The first method is based on a correlation between USDA soil texture and infiltration rates for homogeneous soils, as summarized in Table E.1. The manual indicates that infiltration rates provided through this correlation represent "short-term conservative rates for homogeneous soils." The Department of Ecology recommends that the short-term infiltration rates be reduced by dividing them by a correction factor of 2 to 4, depending on the soil textural classification. These correction factors are included in Table E.1. The WDOE manual specifies that factors higher than those included in Table E.1 should be considered "for situations where long-term maintenance will be difficult to implement, where little or no pretreatment is anticipated, or where site conditions are highly variable or uncertain."

The second method for estimating infiltration rates included in the Department of Ecology manual is based on soil gradation parameters measured with the ASTM soil gradation procedure. The recommended infiltration rates are included in Table E.2. These estimates are described as "long-term rates" that represent average conditions regarding site variability, the degree of long-term maintenance, and storm water pretreatment.

The third approach recommended in the Department of Ecology manual is to use large-scale in-situ infiltration measurements by using a procedure termed the Pilot Infiltration Test (PIT). For this test, water is added to a pond or an excavated pit at a rate

that will maintain the water level between 3 and 4 feet above the bottom of the pond or pit. The infiltration rate is recorded both as the pond is filled and then as it empties. Estimates from these in-situ tests are also considered short-term rates that must be reduced through correction factors. The typical range of correction factors to account for these issues is summarized in Table E.3

The second major reference for storm water management in the state of Washington is the *King County Surface Water Design Manual* (1998). Procedures to estimate the infiltration rate outlined in the King County manual include the EPA falling-head percolation test procedure and the double-ring infiltrometer test. The King County manual suggests that at least three tests should be performed for each proposed infiltration facility site. Correction factors to be applied to measured infiltration rates are included in the King County manual. These correction factors account for uncertainties in testing, depth to the water table or impervious strata, infiltration receptor geometry, and long-term reductions in permeability due to bio-buildup and accumulation of fines. Table E.4 provides the correction factors that are multiplied by the measured infiltration rate to determine a design infiltration rate.

E.4 Estimating Hydraulic Conductivity from Air Flow Experiments and from Grain Size Curves

One of the objectives of this study was to develop estimates of the saturated hydraulic conductivity of disturbed soil samples obtained from infiltration ponds. Two approaches were used: one approach was based on measuring air flow in synthetic and natural soil samples, and the second approach was based on soil texture information obtained from grain size curves. Both approaches are relatively simple and do not require sophisticated laboratory techniques or equipment. The intent is to develop an

approach for estimating saturated hydraulic conductivity that is more sophisticated and site-specific than the approach based on USDA soil classifications that was described in Table E.1, but that is more simple than traditional laboratory methods.

A relationship between grain size distribution and saturated hydraulic conductivity is of value because grain size information can be more easily obtained than laboratory measurements of hydraulic conductivity. Because grain size analyses are generally simple and inexpensive, estimates from relatively many samples can be obtained rapidly and inexpensively. It may be more effective to obtain rough estimates of saturated hydraulic conductivity from grain size distributions from many samples rather than a few laboratory measurements that require substantially more effort, especially in soils that exhibit significant spatial heterogeneity. A relationship between grain size and hydraulic conductivity may provide adequate estimates for hydraulic conductivity where more detailed data are not available or justified (Rawls et al., 1982).

E.4.1 Hydraulic Conductivity from Airflow Experiments

Using air conductivity to estimate saturated hydraulic conductivity is attractive because air conductivity can be measured rapidly and with fewer practical problems than saturated hydraulic conductivity (Loll et al., 1999). The approach introduced in this study requires relatively few technical laboratory procedures and can be done in minutes for each soil sample. This approach is based on Darcy's law, which has been shown to be valid for airflow in most soils (Massmann, 1989). A stand-alone permeameter developed at the University of Washington (Massmann and Johnson, 2001) was used in the current study to measure air conductivity. This permeameter is an inexpensive instrument that requires no specialized laboratory equipment or instrumentation.

E.4.2 Hydraulic Conductivity from Soil Gradation Information

The measured air conductivity values were converted to saturated water or hydraulic conductivity, and a regression equation was derived to estimate saturated hydraulic conductivity, using selected grain-size parameters of the synthetic soil samples. These regressions were developed for both "natural" and "synthetic" soil samples.

The synthetic soils, which were developed by mixing different portions of four soil textures, were used because they allowed a relatively quick method of obtaining a wide distribution of soil "types." The soil gradation curves could be calculated for these synthetic samples, rather than measured in the laboratory. This resulted in significant savings in time. Seventy-one synthetic soil samples were included in the study. The natural soils were collected at 15 field sites with infiltration ponds. A total of 67 soil samples were taken from these sites.

The air permeameter was used to estimate hydraulic conductivity for each different soil sample, and these hydraulic conductivity values were then used to develop regression equations relating soil texture information and hydraulic conductivity. Three different sets of regression equations were developed. The first set of equations was derived from data collected from the synthetic soils. The second set of equations was derived from data collected from the field (natural) soils. Data from the synthetic and natural soils were combined to derive the third set.

The effective grain diameters d_{10}, d_{60}, and d_{90} were obtained from grain size curves. These effective grain diameters, which correspond to an equivalent "percent passing" on the grain size distribution curve, were used as the parameters in the regression equations.

Regression equations were derived by using different combinations of the three grain size parameters. The general form of these regression equations is:

$$K_{s-predicted} = c_1 + c_2 d_{10}^m + c_3 d_{60}^m + c_4 d_{90}^m \qquad \text{(E.1)}$$

where $K_{s\text{-}predicted}$ is saturated hydraulic conductivity in units of cm/s (L/t); c_1, c_2, c_3, and c_4 are coefficients; and the exponent, m, is 1 or 2.

Three regression equations were selected for a best-fit comparison. These three equations are presented in Table E.5. The measured saturated hydraulic conductivity obtained with the air permeameter and the predicted hydraulic conductivity values from the regression equations are plotted in figures E.1, E.2, and E.3.

E.5 Full-Scale Infiltration Tests

In comparison to other field and laboratory methods, full-scale tests provide the most reliable estimates of how infiltration ponds will perform. These tests, which are often termed "flood tests," are conducted by discharging water into a pond and measuring the change in water level in the pond as a function of time. Data are collected both during the filling stage of the test and during the draining stage after the discharge into the pond has been stopped. The primary advantage of these full-scale tests is that the infiltration rate is measured directly. The approach does not require modeling or significant analytical tools to estimate or infer infiltration rate from some other measured parameter. Sampling errors that can be introduced with small-scale measurements in heterogeneous soils are avoided. The primary disadvantage is that these tests require a source of water that can be delivered at a high enough flow rate to cause ponding within the facility, and they can only be completed after the facility is largely in place.

Each test included a filling stage and a draining stage. During the filling stage of the test, which typically lasted several hours, water from fire hydrants was discharged into the pond and the depth of water increased. The draining stage of the test started when the discharge was terminated. The water level in the pond decreased with time during this draining stage as the water infiltrated through the bottom and sides of the pond. The draining stage lasted from 12 hours to several days, depending upon the rate of infiltration. The rate of infiltration was estimated from full-scale test data by performing a water balance on the infiltration pond.

E.5.1 Description of Sites Used for the Full-Scale Tests

Full-scale flood tests were conducted at four infiltration facilities in western Washington. One facility was located in Clark County, one facility as in King County, and two facilities were located in Kitsap County, Krista Firs and Balsam 7-11. These particular locations were chosen on the basis of the size of the ponds, the expected infiltration rate, and the willingness of the storm water managers in these counties to cooperate in the study. Small- to medium-sized ponds, in the range of 2,000 to 10,000 ft^3 were chosen to reduce the amount of water that would be required for the flood tests. Ponds with anticipated infiltration rates in the range of 0.1 to 10 inches per hour were chosen because these represent "typical" sites. Sites with infiltration rates significantly less than this are generally undesirable because of the size of the pond that would be required to infiltrate water from a typical design storm. Sites with infiltration rates significantly larger than this are undesirable because of water quality considerations (WDOE, 2001).

E.5.2 Estimates of Infiltration Rates Based on the Full-Scale Tests

The basic data that describe the infiltration tests are included in Table E.6. Figure E.4 shows example results for the test that was completed in Clark County. The results at the other sites were similar to those shown for Clark County. The water level data shown in Figure E.5 can be used to estimate the infiltration rate as a function of time. Figure E.6 shows the infiltration rate averaged over each 30-minute period for the Clark County pond. The infiltration rate increased with time during the filling portion of the test and reached a maximum rate of approximately 2.0 in/hr. After the discharge to the pond had been stopped, the infiltration rate quickly decreased to approximately 0.25 in/hr. This rate remained roughly constant for the duration of the test.

The rapid increase in infiltration during the filling portion of the test may have been caused in part by lateral flow along the sides of the ponds. This is similar to "bank storage" that occurs in stream channels. As the water level in the pond increases, flow is induced horizontally into the banks of the pond. This infiltration is in addition to the infiltration that occurs along the pond bottom. Once the water level in the pond begins to decrease, the horizontal flow is reversed and water drains into the pond along the sides and out of the pond along the bottom. This inflow, which reduces the net infiltration rate, decreases with time.

A constant infiltration rate after filling has stopped suggests that the hydraulic gradient that causes flow is also approximately constant during this period. Given that the water level in the pond was decreasing from approximately 10 inches at 30 hours to less than 1 inch at 70 hours, it appears that the water level or water pressure in the pond

was not a primary component of the forces causing infiltration. This behavior was also observed at other ponds.

E.5.3 Implications of the Full-Scale Test Data

Lateral or horizontal flow may have occurred during the filling phases at all four ponds. This suggests that the ponds may have had a higher infiltration rate during the initial inflow of stormwater discharge. Once a maximum water level in the pond had been reached and the water level began to decline, the infiltration rate would decrease if the horizontal flow reversed and flowed back into the pond. The infiltration rates for the ponds eventually reached a nearly constant value. The early-time and long-term infiltration rates for the four ponds included in this study are summarized in Table E.7.

If lateral flow is consistently important, more efficient designs may require a larger ratio of side area to bottom area. This design approach would necessitate maintenance for the sides as well as the bottom of the pond. If the soil on the sides and bottom are preserved with respect to vegetation and silt build-up, the horizontal as well as the vertical flow could be an effective means of infiltrating stormwater runoff into the subsurface.

Infiltration rates based on soil texture for the four sites included in Table E.7. These estimates are from *Stormwater Management Manual for Western Washington: Volume III—Hydrologic Analysis and Flow Control Design/BMPs* (WDOE, 2001). The infiltration rates based on soil textures over-estimated the actual full-scale measured rate at Krista Firs, in Kitsap County and at Cimarron in King County. The soil texture rate for Balsam 7-11 (Kitsap County) under-estimated the actual full-scale rate, and the soil texture rate for Clark County closely estimated the actual full-scale rate. This reinforces

that grain size texture alone does not include site-specific characteristics that may affect infiltration rates.

E.6 Comparison of Field-Scale Infiltration Rates with Small-Scale, Saturated Hydraulic Conductivity Values

Saturated hydraulic conductivity values estimated from measuring air conductivity and from regression equations derived from grain size parameters were compared to full-scale infiltration rates calculated during this study and given in literature. Table E.8 summarizes the measured full-scale infiltration rates and estimated saturated hydraulic conductivity rates for 15 sites.

The estimated saturated hydraulic conductivity values given in columns B, C, and D in Table E.8 were calculated from data for multiple soil samples at each site. The estimated hydraulic conductivity from each sample was used to calculate an equivalent saturated hydraulic conductivity value by using harmonic means (Freeze and Cherry, 1979). These equivalent or effective hydraulic conductivity values are included in Table E.8.

Three methods were used to estimate the saturated hydraulic conductivity values. The estimates in columns "B" and "C" in Table E.8 were derived from regression equations that are included in Table E.5. The estimates in column "D" were calculated from the air flow tests. The most conservative regression equation was a form of the Hazen equation ($K_s = 0.87 d_{10}^2$). The estimated saturated hydraulic conductivity rates measured with the air permeameter method ("Lab K_s") over-predicted the monitored infiltration rates for all 15 ponds.

E.7 Comparison of Modeling Approaches

The results included in Table E.8 clearly show that infiltration rates cannot be reliably estimated on the basis of soil properties alone. Information related to the hydraulic gradient is also required. Computer models provide one means for estimating the hydraulic gradients and infiltration rates for infiltration facilities. A variety of models and modeling approaches are available for simulating flow from infiltration facilities. Results from a steady-state saturated flow model were compared to results from a transient unsaturated model to evaluate errors that are introduced when the simplified model is used to simulate flow from infiltration ponds.

The groundwater flow model MODFLOW was used for the steady-state saturated flow simulations (McDonald and Harbaugh, 1988). The model output gives the location of the water table location and the flow exiting the pond. The infiltration rate for the pond is calculated by dividing the flow by the wetted perimeter of the pond.

The saturated-unsaturated finite-difference model VS2DH 3.0 was used for the transient unsaturated flow model simulations (Hsieh et al., 2000). The unsaturated hydraulic characteristics were represented by the Van Genuchten equation (Van Genuchten, 1980).

The transient unsaturated flow model is more complicated to use than the steady-state saturated flow model. The unsaturated forms of the governing equations are highly nonlinear and are difficult to solve numerically (Anderson and Woessner, 1992). Also, the additional relationships that must be specified in unsaturated flow modeling, such as between hydraulic conductivity and pressure head, are very sensitive to small changes in moisture content. This sensitivity causes instabilities to develop during the numerical

solution. Using small nodal spacing (on the order of centimeters) and small times steps (on the order of seconds) can minimize these instabilities but requires long computational times.

E.7.1 Comparison of Infiltration Rates

The evaluation of the steady-state, saturated flow assumption is separated into two distinct parts. The first part considers errors in assuming that the infiltration exiting the pond has reached steady-state. The second part considers the assumption of saturated flow. In evaluating these assumptions, the two numerical models presented above were used to compare calculated infiltration rates exiting the infiltration pond in both models. For each unique situation, both models simulated flow using the same boundary conditions, hydraulic parameters, and model dimensions.

Two scenarios were developed to examine how quickly the flow from an infiltration pond will reach steady-state and how the infiltration rate depends on the proximity of the constant head boundary condition to the pond. The length from the center of the pond to the outer edge of the constant head boundary was set to 10 and 50 meters for the first and second scenarios, respectively. In scenario 1, the transient model reached a steady infiltration rate after approximately 5 hours, as shown in Figure E.6. This quick response occurred because the wetting front reached the boundary condition, which set the gradient. When the boundaries were extended to a distance of 50 meters in the second scenario, the infiltration rates from the transient model were significantly larger than the steady-state values, as shown in Figure E.7. These results show that the steady-state assumption may significantly under-estimate infiltration rates and that the amount of this under-estimation is dependent upon site-specific hydrologic information.

In addition to modeling under the assumption of steady-state flow, the assumption of saturated flow instead of unsaturated flow was also evaluated. Additional simulations were run to quantify the difference in infiltration rates that occur when a saturated flow model is used versus an unsaturated flow model. The difference between the saturated and unsaturated flow models was lowest in highly permeable soils and increased as the hydraulic conductivity of the soil decreased. The modeling results suggest that the error in the final steady-state infiltration rate varies from 20 to 40 percent over a range of hydraulic conductivities typically found beneath infiltration ponds in Western Washington.

E.7.2 Validity of the Steady-State Saturated Flow Assumption

The results of the model comparison suggest that, under certain hydraulic conditions, the errors introduced by assuming steady-state saturated flow may be acceptable for simulating flow from infiltration ponds. In permeable materials, the system will reach steady-state within a relatively short amount of time, and differences between saturated flow and unsaturated flow will be low. Conversely, when a lower permeable unit is below the pond, the errors in the steady-state saturated flow model results may be large. Note, however, that the results from the steady-state saturated flow simulations always give conservative infiltration rate estimates because infiltration rates calculated under these assumptions are always less than transient unsaturated flow infiltration rate estimates. Additionally, the relative relationships that are established in the evaluation that follows will still hold true. The absolute values of infiltration will have large errors for systems with low permeable soils.

Errors in the steady-state saturated assumptions should be considered relative to errors introduced by characterization and generalization of aquifer properties and by the enforcement of boundary conditions. There is significant uncertainty in any hydraulic conductivity estimate, which can vary over an order of magnitude from one point to another. Also, treating the boundary conditions for the models as constant head introduces error because uncertainty is associated with the water table level.

E.8 Computer Models of Infiltration Pond Performance

Three-dimensional, steady-state, saturated flow model simulations were used to examine the influence of different parameters on the overall effectiveness of infiltration ponds. A base model of a "typical" pond was developed in MODFLOW to evaluate different design alternatives. This model was loosely based on the geometry and observed geology beneath the Lacey-Lid infiltration pond in Thurston County, as described in the *Water Resources Investigations Report 92-4109* (Drost et al., 1999).

E.8.1 Site Characteristics and Design Alternatives That Affect Pond Performance

Water Table Elevation and Lateral Flow

A series of simulations were performed to quantify the change in the infiltration rate that occurs from water table fluctuation and to determine the amount of lateral flow from infiltration ponds. The results show that the infiltration rates decrease substantially when the water levels rise. These results emphasize the importance of understanding regional water table variations at a proposed infiltration pond site. If, for example, a PIT is performed in the summer when regional water table elevations are low, the measured infiltration rate could be twice the rate that would be observed in the winter when the water table levels rise.

Changes in water table elevation have little effect on the percentage of the flow that occurs through the sides of the infiltration pond. Under all the conditions modeled, there was a slight increase in the lateral flow as the water table approached the pond bottom, but nearly one-third of the flow from the infiltration pond left through the sides.

Pond Geometry

Infiltration rates were calculated for different pond shapes. For all the ponds the area of the footprint, the depth of the pond and the water level in the pond were the same. Only the shape was changed. The results illustrate how the infiltration rate increases linearly as a pond becomes more elongate. The increase in the infiltration rate can be attributed to the increase in the lateral flow that occurs as the pond perimeter increases.

Water Level in the Pond

The results suggest that the decrease in the total infiltration rate that accompanies lowering the water level in a pond is a result of a decrease in the amount of lateral flow. The amount of water that exited the bottom of the pond was similar for all pond depths.

Gravel Base

A series of simulations were run to quantify changes in infiltration rate due to replacement of the natural soil beneath a pond with a gravel material. The increase in the total infiltration rate ranged from 0.8 percent to 1.8 percent for all the water table elevations considered. While the amount of flow out the bottom of the pond increased substantially, this was counteracted by the decrease in the amount of lateral flow, which resulted in an insignificant increase in total infiltration rate.

Gravel Column Modification

A gravel column with a high hydraulic conductivity was simulated from the pond bottom down to the regional groundwater table. The addition of the column increased the infiltration rate by less than 1 percent. This insignificant change indicates that adding a gravel column will not affect the pond's performance during steady-state saturated conditions. The small effect is due to the hydraulic gradient term. Adding a gravel chimney has little impact if no significant hydraulic gradient exists to drive groundwater flow.

The major caveat to these results is that they were determined under the assumption of steady-state saturated flow. Results reported in Section 6.3 demonstrated that the error in these assumptions varies according to the subsurface properties, but in general are small in comparison to errors introduced in the characterization and generalization of subsurface aquifer parameters and enforcement of boundary conditions.

E.8.2 Evaluations of Hydraulic Gradients Beneath Infiltration Ponds

Reliable designs of infiltration ponds require an accurate estimation of the hydraulic gradient. Some design approaches found in the literature (Ferguson, 1994; Stahre and Urbonas, 1990) recommend using a constant vertical hydraulic gradient of 1.0. This assumption makes the infiltration rate equal to the hydraulic conductivity of the subsurface material. This simplified method, which is common practice, does not account for the possibility of hydraulic gradients being less than 1.0. If a hydraulic gradient of 1.0 is used in the design process, the pond size may be undersized. Prolonged gradients of less than 1.0 will cause flooding from the infiltration pond.

A transient unsaturated flow model was used to monitor the time evolution of the hydraulic gradient beneath an infiltration pond for different soil types during a 30-hour recharge period. The results demonstrated that, in highly permeable soils, assuming a hydraulic gradient of 1.0 is not conservative. Conversely, in low permeable soils, assuming a hydraulic gradient of 1.0 may be conservative.

E.9 Conclusions and Design Recommendations

The following conclusions and design recommendations were developed from the results of the studies described in this report.

E.9.1. Effects of Hydraulic Gradient

- Short-term infiltration tests will tend to over-estimate long-term infiltration rates, as shown by the Green-Ampt approximation. The initial infiltration rate is significantly larger than the saturated hydraulic conductivity because the hydraulic gradient term is larger than 1.0. As more water infiltrates, the gradient approaches a value of 1.0, and the infiltration rate approaches the saturated hydraulic conductivity.
- If recharge or infiltration is sufficient to cause the wetting front to reach a regional or perched water table, the hydraulic gradient may drop to a value significantly less than 1.0, and the infiltration rate may be much less than the saturated hydraulic conductivity. This is a very important concept and one that is overlooked in design approaches in which infiltration rates are estimated solely on the basis of soil types or saturated hydraulic conductivity estimates.
- A transient, unsaturated flow model was used to monitor the time evolution of the hydraulic gradient beneath an infiltration pond for different soil types during a 30-

hour recharge period. The results demonstrated that, in highly permeable soils, assuming a hydraulic gradient of 1.0 is not conservative. Conversely, in low permeable soils, assuming a hydraulic gradient of 1.0 may be conservative.

E.9.2 Regressions for Saturated Hydraulic Conductivity

- Equation C-8, shown in Table E.5, produces estimates of hydraulic conductivity that have a sum of mean square errors that is approximately 35 percent smaller than the mean square errors produced by the Hazen equation for the set of synthetic and natural soils used in this study. This polynomial equation uses data that are readily available from grain size analyses and should be considered an alternative for the Hazen equation, especially for more coarse-grained soils with a hydraulic conductivity larger than approximately 0.05 cm/s.

E.9.3 Full-Scale Infiltration Tests

- Full-scale infiltration tests conducted at four sites in western Washington showed that the infiltration rate increases with time during the filling portion of the test. After the discharge to the pond is stopped, the infiltration rate quickly decreases to a rate that may be several times smaller than the initial rate. The rapid increase in infiltration during the filling portion of the test may be caused in part by lateral flow along the sides of the ponds. This is similar to "bank storage" that occurs in stream channels. As the water level in the pond increases, flow is induced horizontally into the banks of the pond. This infiltration is in addition to the infiltration that occurs along the pond bottom. Once the water level in the pond begins to decrease, the horizontal flow is reversed and water drains into the pond

along the sides and out of the pond along the bottom. This inflow, which reduces the net infiltration rate, decreases with time.

- Infiltration rates based on soil texture for four sites are included in Table E.7. These estimates are from the WDOE *Stormwater Management Manual for the Puget Sound Basin* (2001). The infiltration rates based on soil textures over-estimated the actual full-scale measured rate at Krista Firs (Kitsap County) and at Cimarron (King County). The soil texture rate for Balsam 7-11 (Kitsap County) under-estimated the actual full-scale rate, and the soil texture rate for Clark County closely estimated the actual full-scale rate.
- Saturated hydraulic conductivity values estimated from measuring air conductivity and from regression equations derived from grain size parameters were compared to full-scale infiltration rates calculated during this study and given in literature. The estimated saturated hydraulic conductivity values were up to two orders-of-magnitude larger that the full-scale infiltration rates for some sites and were two orders-of-magnitude smaller in other cases. This reinforces that grain size texture alone does not include site-specific characteristics that may affect infiltration rate

E.9.4 Comparison of Modeling Approaches

- Results from a steady-state saturated flow model were compared to results from a transient unsaturated model to evaluate errors that are introduced when the simplified model is used to simulate flow from infiltration ponds. These results show that the steady-state assumption may significantly under-estimate

infiltration rates and that the amount of this under-estimation is dependent upon site-specific hydrologic information.

- Computer simulations were used to quantify the difference in estimated infiltration rates that occur when a saturated flow model is used versus an unsaturated flow model. The difference between the saturated and unsaturated flow models is lowest in highly permeable soils and increases as the hydraulic conductivity of the soil decreases. The modeling results suggest that the error in the final steady-state infiltration rate varies from 20 to 40 percent over a range of hydraulic conductivities typically found beneath infiltration ponds in Western Washington.

E.9.5 Design Alternatives from Computer Simulations

- The results of computer simulations suggest the infiltration rate increases linearly as a pond becomes more elongate. The increase in the infiltration rate can be attributed to the increase in the lateral flow that occurs as the pond perimeter increases.
- A gravel column with a high hydraulic conductivity was simulated from the pond bottom down to the regional groundwater table. The addition of the column increased the infiltration rate by less than 1 percent. This insignificant change indicates that adding a gravel column will not affect the pond's performance during steady-state saturated conditions. The small effect is due to the hydraulic gradient term. Adding a gravel chimney has little impact if no significant hydraulic gradient exists to drive groundwater

- If lateral flow is consistently important, more efficient designs may require a larger ratio of side area to bottom area. This design approach would necessitate maintenance for the sides as well as the bottom of the pond. If the soil on the sides and bottom are preserved with respect to vegetation and silt build-up, the horizontal as well as the vertical flow could be an effective means of infiltrating storm-water runoff into the subsurface.

Table E.1—Recommended infiltration rates based on USDA soil textural classification (after WDOE, 2001)

	Short-Term Infiltration Rate (in/hr)	Correction Factor	Estimated Long-Term Infiltration (Design) Rate (in/hr)
Sandy gravels/gravelly sands	20	2	10
Sand	8	4	2
Loamy Sand	2	4	0.5
Sandy Loam	1	4	0.25
Loam	0.5	4	0.13

Table E.2—Recommended infiltration rates based on ASTM gradation testing (WDOE, 2001)

D10 Size from ASTM D422 Soil Gradation Test (mm)	Estimated Long-Term (Design) Infiltration Rate (in/hr)
>0.4	9
0.3	6.5
0.2	3.5
0.1	2.0
0.05	0.8

Table E.3—Correction factors to be used sith in-situ infiltration measurements to estimate long-term design infiltration rates (WDOE, 2001).

Issue	Partial Correction Factor
Site variability and number of locations tested	CFv = 1.5 to 6
Degree of long-term maintenance to prevent Siltation and bio-buildup	CFm = 2 to 6
Degree of influent control to prevent siltation and bio-buildup	CFi = 2 to 6
Total correction factor	CF = CFv + CFm + CFi

Table E.4—Correction factors from the King County *Surface Water Design Manual* (King County, 1998).

$F_{testing}$	$F_{geometry}$	$F_{plugging}$
0.30 - 0.50	0.25 - 1.0	0.7 for loams and sandy loams
		0.8 for fine sands and loamy sands
		0.9 for medium sands
		1.0 for coarse sands or cobbles

Table E.5—Sum of mean square error of synthetic and natural soils for selected equations.

	Regression Equation	Sum of mean square error
C.1	$0.87\,d_{10}^2$	5.43
C.6	$0.0029 + 1.0\,d_{10} - 0.014\,d_{60} - 0.0011\,d_{90} - 0.19\,d_{10}^2 + 3.1(10^{-4})\,d_{60}^2 - 2.5\,(10^{-5})\,d_{90}^2$	3.45
C.8	$0.019 + 0.82\,d_{10} + 2.8(10^{-5})\,d_{60}^2 - 0.0045\,d_{90}$	3.50

Table E.6—Summary of data for full-scale infiltration tests.

A. Site	B. Inflow Rate (ft^3/hr)	C. Inflow Duration (hours)	D. Total Inflow (ft^3)	E. Draining Duration (hours)	F. Max. Water Depth (inches)	G. Bottom Area (ft^2)	H. Side Slope	I. Total Infiltration (ft^3)
Clark	2060	2.5	4710	67.8	21.5	1860	0.3	4820
Balsam	1000	2.2	2290	12.4	31.2	370	0.7	2260
Krista	1840	2.3	4190	78.9	26.1	1030	0.4	3960
Cimarron	1220	1.7	2070	102.9	12.9	2040	0.6	1370

Table E.7—Summary of calculated infiltration rates.

Site	**Long-term infiltration rate (in/hr)**	**Short-term infiltration rate (in/hr)**	**Soil Texture Description**	**Estimated long-term rate from soil texture (WDOE, 2001) (in/hr)**
Clark County	0.23	2.5	Loam/Silty Loam	0.13/0.25
Balsam 7-11	2.1	13.2	Silty Loam	0.25
Krista Firs	0.33	2.8	Sand	2
Cimarron	0.1	1.9	Silty sand loam	0.25

Table E.8—Comparison of estimated saturated hydraulic conductivity and long-term full-scale infiltration rates.

Site	A. Long-term Full-scale (in/hr)	B. Regression Equation C.1 (in/hr)	C. Regression Equation C.8 (in/hr)	D. Air Flow Tests (in/hr)
Clark County Pond	0.23	0.01	0.01	20
Beaverdam, King County	1.9	403	351	183
Balsam 7-11, Kitsap County	2.1	0.03	0.04	17
Krista Firs, Kitsap County	0.33	41	36	204
Airdustrial, Thurston County	0.92	24	35	81
Bush, Thurston County	9.8	122	106	232
Echo Glen, Thurston County	13.5	428	372	n.a.
Lacey Lid, Thurston County	0.33	21	23	60
Margaret McKenny, Thurston Co.	1.64	59	43	145
Ridgeview, Thurston County	4.0	787	571	n.a.
Springfield, Thurston County	3.0	10	9	14
State Farm, Thurston County	4.26	52	45	83
Sweetbriar, Thurston County	0.26	34	37	28
Westwood Baptist, Thurston Co.	0.5	na	na	30
Wood Glen, Thurston County	1.28	51	56	104

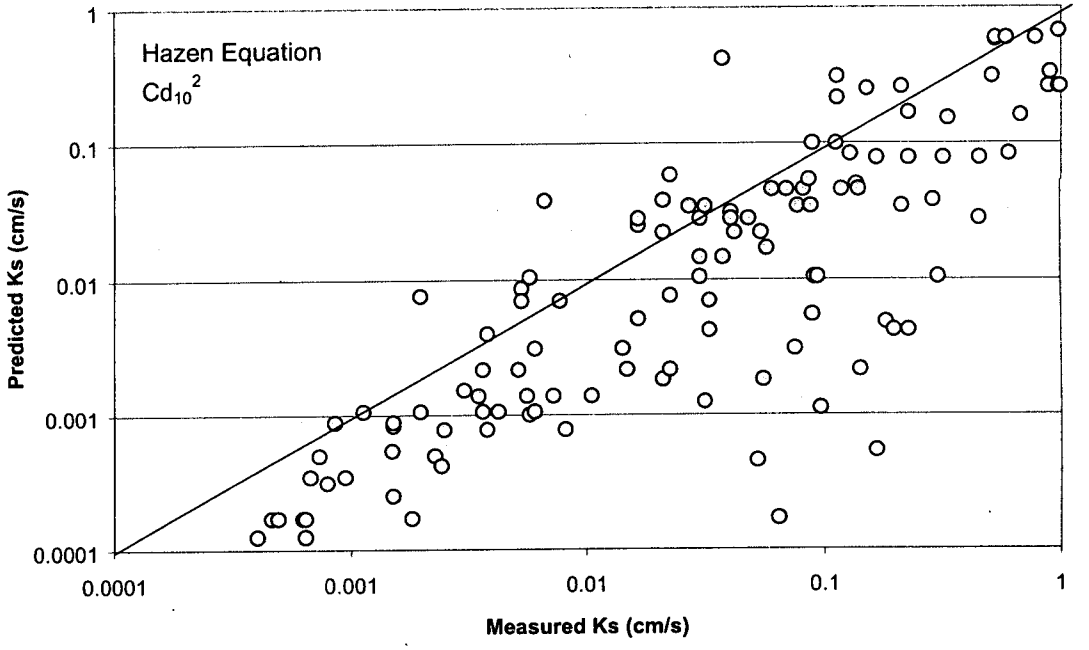

Figure E.1—A comparison of measured hydraulic conductivity of natural soils and synthetic soils with predictions made with the Hazen equation (Regression Equation C.1).

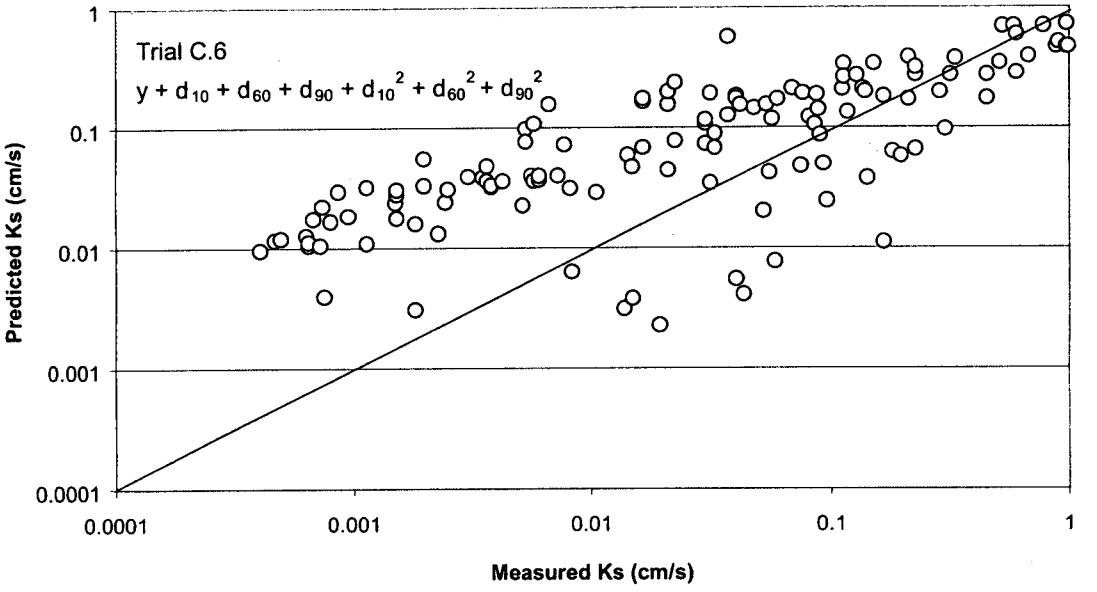

Figure E.2—A comparison of measured hydraulic conductivity of natural soils and synthetic soils with predictions made with Regression Equation C.6.

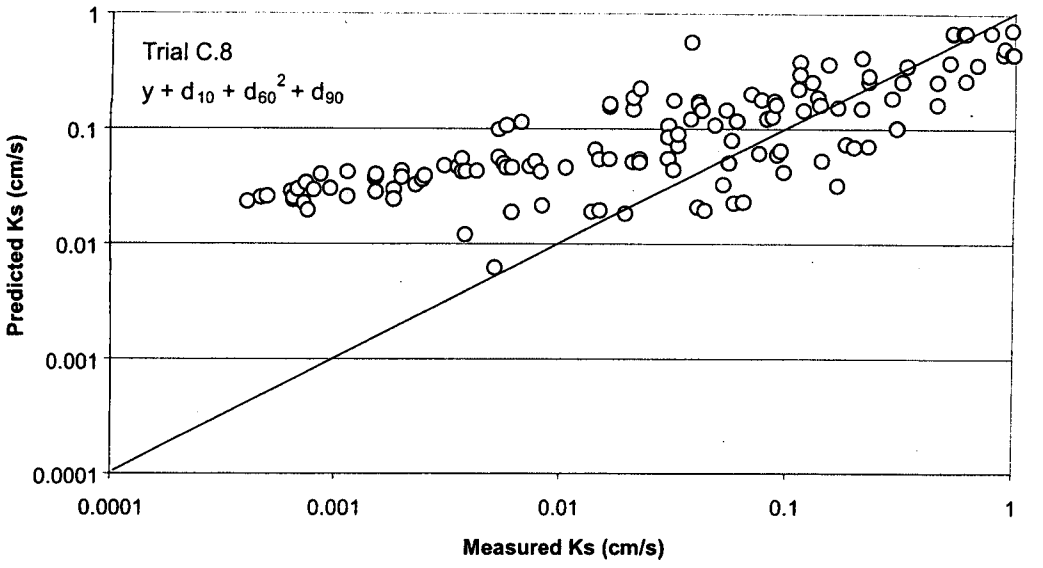

Figure E.3—A comparison of measured hydraulic conductivity of natural soils and synthetic soils with predictions made with regression equation C.8.

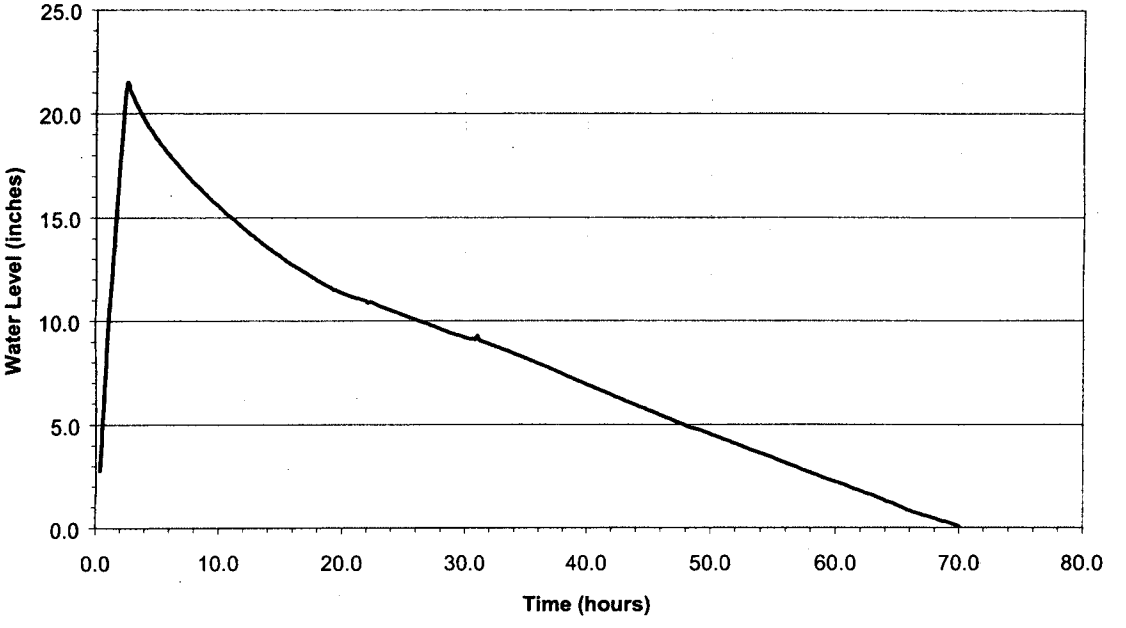

Figure E.4—Water levels during the full-scale test at the Clark County pond.

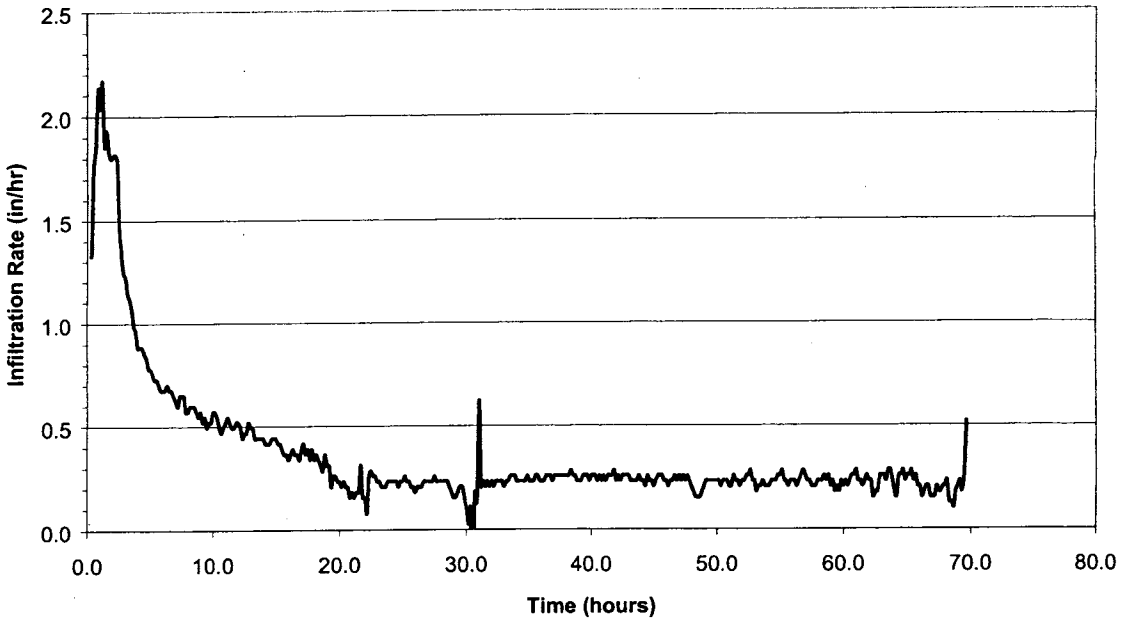

Figure E.5—Infiltration rate for Clark County averaged over 30-minute intervals.

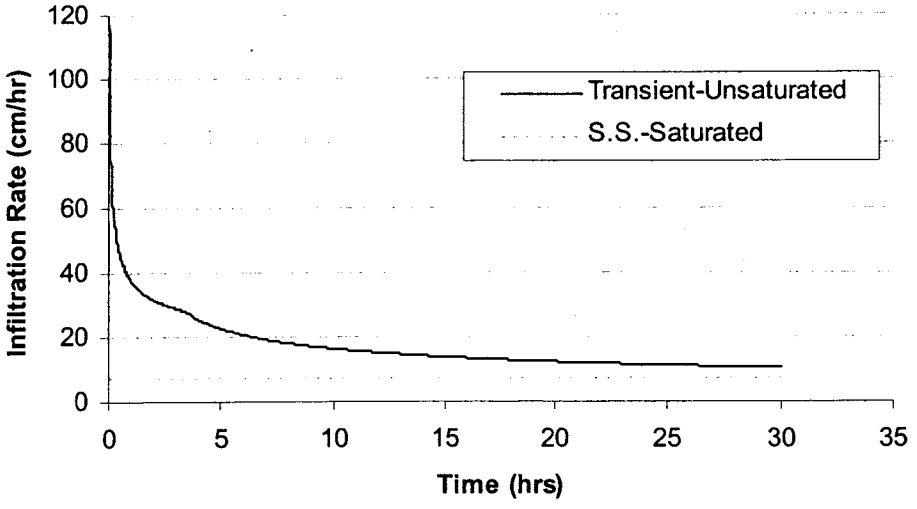

Figure E.6—Infiltration rate versus time for K = 0.0024 cm/s in Scenario 1

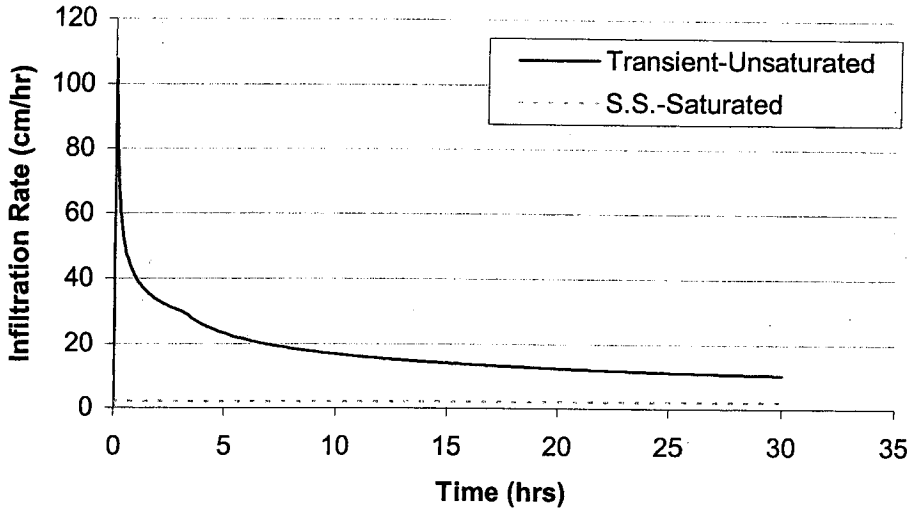

Figure E.7—Infiltration rate versus time for K = 0.0024 cm/s in Scenario 2

1 INTRODUCTION

Storm water infiltration facilities are used to reduce the hydrologic impacts of residential and commercial development. Increased runoff caused by impervious surfaces may destabilize stream channels and may degrade or destroy fish and wildlife habitat. Impervious surfaces also prevent rain and snowmelt from seeping into the ground and recharging streams, wetlands, and aquifers (Ferguson, 1994). Infiltration facilities, such as ponds, dry wells, infiltration galleries, and swales, are designed to capture and retain runoff and allow it to infiltrate rather than to discharge directly to surface water.

Important benefits of groundwater infiltration facilities include reducing surface-runoff volume, reducing pollutant discharge, reducing thermal impacts on fisheries, increasing groundwater recharge, and augmenting low-flow stream conditions (Duchene et al., 1992).

The design of infiltration facilities is particularly challenging because of the large uncertainties associated with predictions of both short-term and long-term infiltration rates. These uncertainties in infiltration rates translate into uncertainties in the area and volume that are required for infiltration ponds. Under-sized ponds may result in flooding, while over-size ponds may be inefficient in terms of land use and expensive in terms of property acquisition.

The overall objective of the studies described in this report was to provide recommendations for improving approaches used to design infiltration facilities, with particular emphasis on infiltration ponds. These studies involved two main components:

a data-collection component and a numerical-modeling component. The primary objective of the data-collection component was to investigate the relationship between field-measured infiltration rates and estimates of saturated hydraulic conductivity. The data-collection component involved compiling existing data on field-scale infiltration rates from previous studies. Field-scale infiltration rates were also measured at selected ponds in western Washington. These field-measured infiltration rates were then compared to estimates of hydraulic conductivity obtained from soil samples collected in the field. The hydraulic conductivity estimates were based on soil gradation analyses and air conductivity tests. The goal was to evaluate how the hydraulic conductivity of near-surface soils compared to field-scale values of infiltration rates. The data collection component of this report is from Butchart (2001) and is included in sections 2, 3, and 4 of this report.

The primary objectives of the numerical-modeling component were to compare different modeling approaches, to quantify the sensitivity in the overall function of infiltration ponds to different input parameters, and to develop recommendations for site characterization of and design alternatives for these facilities. Models that simulate both saturated and unsaturated flow were compared with models that consider only saturated flow to identify those flow systems for which saturated models provide reasonable approximations. Both steady-state and transient simulations were developed and compared. The models were used to evaluate the sensitivity of infiltration rates to subsurface stratigraphy, depth to water table, and pond geometry. The models were also used to illustrate the importance of hydraulic gradient in estimating infiltration rates from

these facilities. The numerical-modeling component of this report is from Stolar (2001) and is included in sections 5 and 6 of this report.

The data-collection and numerical-modeling components of this research considered various issues and aspects related to infiltration facilities. The research relates to the relative importance of soil type in controlling infiltration. It relates to the effects of hydraulic gradients and water table configuration. It considered design methodologies that are currently in practice, and it included an evaluation of the importance of lateral flow from infiltration ponds. An overview of these issues and aspects is presented below.

1.1 Quantitative Descriptions of Infiltration Processes

The design of infiltration facilities requires quantitative estimates of infiltration rates. The size and geometry of the infiltration facilities are selected by comparing infiltration rates with estimates of runoff volumes calculated for specified precipitation events. Two equations that are commonly used to describe infiltration are Darcy's Law and the Green-Ampt equation. These equations are described below as a means to illustrate the processes and parameters that control infiltration and that dictate success or failure at infiltration facilities.

1.1.1 Darcy's Law

Darcy's Law can be written in terms of infiltration rate in the following form:

$$f = \frac{Q}{A} = -K\left(\frac{dh}{dz}\right) = -Ki \tag{1.1}$$

where f is the specific discharge or infiltration rate of water through a unit cross-section of the porous material (L/t), Q is the volumetric flow rate (L^3/t), A is the cross-sectional

area perpendicular to flow (L^2), K is the hydraulic conductivity (L/t), dh/dz is the hydraulic gradient (L/L), and i is a "short-hand" notation for the gradient (L/L).

Darcy's law illustrates that the two factors that control infiltration are hydraulic *conductivity* and hydraulic gradient. The hydraulic conductivity, K, is a particularly challenging parameter to estimate because it varies by orders-of-magnitude, depending on the geologic media or soil type (Freeze and Cherry, 1979). Additional uncertainties are introduced in unsaturated soils, where hydraulic conductivity is a function of the water saturation or moisture content.

The hydraulic head in equation 1.1 is the driving force or energy that causes water to move through the soil. This force, which is due to gravity and pressure, is composed of two components: an elevation head, z , and a pressure head, ψ:

$$h = z + \frac{P}{\rho g} = z + \psi \qquad (1.2)$$

where h is the total head, z is the elevation of the point above some datum (L), P is the water pressure ($M/L \cdot t^2$), ρ is the water density (M/L^3), and ψ is the pressure head. At the water table the water pressure is atmospheric (i.e., set equal to 0.0), and the hydraulic head equals the elevation. Water pressure is less than 0.0 in the unsaturated zone above the water table and is greater than 0.0 in the saturated zone below the water table. The negative water pressures in unsaturated soils are caused by capillary forces or capillary pressures (Freeze and Cherry, 1979). These capillary pressures are a function of pore size—smaller pores have greater capillary pressures (Ward and Elliot, 1995). This negative capillary pressure is also a function of soil moisture content. The capillary pressure becomes less negative as the soil moisture content increases. For unsaturated

systems with capillary pressures of less than 0.0, pressure or "suction" head is defined as capillary pressure divided by the unit weight of water (Mays, 1996):

$$\psi = \frac{P_c}{\rho g} \tag{1.3}$$

where P_c is capillary pressure ($M/L \cdot t^2$) and ψ is the suction head (L). Table 1.1 gives typical values for the suction head at the wetting front for various soil types.

Although Darcy's Law was originally developed to describe saturated flow, it also applies to flow in unsaturated systems (e.g., Freeze and Cherry, 1979). In unsaturated flow, the hydraulic conductivity, K, the fluid pressure, P, and the hydraulic gradient, i, are functions of the moisture content. Darcy's Law for unsaturated flow can be rewritten as:

$$f = -K(\theta) \cdot i(\theta) \tag{1.4}$$

where $K(\theta)$ is the unsaturated hydraulic conductivity [L/T], $i(\theta)$ is the head gradient for unsaturated flow, and θ is the volumetric moisture content.

1.1.2 The Green-Ampt Approximation

Darcy's Law is often used to describe infiltration in unsaturated systems through an approximation that is termed the Green-Ampt equation (e.g., Chin, 2000). The Green-Ampt equation was developed by using Darcy's Law in conjunction with a set of assumptions regarding flow field geometry and material properties. This approach assumes ponded water at the ground surface and a wetting front that extends to a depth, L, as shown in Figure 1.1. The wetting front is assumed to move downward as a sharp interface. The soil is assumed to be saturated above the wetting front (the water content is assumed equal to the porosity). The water content below the wetting front is assumed

to be equal to some lower initial value. The rate of infiltration is approximated by the following expression:

$$f(t) = K_{sat}\left[\frac{H_o + L + h_{wf}}{L}\right] \qquad (1.5)$$

where

f(t) = the infiltration rate at time t (L/t),

K_{sat} = saturated hydraulic conductivity (L/t),

H_o = depth of water in the pond or infiltration facility (L),

L = depth of the wetting front below the bottom of the pond (L), and

h_{wf} = average capillary head at the wetting front (L). Approximately equal to the air entry pressure or bubbling pressure.

Equation (1.5) can be solved to estimate infiltration rate as a function of time (e.g., Salvucci and Entekhabi, 1994). Table 1.2 summarizes the values for input variables that were used to compare infiltration rates for different soil types. These values were chosen on the basis of averages reported by Carsel and Parrish (1988) for these soil types. The depth of water in the infiltration facility, H_o, is assumed to be small in these calculations. The general shape of the infiltration curve that derived from Equation 1.5 is shown in Figure 1.2 for a "loamy sand" soil type. Curves for other soil types will have similar shapes, but with different infiltration rates at steady-state and different time periods required to achieve these steady-state rates. The initial infiltration rates are higher than the saturated hydraulic conductivity because of the relatively high gradients when the wetting front is shallow (L in equation (1.5) is small). As the depth of the wetting front increases, the gradient decreases and the infiltration rate approaches the saturated hydraulic conductivity, K_{sat}. Table 1.2 summarizes the results for three different soil types that are often associated with infiltration facilities.

The results presented in Figure 1.2 and Table 1.3 have important implications for the design of infiltration facilities. These results show that short-term infiltration tests will tend to over-estimate long-term infiltration rates. These results also illustrate the importance of the hydraulic gradient term in controlling infiltration rates. The initial infiltration rate is significantly larger than the saturated hydraulic conductivity because the gradient term is larger than 1.0. As more water infiltrates, the gradient decreases and approaches a value of 1.0.

1.1.3 Impact of Regional or Perched Water Tables

Note that once the wetting front reaches a regional or perched water table, the Green-Ampt approximation is no longer valid. Under these conditions, the hydraulic gradient may drop to a value significantly less than 1.0, and the infiltration rate may be much less than the saturated hydraulic conductivity. This is a very important concept and one that is overlooked in design approaches in which infiltration rates are estimated solely on the basis of soil types or saturated hydraulic conductivity estimates.

Figure 1.3 illustrates a flow system near an infiltration pond in which the wetting front has reached the water table. The soils beneath and adjacent to the pond are saturated with water, and the water table slopes away from the pond. The infiltration rate under these conditions is still described with Darcy's Law (Equation 1.1), but the gradient term is more difficult to quantify or predict. This gradient, which is related to the slope of the water table near the pond, will depend upon the soil type, the depth to the water table, the geometry of the pond, and the depth of water in the pond. Under most conditions this gradient will be significantly less than 1.0, and the infiltration rate will be smaller than the saturated hydraulic conductivity, as shown in Darcy's Law.

1.1.4 Infiltration in Layered Systems

The previous discussions related to Darcy's Law and the Green Ampt approximation have focused on homogeneous soils. Infiltration into layered systems can also be described with Darcy's law, with hydraulic conductivity and gradients changing from layer to layer. For infiltration at a site with a higher conductivity layer overlaying a layer of lower conductivity, the top layer initially controls the infiltration rate. When the wetting front reaches the less conductive layer, the infiltration rate will drop, and the rate of infiltration will be controlled by the less conductive layer (Chow et al., 1988). After a sufficient time, a positive pressure head in the form of a perched water table (mound) can develop above the lower conductivity soil. Ponding, or mounding, results in a head gradient of less than 1.0, much the same way as when the wetting front reaches the water table. The shape and growth of the mound depends on the infiltration rate, the dimensions of the infiltration area, and the hydraulic characteristics of the soil (Ferguson, 1994).

1.2 Infiltration Rates from Design Manuals for Storm Water Infiltration Facilities

Two widely recognized references are used to design of storm water infiltration facilities in Washington State. One is the Washington Department of Ecology's *Stormwater Management Manual for Western Washington* (WDOE, 2001), and the second is the *King County Surface Water Design Manual* (King County, 1998).

The Department of Ecology manual recommends three methods for estimating long-term infiltration rates. The first method is based on a correlation between USDA soil texture and infiltration rates for homogeneous soils. The infiltration rates that the Department of Ecology has recommended, which are reproduced in Table 1.2, are based

on a correlation developed by Rawls, et al. (1982) with minor changes based on the Water Environment Federation (1998). The manual indicates that infiltration rates provided through this correlation represent "short-term conservative rates for homogeneous soils." These estimates do not consider the effects of long-term clogging due to siltation and biomass buildup in the infiltration facility. The Department of Ecology recommends that the short-term infiltration rates be reduced by dividing them by a correction factor of 2 to 4, depending on the soil textural classification. These correction factors, which are included in Table 1.2, can be reduced if approved by the local jurisdiction for sites with little soil variability, sites that will require a high degree of long-term facility maintenance, or sites where pretreatment will be employed to reduce the total suspended solids entering the infiltration facility. The WDOE manual specifies that correction factors must be greater than or equal to 2.0 and that factors higher than those included in Table 1.2 should be considered "for situations where long-term maintenance will be difficult to implement, where little or no pretreatment is anticipated, or where site conditions are highly variable or uncertain."

The second method for estimating infiltration rates included in the Department of Ecology manual is based on soil gradation parameters measured with the ASTM soil gradation procedure. These estimates are based on studies that compare infiltration measurements from full-scale infiltration facilities to soil gradation data developed with the ASTM procedure (ASTM D422). The recommended infiltration rates are included in Table 1.3. These estimates are described as "long-term rates" that represent average conditions regarding site variability, the degree of long-term maintenance, and pretreatment for TSS control. The Ecology manual indicates these long-term infiltration

rates may need to be decreased if the site is highly variable, or if maintenance and influent characteristics are not well controlled. The manual also notes that the data that form the basis for the estimates in Table 1.3 were from soils that would be classified as sands or sandy gravels and that no data were available for finer soils. The manual recommends that these vales not be for soils with a d_{10} size (10 percent passing the size listed) of less than 0.05 mm (U.S. Standard Sieve). The estimated infiltration rates included in tables 1.2 and 1.3 apply to homogeneous soils. If more than one soil unit is encountered beneath the facility, the Ecology manual requires that the lowest infiltration rate determined from each of the soil units be used as the representative site infiltration rate.

The third approach recommended in the Department of Ecology manual is to use large-scale in-situ infiltration measurements by using a procedure termed the Pilot Infiltration Test (PIT). For this test, water is added to a pond or an excavated pit at a rate that will maintain the water level between 3 and 4 feet above the bottom of the pond or pit. The instantaneous flow rate and cumulative volume required to maintain the constant water level are recorded at 15- to 30-minute intervals. Water is added to the pit for a recommended minimum of 17 hours. The infiltration rate is recorded both as the pond is filled and then as it empties. Estimates from these in-situ tests are also considered short-term rates that must be reduced through correction factors to account for site variability and number of tests conducted, degree of long-term maintenance and influent pretreatment/control, and potential for long-term clogging due to siltation and bio-buildup. The typical range of correction factors to account for these issues is summarized in Table 1.4.

The second major reference for storm water management in the state of Washington is the *King County Surface Water Design Manual* (1998). Procedures to estimate the infiltration rate outlined in the King County manual include the EPA falling-head percolation test procedure and the double-ring infiltrometer test. In a single-ring infiltrometer test, a cylinder (typically less than 1 m in diameter) is inserted into the ground, and water is poured into the cylinder. The water level is held constant by continually adding water from a graduated cylinder. The quantity of water added during a specified time period is recorded, and the infiltration rate versus time can then be calculated. The double-ring system attempts to measure only vertical infiltration by eliminating the effects of lateral flow. In this method, an outer ring surrounds the infiltrometer. This outer ring acts as a buffer zone, eliminating lateral flow within the infiltrometer. The infiltration rate is measured with the inner ring and results in a more accurate vertical rate (Ferguson, 1994).

The King County manual suggests that at least three tests should be performed for each proposed infiltration facility site. Correction factors to be applied to measured infiltration rates are included in the King County manual. These correction factors account for uncertainties in testing, depth to the water table or impervious strata, infiltration receptor geometry, and long-term reductions in permeability due to bio-buildup and accumulation of fines. Table 1.5 provides the correction factors that are multiplied by the measured infiltration rate to determine a design infiltration rate. The factor $F_{testing}$ refers to uncertainties in small-scale testing; $F_{geometry}$ refers to infiltration receptor geometry; and $F_{plugging}$ refers to biological accumulation on the pond bottom.

1.3 Other Criteria and Considerations for Infiltration Ponds

1.3.1 Siting Criteria and Considerations

Different regulatory organizations have attempted to improve the likelihood of an infiltration pond functioning properly by developing criteria that must be met before a pond location is selected. The common thread in these criteria is that infiltration ponds function best when the soil is highly permeable, the slope of the infiltration surface is low, and the pond is high above the water table. Specifically, the Department of Ecology requires the soil infiltration rate to be at least 0.5 in/hr, the slope to be no greater than 15 percent, and the bottom of an infiltration facility to be a minimum of 5 feet from the seasonal high water mark (WDOE, 2001). The provision for the minimum distance to the water table is in place as an effort to avoid the low hydraulic gradients that develop when the wetting front from the infiltration pond reaches the water table. These types of requirements are similar to those used in other states and jurisdictions. For example, the design guidelines prepared by the State of Maryland (2000) state that the bottom must be 4 feet from the water table, the infiltration rate may not be lower than 0.52 in/hr, and the slope must be less than 20 percent.

The approach used to site infiltration ponds developed by the Swedish Association of Water and Sewage Works is based on a point system (Stahre and Urbonas, 1990). Points are assigned to potential sites according to the ratio between the tributary connected impervious area and the infiltration area, the nature of the surface and underlying soils, the slope of the infiltration surface, the vegetation cover, and the degree of traffic on the surface. Sites with high scores are considered suitable, whereas sites that score low are not considered.

1.3.2 Clogging

The formation of a clogging layer on the surface of infiltration ponds is a common occurrence along the wetted perimeter. Clogging may be caused by the accumulation of silt, clay, or other fine material that was suspended in the water entering the recharge basin, by algae growth on the bottom or in the water, by precipitation of calcium carbonate in the water due to increases in pH caused by algae activity, and by biological activity on the wetted perimeter (Bouwer and Rice, 1989). Duchene et al. (1992) used a two-dimensional unsaturated flow model to investigate the influence of clogging on the performance of an infiltration trench. They found that placing a 5-cm-thick layer of soil with a low hydraulic conductivity at the bottom of the trench reduced the infiltration rate by 20 percent, 7 percent, and 4 percent for depths of water in the trench of 0.25 m, 0.50 m, and 1.0 m, respectively. These results conflict with field observations that have found that the hydraulics of infiltration ponds are controlled to a large extent by the formation of a clogging layer on the surface of the soils (Schuh, 1990).

1.3.3 Water Table Elevation

Traditional methods of measuring infiltration rates either have no relationship to the water table elevation or do not consider water level fluctuations over time periods longer than several days. Because water table elevations change throughout the year, it is important to understand the effect that these variations have on the infiltration rate. While infiltration ponds are known to function best when they are well above the water table, relatively little quantitative analysis has been conducted to determine how pond performance is affected by fluctuations in the water table.

1.3.4 Lateral Flow

Currently, information in the literature conflicts regarding what area to use as the available infiltration area in the Darcy's law design approach. The design guidelines prepared by the State of Maryland (1984) suggest using only the bottom area of an infiltration pond when calculating the infiltration rate. Conversely, Stahre and Urbanas (1990) suggest using only the sides of the pond, since the bottom will most likely become clogged over time. Duchene et al. (1992) estimated the percentage of infiltration that occurred through the sides of an infiltration trench and concluded that approximately three-quarters of the water flows through the bottom of the trench. The amount of lateral flow depends on site-specific factors such as height-area ratio of the pond and the degree of anisotropy in the soils around the pond.

Table 1.1—Wetting front suction head for different soil textures (after Mays, 1996).

Soil Class	Wetting front soil suction head, ψ, (in)
Sand	2
Loamy sand	2.5
Sandy loam	4.
Loam	3.5
Silt loam	6.5

Table 1.2—Parameters used to estimate infiltration rates shown in Figure 1.2

	Sand	Loamy Sand	Sandy Loam
Input parameters			
Capillary head at wetting front (cm)	4.1	5.8	11.2
Saturated hydraulic conductivity (cm/min)	0.49	0.24	0.07
Output description			
Time at which infiltration rate equals 1.5 times the saturated hydraulic conductivity (hrs)	0.05	0.1	0.9
Time at which infiltration rate equals 1.1 times the saturated hydraulic conductivity (hrs)	0.4	1.1	8.5

Table 1.3—Recommended infiltration rates based on USDA soil textural classification (WDOE, 2001)

	Short-Term Infiltration Rate (in/hr)	**Correction Factor**	**Estimated Long-Term Infiltration (Design) Rate (in/hr)**
Clean sandy gravels and gravelly sands (i.e., 90% of the total soil sample is retained in the #10 sieve)	20	2	10
Sand	8	4	2
Loamy Sand	2	4	0.5
Sandy Loam	1	4	0.25
Loam	0.5	4	0.13

Table 1.4—Recommended infiltration rates based on ASTM gradation testing (WDOE, 2001)

D10 Size from ASTM D422 Soil Gradation Test (mm)	**Estimated Long-Term (Design) Infiltration Rate (in/hr)**
>0.4	9
0.3	6.5
0.2	3.5
0.1	2.0
0.05	0.8

Table 1.5—Correction factors to be used with in-situ infiltration measurements to estimate long-term design infiltration rates (WDOE, 2001).

Issue	Partial Correction Factor
Site variability and number of locations tested	CFv = 1.5 to 6
Degree of long-term maintenance to prevent siltation and bio-buildup	CFm = 2 to 6
Degree of influent control to prevent siltation and bio-buildup	CFi = 2 to 6
Total correction factor	CF = CFv + CFm + CFi

Table 1.6—Correction factors from the *King County Surface Water Design Manual* (King County, 1998).

$F_{testing}$	$F_{geometry}$	$F_{plugging}$
0.30 - 0.50	0.25 - 1.0	0.7 for loams and sandy loams
		0.8 for fine sands and loamy sands
		0.9 for medium sands
		1.0 for coarse sands or cobbles

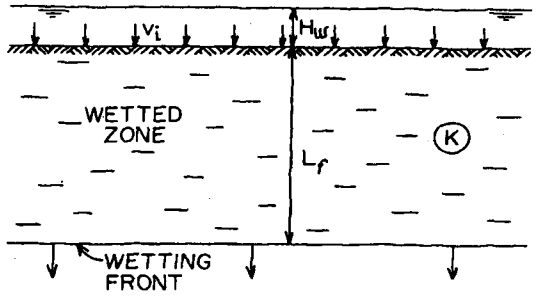

Figure 1.1—Moisture zones during infiltration (Bouwer, 1978).

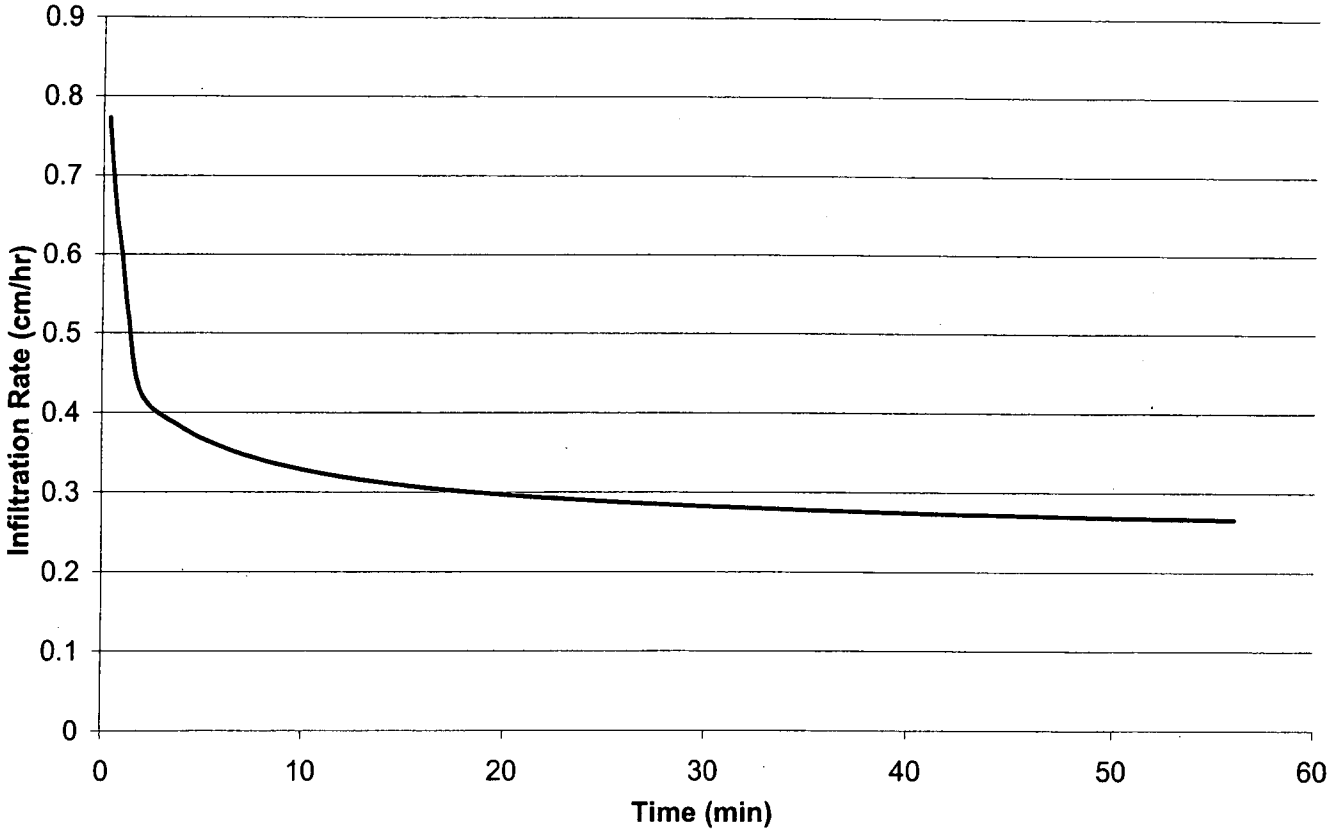

Figure 1.2 —Estimated infiltration rate for loamy sand using the Green and Ampt equation.

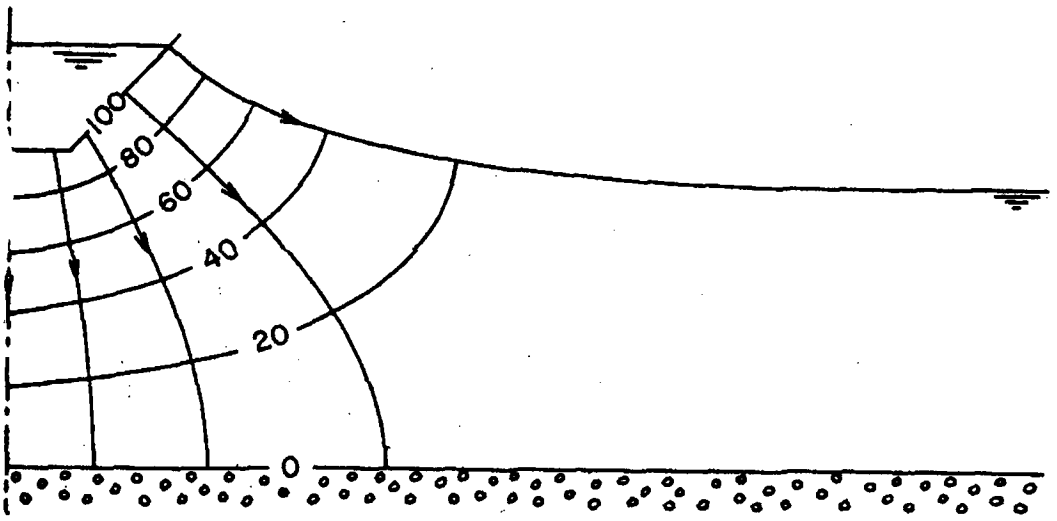

Figure 1.3—Flow system for a wetting front that has reached the water table (Bouwer, 1978).

2 ESTIMATING HYDRAULIC CONDUCTIVITY FROM AIR FLOW EXPERIMENTS

One of the objectives of this study was to develop estimates of the saturated hydraulic conductivity of disturbed soil samples obtained from infiltration ponds. Two approaches were used: one approach was based on measuring air flow in synthetic and natural soil samples, and the second approach was based on soil texture information obtained from grain size curves. Both approaches are relatively simple and do not require sophisticated laboratory techniques or equipment. The intent is to develop an approach for estimating saturated hydraulic conductivity that is more sophisticated and site-specific than the approach based on USDA soil classifications that was described in Chapter 1, but that is also more simple than traditional laboratory methods. The air-flow approach is described in this chapter, and the soil-texture approach is described in Chapter 3.

Finding a relationship between air conductivity and saturated hydraulic conductivity is beneficial because air conductivity can be measured rapidly and with fewer practical problems than saturated hydraulic conductivity (Loll et al., 1999). The approach introduced in this study requires relatively few technical laboratory testing procedures and can be done in minutes for each soil sample.

2.1 Relationship Between Air Conductivity and Hydraulic Conductivity

The approach for estimating saturated hydraulic conductivity using air-flow experiments is based on Darcy's law. Although originally developed for water as the fluid, Darcy's law has been shown to be valid for air flow in most soils (Massmann, 1989). The exceptions are relatively fine-grained soils, such as clays, and systems with

very high flow rates. For the pressures and soil types that will be used in this study, the flow of air through soils can be described by the following form of Darcy's law:

$$Q_{air} = -K_{air}\left(\frac{dh_{air}}{dz}\right)A \qquad (2.1)$$

where Q_{air} is the volumetric flow rate for the air (L^3/t), dh_{air}/dz is the head gradient across the permeameter (L/L), and K_{air} is the conductivity of the sample for air (L/t). The subscript *"air"* is used to denote that air is the mobile fluid in this experiment.

The pneumatic head, h_{air}, is a measure of the mechanical energy per unit mass of air. For the relatively low pressures used in the laboratory experiments in this study, the air can be treated as an incompressible fluid (Massmann, 1989), and the fluid head at a point is given by the following expression:

$$h_{air} = z + \frac{P_{air}}{\rho_{air} g} \qquad (2.2)$$

where P_{air} is the air pressure ($M/L{\cdot}t^2$) and ρ_{air} is the air density (M/L^3).

The air conductivity, K_{air}, is given by the following expression (Massmann, 1989):

$$K_{air} = \frac{k\rho_{air} g}{\mu_{air}} \qquad (2.3)$$

where k is permeability (L^2), ρ_{air} is the air density (M/L^3), and μ_{air} is the dynamic viscosity of the air ($M/L{\cdot}t$).

The permeability, k, that is measured with air-flow experiments with a dry soil is assumed to be nearly equal to the permeability that is measured with water-flow experiments with saturated soil. Differences in permeability from gas-flow and water-flow experiments may arise because of gas slippage along the solid boundaries. The permeability for a dry soil measured with air flow is always larger than the permeability for a saturated soil measured with water flow. This fact was studied by Klinkenberg in 1941 and is known as the "Klinkenberg effect" (Corey, 1986). The differences in permeability estimates are generally small for coarse-grained soils such as silts, sands, and gravels (Massmann, 1989).

Equation 2.3 can be combined with a similar expression for hydraulic conductivity (e.g., Freeze and Cherry, 1979) to give hydraulic conductivity as a function of air conductivity:

$$K_s = \frac{k\rho_w g}{\mu_w} = \frac{\mu_{air}\rho_w}{\mu_w \rho_{air}} K_{air} = C_f K_{air} \qquad (2.4)$$

The correction factor C_f is dependent upon the viscosity and density of air and water. Each of these variables is in turn dependent upon temperature, as summarized in Table 2.1. If the air conductivity is measured at laboratory temperatures, and if the hydraulic conductivity is also for laboratory temperatures, then the correction factor is equal to 15. This is based on an assumed laboratory temperature of 20° C. If the air conductivity is measured at laboratory temperatures, and if the hydraulic conductivity is for field temperatures, then the correction factor is approximately 11.5. This is based on an assumed field temperature of 10° C.

2.2 Measuring Air Conductivity

The conventional method for measuring the air conductivity of porous media involves continuous-flow permeameters (e.g., Stonestrom and Rubin, 1989; Springer et al., 1998). Air flow is induced through a sample with a mechanical air pump or a source of compressed air. The pressure drop across the sample is measured with pressure transducers or manometers, and the flow rate is measured with rotameters or soap-film flow meters. More recently, air permeameters have also been developed with pistons and syringes to induce air flow and photosensors to measure flow rates (e.g., Davis et al., 1994).

The stand-alone permeameter that was used in the current study is shown in Figure 2.1. This permeameter, which was developed at the University of Washington (Massmann and Johnson, 2001), is constructed with two sections of clear, rigid plastic tubing connected with a plastic fitting or coupling. The upper section of the tubing holds the soil sample, and the lower section is used as a reservoir for pressurized air. Tubes with an inside diameter of 1 to 10 cm and with upper and lower sections each approximately 30 to 50 cm long work well for fine to medium sands. Longer sections may be required for more permeable materials. A nylon or steel mesh is glued to the bottom of the upper section to hold the sample.

The air permeability or conductivity is measured by first placing a sample of dry soil in the upper section of the permeameter. The top of the permeameter is sealed, and the lower section is submerged in a container of water. The seal can be made with a cork or rubber stopper or simply with a thumb. Water will enter the bottom section of the permeameter and will pressurize the air. Because the air pressure in the lower section is

greater than atmospheric pressure, air will flow through the sand when the top of the permeameter is opened. As the air flows upward through the permeameter, the air pressure in the lower section decreases, and H, the distance from the water level in the lower section of the permeameter to the water level in the water container, becomes smaller. If the diameter of the water reservoir is large relative to the diameter of the permeameter, the rate of flow through the permeameter, Q_{air}, is directly proportional to the rate of change in H.

The air conductivity can be estimated by measuring how quickly the water level in the lower section raises. The following expression gives this relationship (Massmann and Johnson, 2001):

$$K_{air} = \left(\frac{\rho_{air}}{\rho_w}\right)\frac{L}{(t_1 - t_0)}\ln\left(\frac{\frac{\rho_w}{\rho_{air}}H_o + L}{\frac{\rho_w}{\rho_{air}}H_1 + L}\right) \qquad (2.5)$$

where H_o and H_1 are measured at times t_0 and t_1 (Massmann and Johnson, 2001). All values on the right side of the equation (2.5) are either known or can be measured directly with the permeameter. In most cases, the first term on the right side of equation (2.5) will be large relative to L. In these cases, equation (2.5) can be reduced to the following:

$$K_{air} = \left(\frac{\rho_{air}}{\rho_w}\right)\frac{L}{(t_1 - t_0)}\ln\left(\frac{H_o}{H_1}\right) \qquad (2.6)$$

2.3 Sensitivity to Permeameter Scale

Three different sizes of air permeameters were used to evaluate the sensitivity of the results to the scale of the permeameter. The inside diameters of the three

permeameters were 1.25 cm, 6.4 cm, and 10.2 cm, and the lengths of the permeameters were 31 cm, 46 cm, and 61 cm, respectively. The soil samples used in these tests comprised #50 and #125 silica sand. Grain size curves for these soils are included in tables C2 and C3 in Appendix C.

The results for the two larger-diameter permeameters, which are included in Table 2.2, were reasonably consistent, and differences were likely due to differences in sample porosity. However, the smallest permeameter tended to give air conductivity values higher than those obtained with the larger permeameters. This can be seen by comparing the results from the #50 samples in Table 2.2. For #50 samples with similar porosity, the air conductivity estimated with the smallest permeameter was twice as large as the air conductivity estimated using the larger permeameter. Similarly, this can be seen in comparing the first two trials of the #50 samples for the smallest permeameter (the ones with the lowest porosity) with the two trials for the medium and large permeameter. The lower porosity samples in the small permeameter produced estimates of air conductivity similar to those from the higher porosity samples for the medium and large permeameters. One explanation for the higher values with the smaller permeameter is leakage along the side walls of the permeameter. The side wall area is proportional to the permeameter diameter while the resistance caused by the soil is proportional to the diameter squared. For small diameter samples, the side wall area becomes larger relative to the soil area.

Reproducibility was also investigated for each permeameter. The difference between estimates for samples with approximately the same porosity for the #50 and #125 soils was generally on the order of 30 percent or less. These differences were

smaller for the larger permeameters. This magnitude of error may be acceptable for many applications, especially at sites with significant spatial heterogeneity.

The advantages of a larger permeameter include reduced edge effects relative to the soil sample, and the ability for larger soil particles to fit into the column without taking up the whole cross-sectional area of the column. A larger permeameter also allows for larger volumes of soil samples, which achieve more precise results for more permeable and non-uniform soils. The 6.4-cm-diameter permeameter was chosen for the laboratory tests because it was easier to manage than the 10.2-cm-diameter permeameter, and the differences in measured results between the two permeameters were within an acceptable range.

2.4 Measuring Air Conductivity for Synthetic Soils

The objective of measuring air conductivity for synthetic soils was to develop regression equations to estimate saturated hydraulic conductivity, K_s, from grain-size analyses. The measured air conductivity values were converted to saturated water conductivity, and a regression equation was derived to estimate saturated hydraulic conductivity using selected grain-size parameters of the synthetic soil samples. The expectation was to use the regression equation to estimate K_s for field soil samples.

Four different soil textures were selected to encompass a wide range of saturated hydraulic conductivity values. The soil textures included #16 silica sand, #50 silica sand, #125 silica sand, and rock flour (pulverized sand that has the consistency of flour). Mixing different portions of these four soil types created a series of soil textures. The air permeameter was then used to estimate hydraulic conductivity for each different soil sample using a C_f of 15. The mixtures used to develop the different soil samples, the

measured K_{air} values, and the estimated saturated hydraulic conductivity are given in Appendix A. These hydraulic conductivity values were used to develop regression equations relating soil texture information and hydraulic conductivity.

Equation 2.6 was used to calculate K_{air}. H_0 was measured from a metric ruler that was taped to the lower cylinder. When the seal was released from the upper cylinder, a stopwatch was used to record the time for the water to rise inside the lower cylinder. H_1 was measured when the timer was stopped. The length of the soil sample was recorded with a metric ruler.

The porosity, n, for each sample was estimated by measuring the volumes of solids and the bulk sample. Porosity was then calculated with the following expression:

$$n = \frac{V_{pores}}{V_{sample}} = \frac{V_{sample} - V_{solids}}{V_{sample}} = 1 - \frac{V_{solids}}{V_{sample}} \qquad (2.7)$$

where V_{pores} is the volume of the pore space, V_{sample} is the volume of the soil sample, and V_{solids} is the volume of the solid particles.

The volume of the soil sample, V_{sample}, was determined by multiplying the length of the soil sample by the cross-sectional area of the inside cylinder. The volume of the solid particles, V_{solids}, was calculated by dividing the weight of the soil sample by 2.65, which is the accepted density for particles (Danielson and Sutherland, 1986).

2.5 Measuring Air Conductivity for Natural Soils

The objective of measuring air conductivity for natural soils was to derive a regression equation relating hydraulic conductivity and soil texture information that could be compared with the regressions derived for the synthetic soils.

A series of air conductivity tests was conducted on samples collected at 15 sites with infiltration ponds. Test holes to collect soil samples were drilled to depths between 10 inches (25 cm) to 70 inches (178 cm). The depths of the test holes depended upon the physical ability to reach lower depths and the soil uniformity. The shallower depths were a result of either soil conditions that prohibited deeper depths, observed uniformity of the soil column throughout and therefore the expectation that deeper depths would not provide new soil textures, or encountering of the water table. Each test hole was visually inspected for a change in soil texture. Soil samples were taken for each soil texture throughout the soil column and identified by the soil layer and depth of the layer. The samples were air dried in the laboratory and tested for air conductivity with the air permeameter. The air conductivity test was repeated for each sample until a minimum of three consistent measurements had been obtained.

Measured air conductivity and the corresponding saturated hydraulic conductivity for each measurement is given in Appendix B.

2.6 Limitations of the Approach

There are limitations in using the air permeameter with coarse-textured soils. When the measured air conductivity is larger than approximately 0.1 cm/s, accurately measuring the time to move air through the soil sample becomes difficult once the upper column seal has been released. This air conductivity value corresponds to a saturated hydraulic conductivity of 1 cm/s, which is typical of coarse gravel.

Non-uniform soil textures within a soil layer resulted in another limitation for the air permeameter. Packing non-uniform soil sometimes resulted in large macropores or continuous air gaps within the soil sample and between the sample and the test cylinder.

This can result in preferential flow paths through the column. A large diameter permeameter has the advantage of reducing this effect. The soil can be agitated in the permeameter until the "holes" are filled in with the finer soil.

Table 2.1—Density and viscosity of water and air at different temperatures (from Janna, 1993).

Temperature °C	$\rho_{water}(kg/m^3)$	$\mu_{water}(kg/m \cdot s)$	$\rho_{air}(kg/m^3)$	$\mu_{air}(kg/m \cdot s)$
10	1000	$1.3(10^{-3})$	1.25	$1.76(10^{-5})$
20	998	$1(10^{-3})$	1.2	$1.8(10^{-5})$

Table 2.2—Comparison of measured air conductivity values for different size permeameters.

Synthetic Sample	D = 1.25 cm		D = 6.35 cm		D = 10.16 cm	
	K_{air} (cm/s)	*porosity*	K_{air} (cm/s)	*porosity*	K_{air} (cm/s)	*porosity*
#16	0.058					
#50	2.00E-03	0.26	2.10E-03	0.35	2.00E-03	0.34
#50	2.10E-03	0.26	2.20E-03	0.35	2.50E-03	0.35
#50	3.60E-03	0.31				
#50	4.30E-03	0.32				
#50	4.10E-03	0.33				
#125	1.90E-04	0.37	2.50E-04	0.44	2.50E-04	0.43
#125	2.70E-04	0.37	1.80E-04	0.45	3.10E-04	0.46
#125			2.80E-04	0.45		
#125			3.00E-04	0.46		

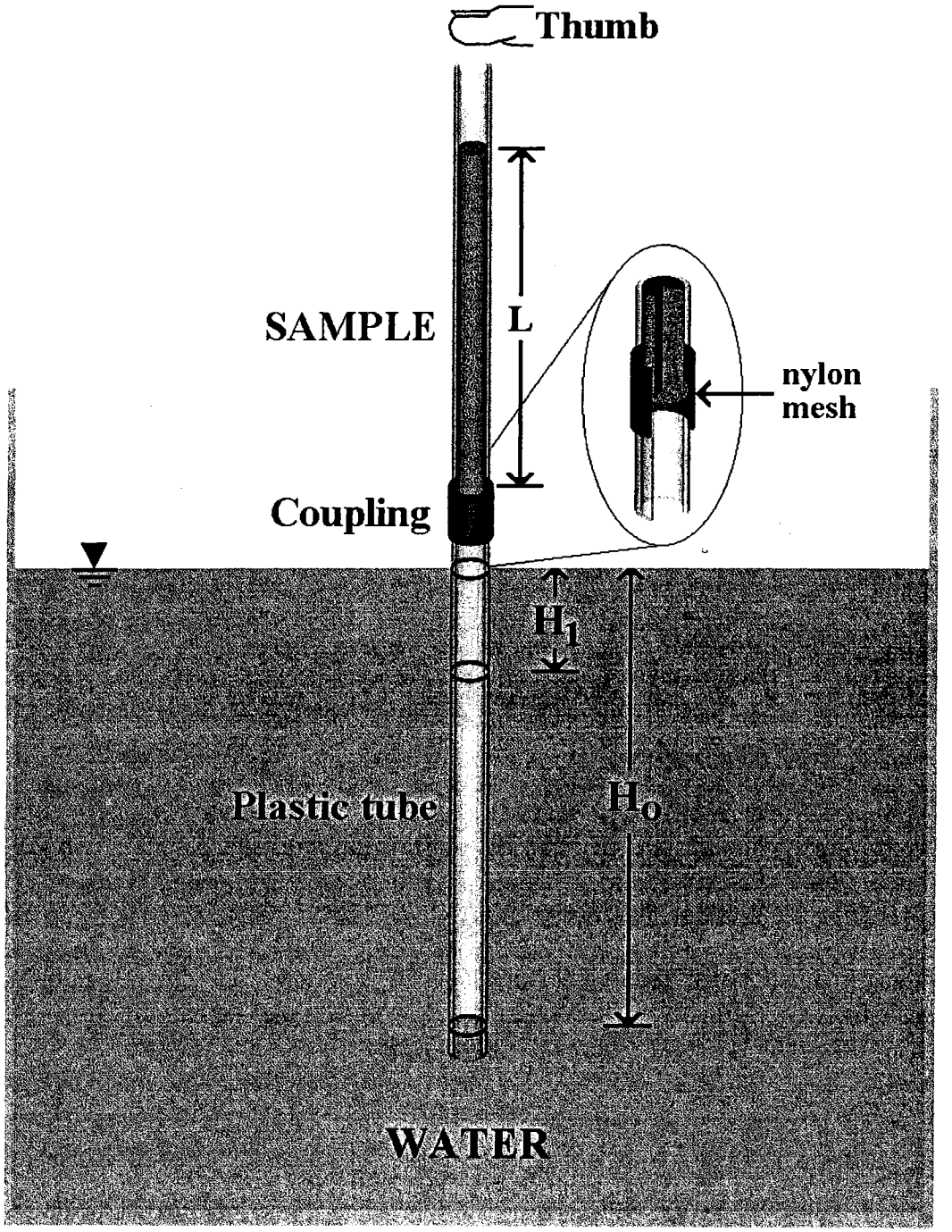

Figure 2.1—Stand-alone air permeameter (from Massmann and Johnson, 2001).

3 ESTIMATING SATURATED HYDRAULIC CONDUCTIVITY FROM GRAIN SIZE CURVES

Regression equations that were derived with grain size parameters from synthetic and field soil samples were used to estimate saturated hydraulic conductivity (K_s). Three different sets of regression equations were developed. The first set of equations was derived from data collected from the synthetic soils described in Chapter 2. The second set of equations was derived from data collected from the field (natural) soils. Data from the synthetic and natural soils were combined to derive the third set.

A relationship between grain size distribution and saturated hydraulic conductivity is of value because grain size information can be obtained more easily than laboratory measurements of hydraulic conductivity. Because grain size analyses are generally simple and inexpensive, estimates from relatively many samples can be obtained rapidly and inexpensively. It may be more effective to obtain rough estimates of saturated hydraulic conductivity from grain size distributions from many samples rather than from a few laboratory measurements that require substantially more effort, especially in soils that exhibit significant spatial heterogeneity. A relationship between grain size and hydraulic conductivity may provide adequate estimates for hydraulic conductivity where more detailed data are not available or justified (Rawls et al., 1982).

3.1 Approaches for Estimating Saturated Hydraulic Conductivity Using Soil Texture Data

Methodologies have been proposed in the literature for estimating hydraulic conductivity and infiltration rates on the basis of soil texture information. These methodologies range from relatively qualitative estimates based on soil type (e.g. Table 2.2, p. 29, Freeze and Cherry, 1979) to relatively quantitative estimates based on data

from soil gradation analyses. Estimates of hydraulic conductivity from soil gradation analyses include the Hazen formula, which is based on an effective grain size (Freeze and Cherry, 1979); the Krumbein and Monk equation, which is based on the mean and the standard deviation of the grain size (Davis and DeWeist, 1966); and the Fair-Hatch equation, which is based on the complete gradation curve (Freeze and Cherry, 1979). These approaches are generally applicable to relatively uniform sands.

One approach that has been proposed for estimating infiltration rates is to use regression equations based on percentage of sand, percentage of clay, and porosity. The general idea is to measure infiltration rates from a large set of samples and to correlate these rates to measurements of the percentage of sand, percentage of clay, and porosity. The resulting regression equations are then assumed to be valid for other similar soils. This approach was used by Rawls and Brakensiek (1985). Regression equations were developed on the basis of measurements taken from more than 5,000 soil horizons from 1,323 soil types in 32 states. The data used to develop these regression equations were collected from soils with clay content ranging from 5 to 60 percent and with a sand content of from 5 to 70 percent. (Clay content was defined as particle sizes smaller than 0.002 mm. Sand was defined as particle sizes between 0.05 and 2 mm.) The data that were used to develop the regressions are described in Rawls et al., 1982.

Although the regresssions developed by Rawls and Brakensiek were developed with soils with clay contents of between 5 to 60 percent and with sand contents of from 5 to 70 percent, they have been used to describe soils with higher sand contents (Carsel and Parrish, 1988; Meyer et al., 1997). The accuracy of these regressions for soils with higher sand content is not known. Soils considered for infiltration facilities generally

have a relatively low clay content. This may limit the use of these equations for estimating saturated hydraulic conductivity for soils in western Washington.

Note that for layered systems, the soil texture information should be collected for each individual layer. An effective hydraulic conductivity can be calculated from the values estimated for the individual layers. For example, the effective hydraulic conductivity for flow perpendicular to the layers is given by the harmonic mean (Freeze and Cherry, 1979).

3.2 Regression Equations for Synthetic Soils

A regression equation was derived by using saturated hydraulic conductivity estimates from 71 "synthetic" soil samples comprising different fractions of four different soil textures. The saturated hydraulic conductivity for each soil sample was estimated by using the air permeameter described in Chapter 2.

Measuring saturated hydraulic conductivity of synthetic soils with pre-determined grain size parameters provided a relatively quick method of obtaining a wide distribution of grain size soil samples and simple calculation of the parameters used in the regression equation.

Grain size characteristics were selected to obtain samples over a large range of the gradation curve. Coarse, medium, and fine textures were represented by four homogeneous soil textures: #16, #50, #125, and rock flour. The desired distribution of grain size samples was achieved by using the #16, #50 and #125 soil textures in increments of 20 percent. The rock flour was added to the samples in increments of 5 percent, up to a maximum of 20 percent. The rock flour was used to represent

characteristics of clay in a soil. The different synthetic samples used for the regression equation are given in Appendix A.

The effective grain diameters d_{10}, d_{60}, and d_{90} correspond to an equivalent "percent passing" on the grain size distribution curve. These grain diameters and porosity were used as the parameters in the regression equations. Because in-situ porosity cannot be duplicated in the lab, the final evaluation of regression equations did not include porosity.

The grain size parameters for the four soil textures were obtained from grain size curves. The curves were made from sieve analyses for soils #16, #50 and #125. The grain size curve for the rock flour was obtained from a hydrometer test conducted at a commercial laboratory. The grain size curves for the synthetic soils are given in Appendix C.

The representative grain size parameters for the synthetic samples were calculated as a percentage of the parameters from the original four soil textures. Each representative grain size was a summation of the percentage of the original soil texture multiplied by the parameter grain size of that soil texture. For example, the d_{90} for a synthetic soil sample comprising 80 percent #16 soil, 1 percent #50 soil, 5 percent #125 soil, and 5 percent rock flour would be calculated from the following equation:

$$d_{90,soilsample} = 0.80(d_{90,\#16}) + 0.10(d_{90,\#50}) + 0.05(d_{90,\#125}) + 0.05(d_{90,rockflour}) \qquad (3.1)$$

Regression equations were derived using different combinations of the three grain size parameters. Each different combination contains one or more of the parameters raised to the power of one or two. The rationale behind the different combinations was

taken from the Rawls and Brakensiek (1985) regression equations for saturated hydraulic conductivity. The general equation for predicting saturated conductivity is given below:

$$K_{s-predicted} = c_1 + c_2 d_{10}^m + c_3 d_{60}^m + c_4 d_{90}^m \tag{3.2}$$

where $K_{s\text{-}predicted}$ is saturated hydraulic conductivity in units of cm/s (L/t); c_1, c_2, c_3, and c_4 are coefficients; and the exponent, m, is 1 or 2.

The "Solver" routine in Excel spreadsheets was used to calculate the coefficients for each parameter by minimizing the sum of the mean square error, subject to the constraint that the predicted saturated hydraulic conductivity was greater than 0.0. The mean square error is calculated by

$$\left(K_{measured} - K_{predicted}\right)^2 \tag{3.3}$$

where $K_{measured}$ is the measured saturated hydraulic conductivity estimated with the air permeameter (L/t), and $K_{predicted}$ is the calculated saturated hydraulic conductivity from a regression equation (L/t).

Regression equations were also developed on the basis of the lowest normalized sum of the mean square error. The normalized mean square error is calculated by

$$\left(\frac{K_{measured} - K_{predicted}}{K_{measured}}\right)^2 \tag{3.4}$$

Plots of the regression equations that were derived by minimizing the sum of the mean square error and the sum of the normalized mean square error were compared. The comparison revealed that a regression equations derived by minimizing the sum of the mean square error resulted in a closer fit between the measured K_s and the predicted K_s.

The equations that were tested for minimum sum of the mean square error are given in Table 3.2.

Three regression equations were selected for a best-fit comparison. These three equations are presented in Table 3.3. Trial 1 was the Hazen equation, which was selected to compare the derived regression with the original Hazen equation. Trials 6 and 8 were selected because they gave the best overall fit for the regressions derived from synthetic soil samples, natural soil samples, and natural and synthetic soil samples combined.

The measured K_s values obtained using the air permeameter and the predicted K_s values from regression equations A.1, A.6, and A.8 are plotted in figures 3.1, 3.2, and 3.3. The Hazen equation under-predicted K_s for the majority of the measured samples. Equation A.6 over-predicted K_s values for rates of less than 0.1 cm/s. Predicted K_s values of greater than 0.1 cm/s were spread about the direct correlation line. Predicted K_s values for equation 1.8a were spread about the line for measured K_s values under 0.01 cm/s and were below measured K_s values of greater than 0.01 cm/s.

3.3 Estimating Saturated Hydraulic Conductivity for Natural Soils by Using the Regression Equation from Synthetic Soils

Grain size parameters for "natural" soil samples from 15 sites were used in the regression equations A.1, A.6, and A.8 derived from "synthetic" soil samples. Comparisons of predicted versus measured K_s are shown in figures 3.4, 3.5 and 3.6.

The Hazen equation under and over-predicted K_s values. Regression equations A.6 and A.8 over-predicted K_s for the majority of the samples. Regression equation A.6a was non-conservative by up to a factor of 1000 for predicted K_s values measured in this study. This suggests that the coefficients derived for the synthetic soils were too large for estimating K_s for the natural soils.

3.4 Regression Equations from Natural Soil Samples

Regression equations were derived for field soil samples by using the same soil texture parameters as the synthetic-soil regressions. A total of 67 soil samples were taken from 15 sites with infiltration ponds. The K_s values used to derive the regression equations are found in Appendix B. The parameters for the natural soils were obtained from grain size curves generated from sieve analyses. The grain size curves are found in Appendix C.

The results for equations derived by minimizing the sum of the mean square error are given in Table 3.3. Regression equations B.1, B.6, and B.8 were developed from the natural soils. Comparisons between the measured and predicted K_s values for the three selected equations are shown in figures 3.7, 3.8, and 3.9. Similar to the synthetic regression results, the Hazen equation showed a tighter fit for lower K_s rates and was conservative for rates greater than 0.1 cm/s. Regression equations B.6 and B.8 do not give as tight as fit as the Hazen for K_s values of less than 0.1 cm/s and give less conservative K_s values for rates larger than 0.1 cm/s.

3.5 Regression Equation from Both Synthetic and Natural Soil Samples

Regression equations were developed by using a combined data set of measured K_s values from both the synthetic and natural soils. The derived regression equations and sum of the mean square errors are included in Table 3.3 as C.1, C.6, and C.8. Figures 3.10, 3.11, and 3.12 compare the measured and predicted K_s values for the three selected equations.

The Hazen equation under-predicted the majority of K_s values by up to a factor of 1000. For regression equations C.6 and C.8, most of the samples were over-predicted for K_s values of lower than 0.01 cm/s and "spread the line" for K_s values of greater than 0.01 cm/s.

Figure 3.13 compares the difference between the measured and predicted K_s values for all three equations. Again, the Hazen equation produced a better fit between the measured and predicted values of less than 0.1 cm/s and then produced conservative predictions for K_s values of greater than 0.1 cm/s.

Regression equations C.6 and C.8 generally over-predicted lower K_s values and resulted in estimates that were spread about the direct correlation line for K_s values of greater than 0.1 cm/s.

Table 3.1—Coefficients for the Hazen Equation where d_{10} is in mm and K_s is in cm/s (Fetter, 1994).

Very fine sand, poorly sorted	0.40 - 0.80
Fine sand with appreciable fines	0.40 - 0.80
Medium sand, well sorted	0.80 - 1.20
Coarse sand, poorly sorted	0.80 - 1.20
Coarse sand, well sorted, clean	1.20 - 1.50

Table 3.2—Sum of mean square error for synthetic and natural soil samples.

Trial	**d_{10}**	**d_{60}**	**d_{90}**	**d_{10}^2**	**d_{60}^2**	**d_{90}^2**	*Sum of Mean Square Errors*		
							Synthetic	Natural	Combined
1				X			1.25	4.02	5.43
2					X		3.83	8.10	11.25
3						X	2.18	6.53	10.80
4	X	X	X				0.68	2.70	3.50
5				X	X	X	0.79	4.28	3.83
6	X	X	X	X	X	X	0.53	3.05	3.45
7		X	X	X			0.86	3.15	4.28
8	X		X		X		0.69	2.74	3.50
9	X	X				X	0.65	2.93	3.60
10			X	X	X		0.88	3.15	4.28
11		X		X		X	0.77	3.38	4.05
12	X				X	X	0.65	2.93	3.60

Table 3.3—Sum of mean square error of synthetic and natural soils for selected equations.

Trial	Regression Equation	Sum of mean square error
A.1	$1.07\,d_{10}^2$	1.25
A.6	$0.067 + 0.59\,d_{10} + 0.012\,d_{60} - 0.29\,d_{90} + 0.1\,d_{10}^2 - 0.0052\,d_{60}^2 + 0.21\,d_{90}^2$	0.53
A.8	$-0.01 + 0.8\,d_{10} + 2.6(10^{-4})\,d_{60}^2 + 0.034\,d_{90}$	0.69
B.1	$0.77\,d_{10}^2$	4.02
B.6	$-3.1(10^{-4}) + 0.57\,d_{10} - 0.035\,d_{60} + 0.0096\,d_{90} + 0.58\,d_{10}^2 + 9.5(10^{-4})\,d_{60}^2 - 2.9(10^{-4})\,d_{90}^2$	3.05
B.8	$0.024 + 0.8\,d_{10} + 3.4(10^{-5})\,d_{60}^2 - 0.0047\,d_{90}$	2.74
C.1	$0.87\,d_{10}^2$	5.43
C.6	$0.0029 + 1.0\,d_{10} - 0.014\,d_{60} - 0.0011\,d_{90} - 0.19\,d_{10}^2 + 3.1(10^{-4})\,d_{60}^2 - 2.5\,(10^{-5})\,d_{90}^2$	3.45
C.8	$0.019 + 0.82\,d_{10} + 2.8(10^{-5})\,d_{60}^2 - 0.0045\,d_{90}$	3.50

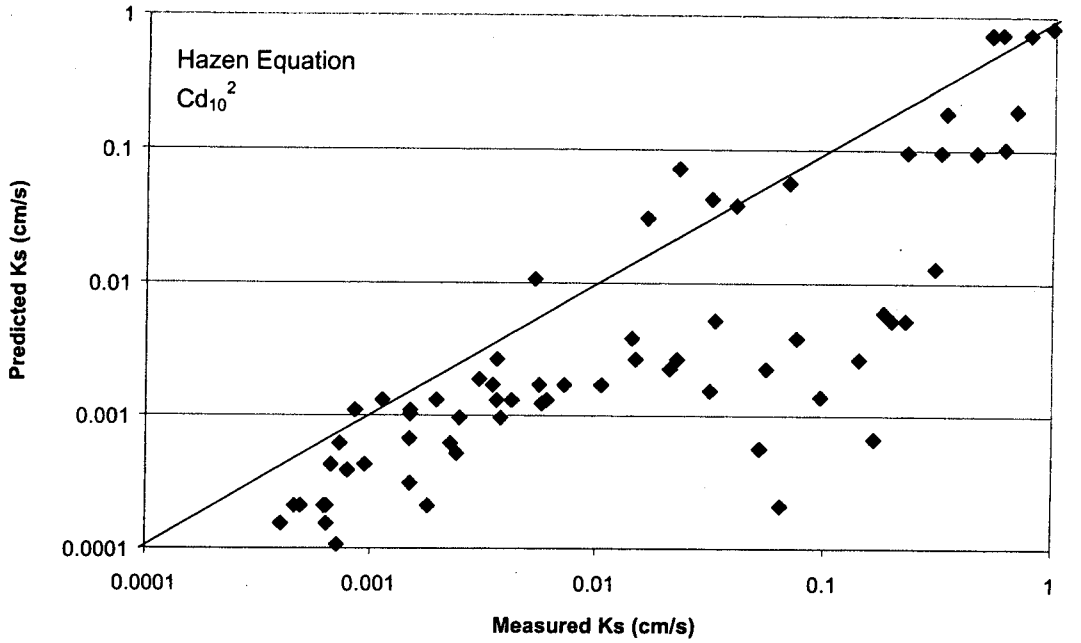

Figure 3.1—A comparison of measured hydraulic conductivity of synthetic soils with predictions made with the Hazen equation (regression equation A.1).

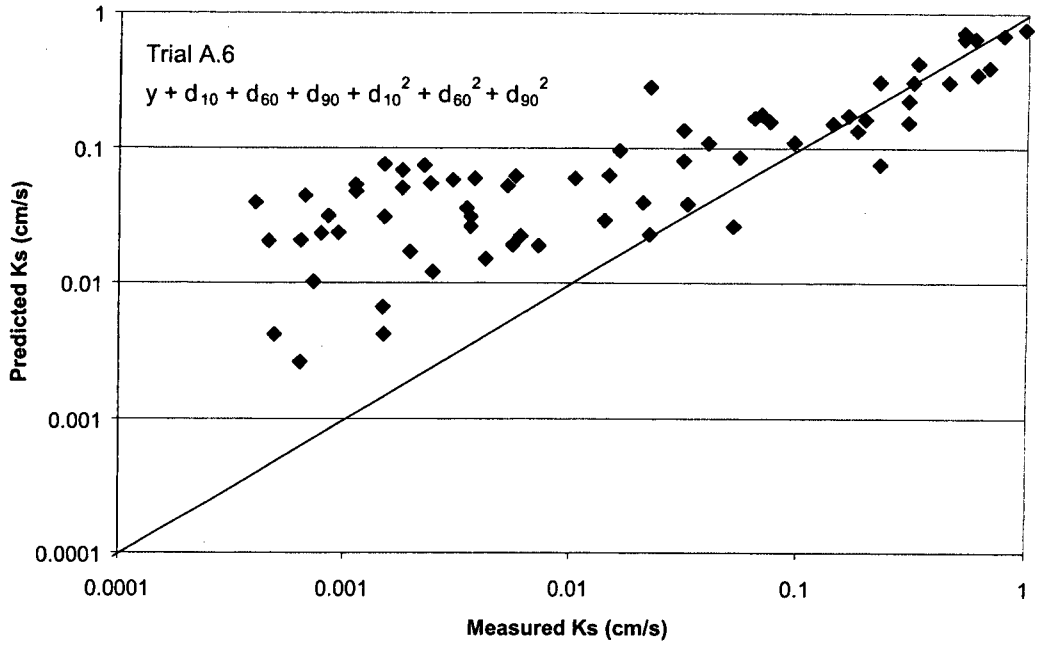

Figure 3.2 - A comparison of measured hydraulic conductivity of synthetic soils with predictions made with regression equation 1.6a.

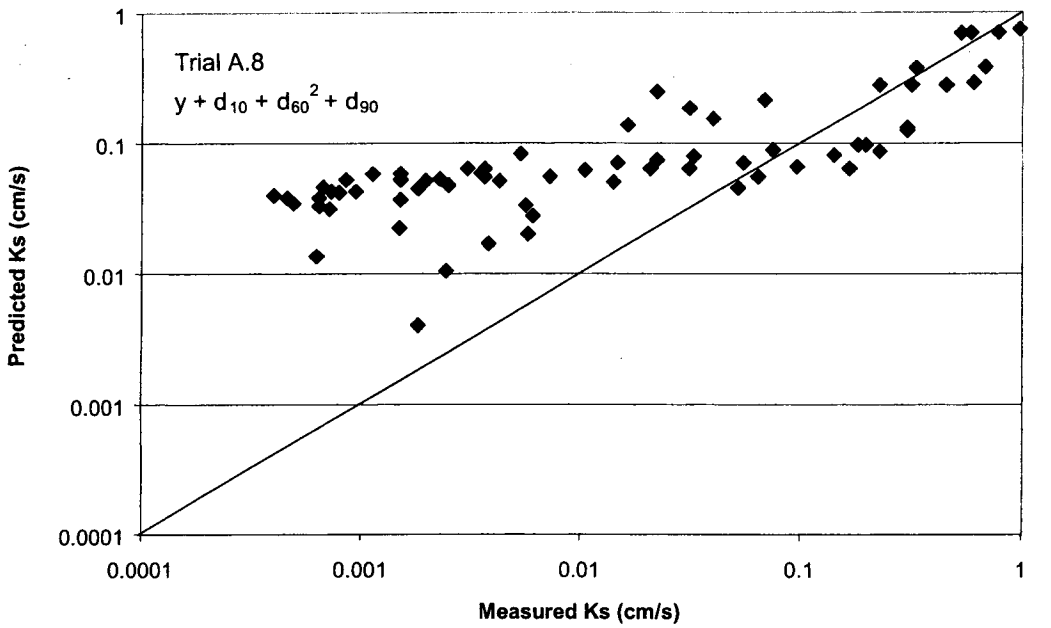

Figure 3.3—A comparison of measured hydraulic conductivity of synthetic soils with predictions made with regression equation A.8.

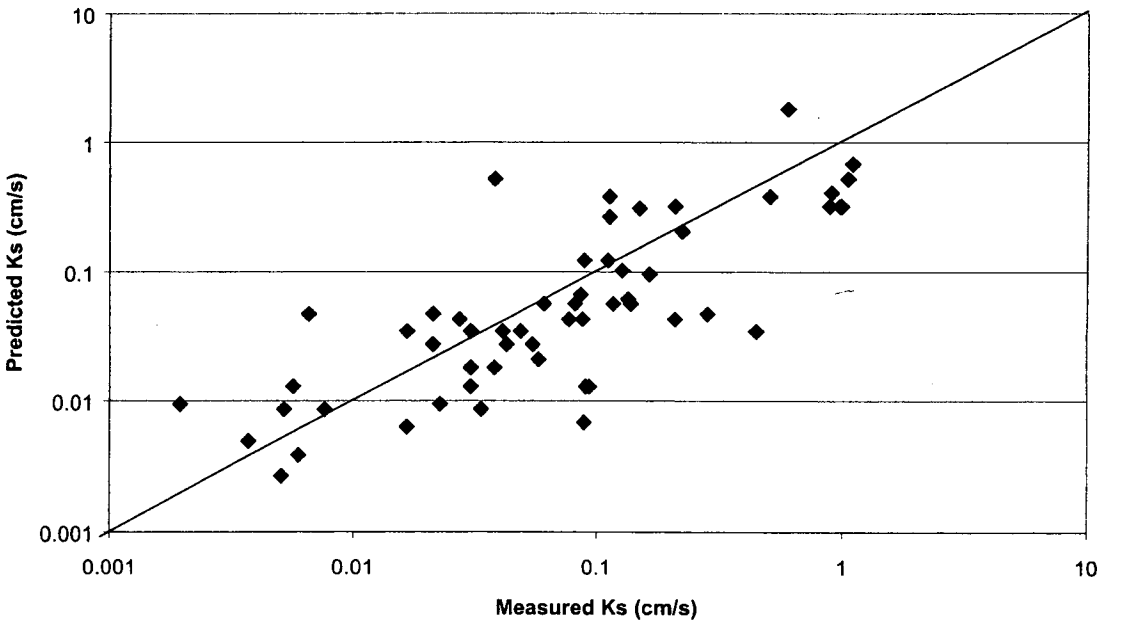

Figure 3.4—Hazen equation A.1 derived from synthetic soil and applied to natural soil parameters.

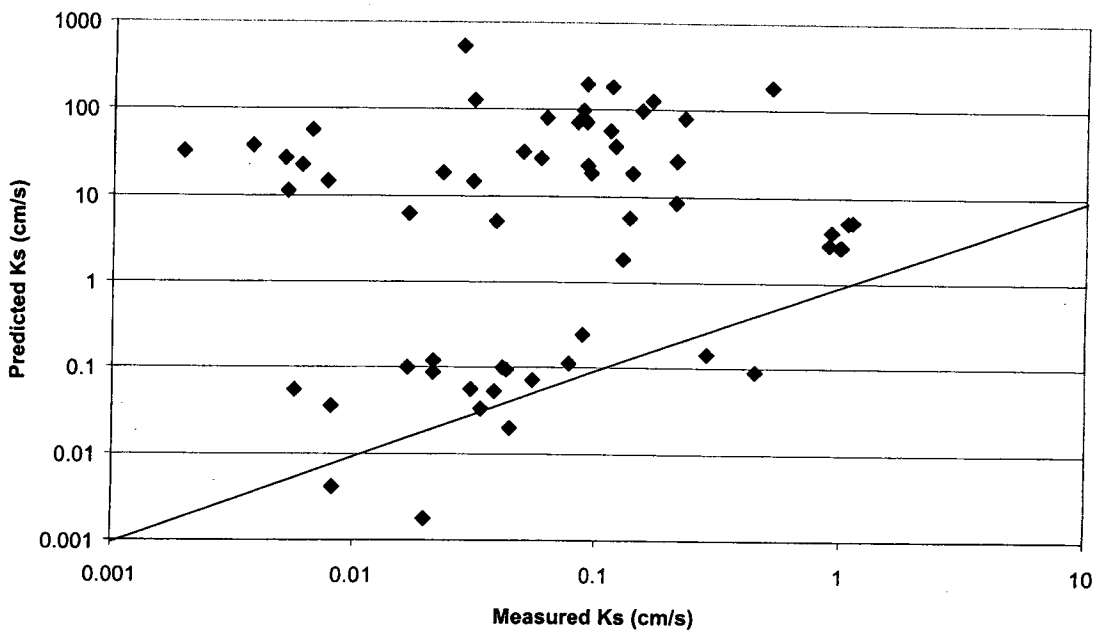

Figure 3.5—Regression equation A.6 derived from synthetic soil and applied to natural soil parameters.

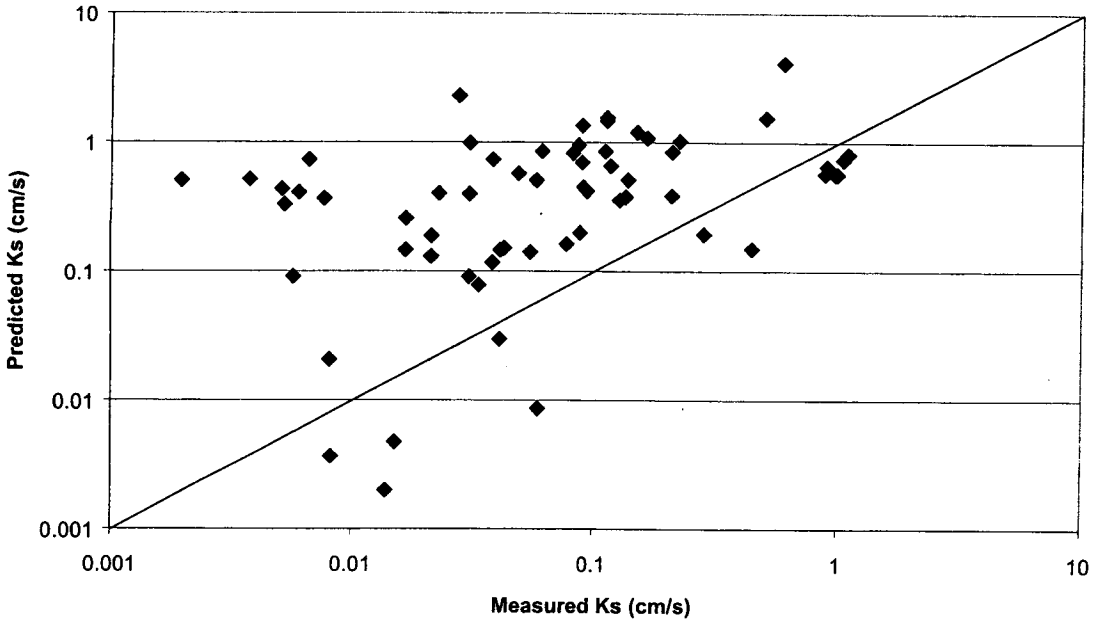

Figure 3.6—Regression equation A.8 derived from synthetic soil and applied to natural soil parameters.

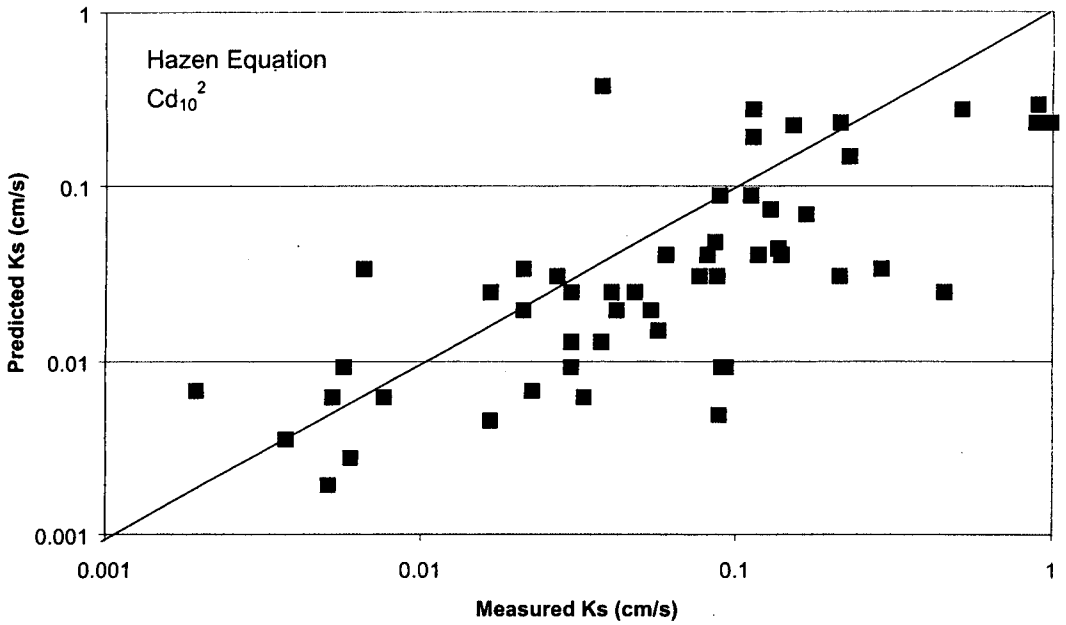

Figure 3.7—A comparison of measured hydraulic conductivity of natural soils with predictions made with the Hazen equation (regression equation B.1).

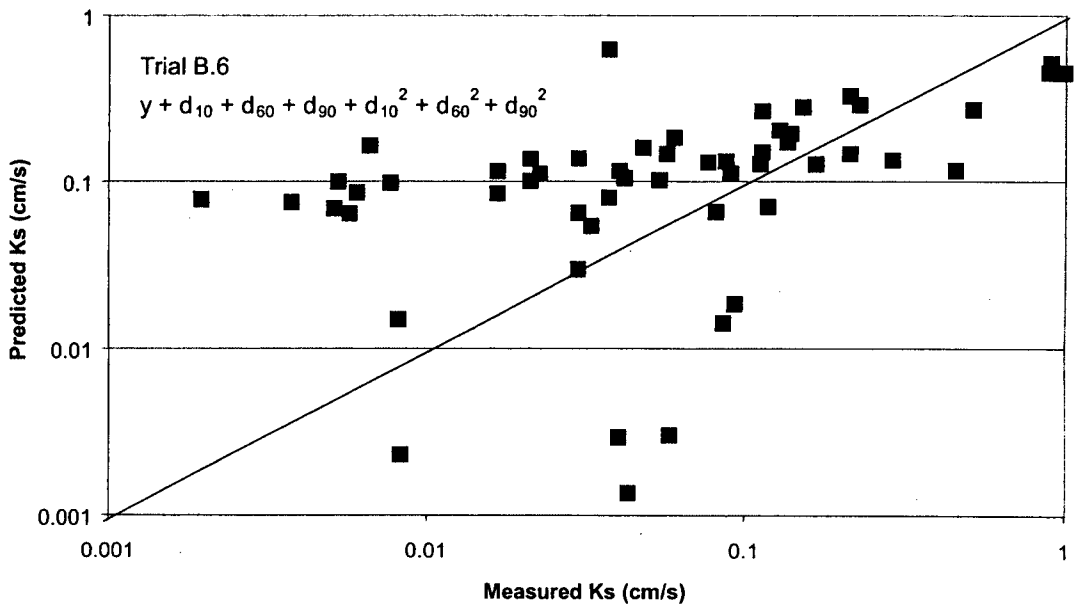

Figure 3.8—A comparison of measured hydraulic conductivity of natural soils with predictions made with regression equation B.6.

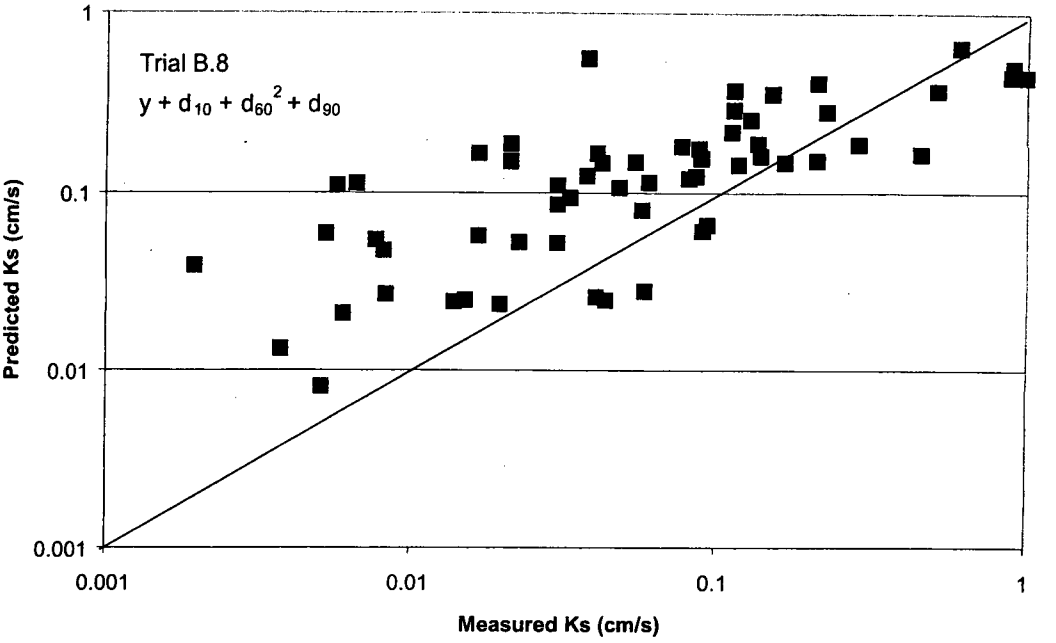

Figure 3.9—A comparison of measured hydraulic conductivity of natural soils with predictions made with regression equation B.8.

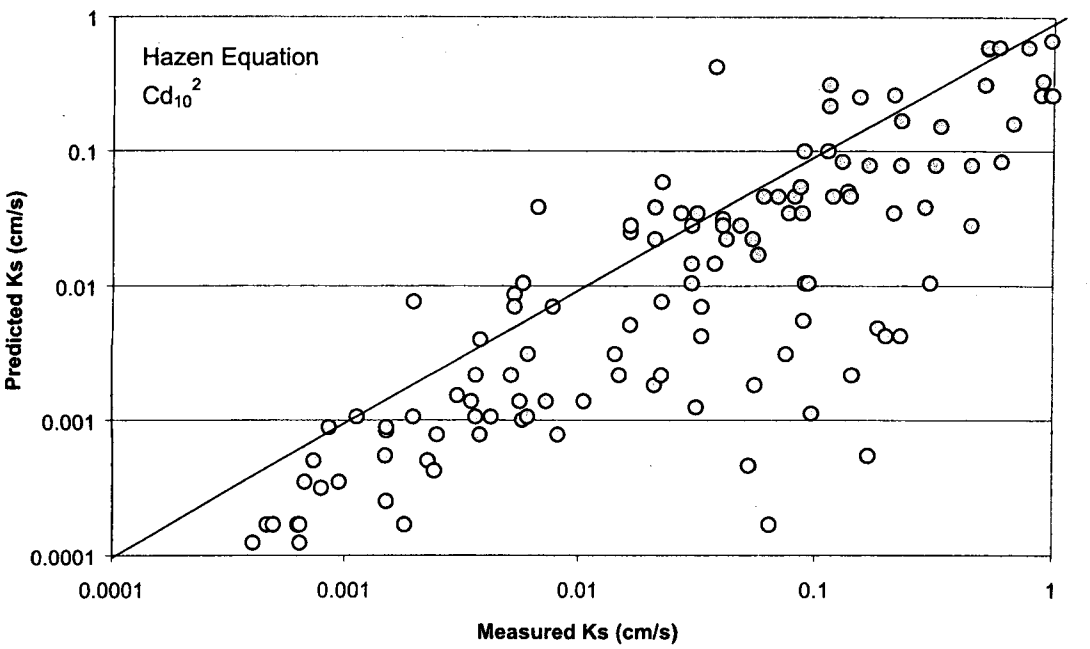

Figure 3.10—A comparison of measured hydraulic conductivity of natural soils and synthetic soils with predictions made with the Hazen equation (regression equation C.1).

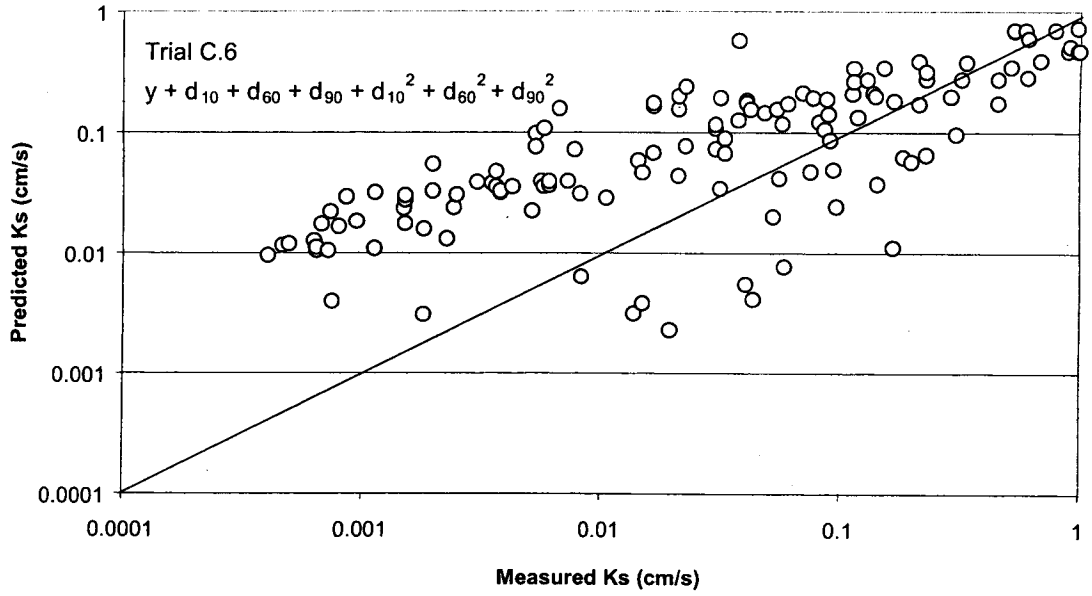

Figure 3.11—A comparison of measured hydraulic conductivity of natural soils and synthetic soils with predictions made with regression equation C.6.

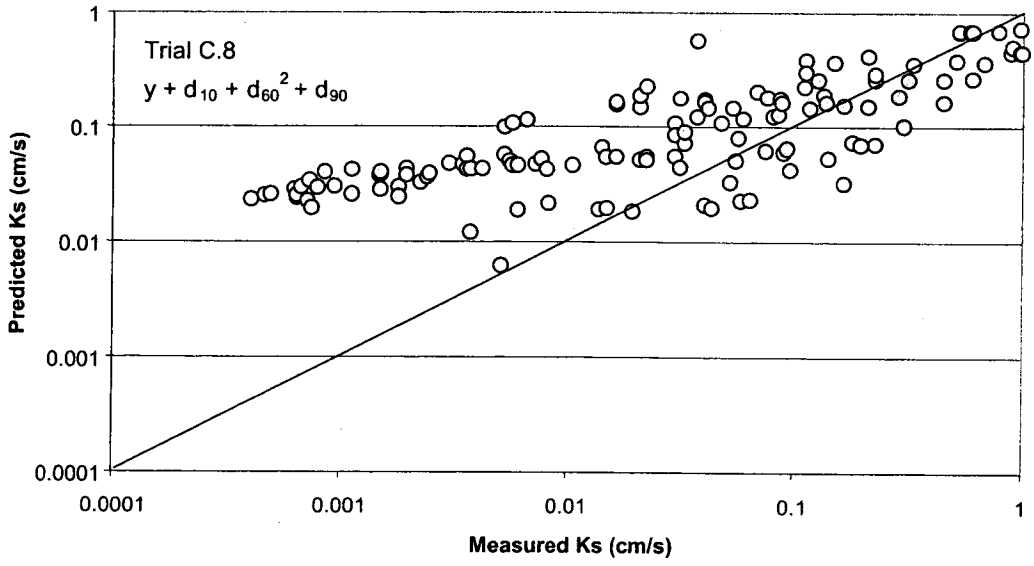

Figure 3.12—A comparison of measured hydraulic conductivity of natural soils and synthetic soils with predictions made with regression equation C.8.

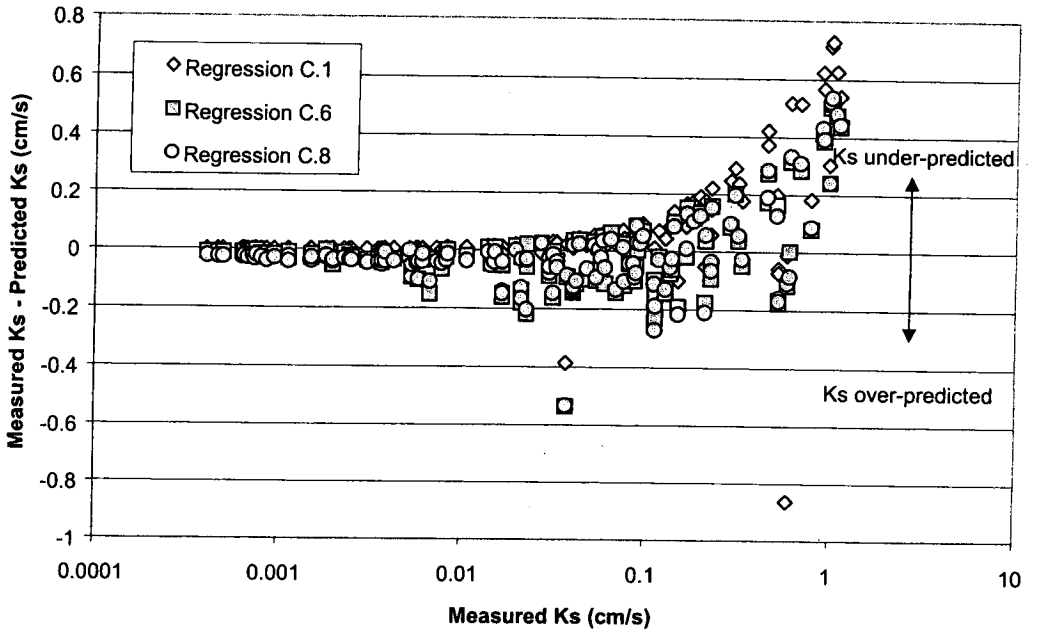

Figure 3.13—Comparison of regressions for natural and synthetic soils.

4 FULL-SCALE INFILTRATION TESTS

This chapter describes the results of full-scale tests that were conducted in this study to estimate infiltration rates for four infiltration facilities in western Washington. The methods used to conduct these tests are described in Section 4.1, and the approach used to analyze the data is described in Section 4.2. The sites that were used for the full-scale test are described in Section 4.3, and the results of the tests are presented in Section 4.4. Some of the implications of the data are discussed in Section 4.5

In comparison to other field and laboratory methods, full-scale tests provide the most reliable estimates of how infiltration ponds will perform. These tests, which are often termed "flood tests," are conducted by discharging water into a pond and measuring the change in water level in the pond as a function of time. Data are collected both during the filling stage of the test and during the draining stage after the discharge into the pond has been stopped. The primary advantage of these full-scale tests is that the infiltration rate is measured directly. The approach does not require modeling or significant analytical tools to estimate or infer infiltration rate from some other measured parameter. Sampling errors that can be introduced with small-scale measurements in heterogeneous soils are avoided. The primary disadvantage is that these tests require a source of water that can be delivered at a high enough flow rate to cause ponding within the facility.

4.1 Field Methods for the Full-Scale Tests

Figure 4.1 illustrates a typical configuration for the full-scale flood tests that were completed as part of the current study. A pressure transducer was used to measure the

water level in the pond as a function of time. During the filling stage of the test, which typically lasted several hours, water was discharged into the pond and the depth of water increased. The draining stage of the test started when the discharge was terminated. The water level in the pond decreased with time during this draining stage as the water infiltrated through the bottom and sides of the pond. The draining stage lasted from 12 hours to several days, depending upon the rate of infiltration.

The pressure transducer, model 15 PSI PS9800 from Instrumentation Northwest, Inc., has an accuracy of 0.1 percent. For a water level in a pond of 24 inches, the degree of accuracy is ± 0.18 inches. The transducer, supported by a steel post that is driven into the pond bottom, measures the height of water above the bottom of the transducer. The transducer is connected to an automatic data acquisition system that collects measurements at pre-determined time intervals. For this study the time interval was 10 minutes.

The water used to fill the ponds was obtained by connecting a 2.5-inch diameter hose to a fire hydrant. The flow rate, which was controlled with a valve at the hydrant, was measured with a water meter provided by the local water utilities. These meters measure to the nearest 10 cubic feet.

Surveying measurements were taken to calculate the pond geometry. A level and tripod were used to measure elevation along the pond bottom and side slopes. Elevation measurements were collected along transects with a horizontal spacing between measurements of approximately 4 to 6 feet, depending on the site. The length and width of the pond bottom were measured with a steel tape measurer. The side slopes (change in

elevation divided by change in horizontal distance) ranged from 0.3 to 0.7 for the three sites.

4.2 Data Analysis for the Full-Scale Tests

The rate of infiltration was estimated from full-scale test data by performing a water balance on the infiltration pond. The following expression gives the volume of water that infiltrates during time interval Δt:

$$V_{\inf} = Q_{in}(\Delta t) - A_{surf}(\Delta z) \qquad (4.1)$$

where V_{inf} is the volume of water that infiltrates during the time interval (L^3), Q_{in} is the flow rate into the pond (L^3/t), A_{surf} is the area of the pond surface (L^2), and Δz is the change in water depth during the time interval (L). The sign convention that is used in equation 4.1 is that a positive Δz denotes an increase in the depth of the water in the pond.

Except for ponds with rectangular cross-sections, the area of the water surface, A_{surf}, will be a function of the depth of the water in the pond, Δz. The surface area for rectangular ponds can be calculated by using the following expression:

$$A_{surf} = (L * W) + \frac{2\Delta z}{s}(L + W) + \frac{4\Delta z^2}{s^2} \qquad (4.2)$$

where L and W are the length and width of the pond bottom and s is the side slope of the pond. The slope is defined as the change in elevation divided by change in horizontal distance.

The infiltration rate is generally defined as the volume of water that infiltrates per unit time per unit area of the wetted pond bottom:

$$I = \frac{V_{\inf}}{A_{wet}\Delta t} \qquad (4.3)$$

where I = infiltration rate (L/t) and A_{wet} is wetted area of the pond bottom (L^2).

Equations 4.1 and 4.3 can be combined to give the following expression for infiltration rate:

$$I = \frac{V_{\inf}}{A_{wet}\Delta t} = \frac{Q_{in}}{A_{wet}} - \frac{A_{surf}\Delta z}{A_{wet}\Delta t} \qquad (4.4)$$

During the early portion of the test when the pond is being filled, the flow rate into the pond (Q_{in}) and the change in depth (Δz) are both positive values. During the later stage of the test the flow rate is 0.0 and the change in depth is a negative number. In both stages the infiltration rate is a positive value.

Except for ponds with vertical sides, the wetted area of the pond bottom will depend upon the depth of water in the pond. The wetted area (A_{wet}) for a rectangular pond is given by the following expression:

$$A_{wet} = L*W + \left(2L + 2W + \frac{4\Delta z}{s}\right)\sqrt{\Delta z^2 + \frac{\Delta z^2}{s^2}} \qquad (4.5)$$

4.3 Description of Sites Used for the Full-Scale Tests

Full-scale flood tests were conducted at four infiltration facilities in western Washington. One facility was located in Clark County, one facility was in King County, and two facilities were located in Kitsap County. The particular locations were chosen on the basis of the size of the ponds, the expected infiltration rate, and the willingness of the storm water managers in these counties to cooperate in the study. Small- to medium-

sized ponds, in the range of 2,000 to 10,000 ft^3, were chosen to reduce the amount of water that would be required for the flood tests. Ponds with anticipated infiltration rates in the range of 0.1 to 10 inches per hour were chosen because these represent "typical" sites. Sites with infiltration rates significantly less than this are generally undesirable because of the size of the pond that would be required to infiltrate water from a typical design storm. Sites with infiltration rates significantly larger than this are undesirable because of water quality considerations (WDOE, 2001).

Site specific data, soil, design infiltration rate, and pond descriptions are found in Appendix D.

4.3.1 Clark County Pond

In November 2000 a flood test was performed at a storm-water infiltration pond in Clark County. The pond, which is shown in Figure 4.2, is located in a residential area in the northern part of Vancouver. The pond is enclosed with a chain-link fence. No information was available regarding the age of the pond or area of the basin that drains into the pond.

The pond bottom is rectangular with dimensions of 75 feet by 25 feet. The side slopes were surveyed to be 0.3 (V:H) and the depth of the pond is approximately 6 feet. A 3-foot-high retaining wall constructed with concrete blocks is located on the north side of the infiltration pond. The retaining wall is permeable because of open spaces between the concrete blocks. The water flows into the infiltration pond from a pre-treatment area located on the grassy plateau above the retaining wall. Stormwater discharges to the pretreatment area from two pipes located at opposite ends of the grassy plateau.

The pond bottom and side slopes are covered with patches of moss and grass. Two trees are located in opposite diagonal corners of the pond. The side slopes of the pond are covered in patches of grass.

4.3.2 Balsam 7-11 Pond, Kitsap County

In September 2000 a flood test was performed at the Balsam 7-11 stormwater infiltration pond in Kitsap County. The infiltration pond (Figure 4.3) is located in east central Kitsap County, south of Sinclair Inlet. The site is located at the eastern end of a convenience store parking lot adjacent to a major thoroughfare. The estimated area of the basin that drains into the pond is 7 acres (Wiltsie, 1998). Stormwater that discharges into the pond comes from both residential and commercial developments. The water outlet pipe is located on the south end. Litter (such as wrappers, old shoes, and other articles of clothing) was found in the bottom of the pond. A chain-link fence encloses the pond.

The pond was designed in 1977. The pond bottom is rectangular, 7 feet wide by 53 feet long. The side slopes were surveyed to be 0.7, and the depth of the pond is approximately 7 feet. There is no pre-treatment for the stormwater that discharges into the pond. The pond bottom and side slopes are dense with wetland plants. Sediment build-up has been removed from Balsam 7-11 within the last three years (Anderson, J., 2001).

4.3.3 Krista Firs Pond, Kitsap County

In October 2000 a flood test was performed at Krista Firs storm water infiltration pond in Kitsap County. This pond, which is shown in Figure 4.4, is located in a residential area less than 3 miles southwest of the Balsam 7-11 facility. The basin area

draining into the pond is approximately 10.6 acres (Wiltsie, 1998). A chain-link fence encloses the pond.

The pond was designed in 1978. The pond bottom is rectangular with dimensions of 26 feet by 39 feet. The pond side slopes were estimated to be 0.4, and the depth of the pond is approximately 6 feet. The water inlet is located in the northwest corner of the pond. There is no pre-treatment for the stormwater that discharges into the pond.

The pond bottom has dense patches of moss and grass. Shrubs and large gravel (ranging from 10 to 100 mm in size) are scattered throughout the bottom of the pond. The side slopes have patches of dry grass and moss. This pattern indicates moist conditions in the pond bottom, but not for the side slopes.

4.3.4 Cimarron Pond, King County

A flood test was performed at the Cimarron storm water infiltration pond in King County in April 2001. This pond, which is shown in Figure 4.5, is located in a residential area on the Sammamish Plateau in eastern King County and was constructed in 1981. The basin area draining into the pond is approximately 14.6 acres. The pond bottom is roughly triangular in shape with side dimensions of approximately 42 feet by 85 feet by 110 ft. The pond side slopes were estimated to be 0.6, and the depth of the pond is approximately 5. A breached swale was included in the design for pre-treatment of the stormwater. The top 6 inches of the pond were filled with well-graded, clean sand and ¾-in. to 2-in. washed gravel placed beneath the sand. The average infiltration rate used for the design was 13.3 in/hr. The photograph included in Figure 4.5, which shows the pond essentially full of water, was taken in January of 2002 after several months of high precipitation. The pre-treatment swale was fully submerged, and an over-flow discharge

pipe was partially submerged at this time. This overflow pipe discharges into a nearby wetlands, which suggests a relatively high water table.

Falling head test infiltrometer tests were conducted at the Cimarron pond in an earlier study (Foley, 2000). The measured infiltration rates from these tests was 2.7 inches/hour. At the time of this earlier study, the soils from the bottom of the pond were found to have a high percentage of fines (12 to 20 percent).

4.4 Estimates of Infiltration Rates Based on the Full-Scale Tests

4.4.1 Clark County Pond

The basic data that were used to estimate infiltration rates at the Clark County site are shown in Table 4.1 and in Figure 4.6. Table 4.1 lists the flow rates, the duration of the test, and the pond geometry. Figure 4.6 shows the depth of water as a function of time, measured at 10-minute intervals. The flow rate into the pond during the filling portion of the test was approximately 2000 ft^3/hr (250 gpm), and the filling stage lasted for approximately 2.5 hours. The water level in the pond reached a depth of approximately 21 inches during the filling portion of the test.

The draining phase, which lasted just under 70 hours, can be divided into two parts. During the first part, which lasted until hour 30, the change in water level followed an exponentially shaped curve that became flatter with time. Between hour 30 and the end of the test, the water level followed a linearly shaped curve with a slope that was essentially constant.

The water level data shown in Figure 4.6 can be used to estimate the infiltration rate as a function of time with Equation 4.4. Figure 4.7 shows the infiltration rate averaged over each 30-minute period. The infiltration rate increased with time during the

filling portion of the test and reached a maximum rate of approximately 2.0 in/hr. After the discharge to the pond was stopped, the infiltration rate quickly decreased to approximately 0.25 in/hr. This rate remained roughly constant for the duration of the test.

The total volume of water that was discharged to the infiltration pond during the full-scale test at the Clark County site was approximately 4710 ft^3. All of this water eventually infiltrated into the ground. Figure 4.8 shows the fraction of the total inflow that had infiltrated from the pond as a function of time. The total inflow is estimated by summing the infiltration rates shown in Figure 4.7 over the duration of the test. This total inflow is given in the last column of Table 4.1. Note that the total inflow that was calculated on the basis of estimated infiltration rates (Column "I" in Table 4.1) is different from the total inflow that was calculated on the basis of discharge to the pond (Column "D" in Table 4.1). These differences are due to uncertainties in pond surface area and wetted pond bottom in Equation 4.4.

The fraction of the total inflow that had infiltrated at each time was calculated by summing the infiltration rates for all earlier times and then dividing this sum by the total inflow. For the Clark County site, approximately 20 percent of the total inflow occurred during the filling stage of the test.

The estimated infiltration rate was nearly constant after approximately 30 hours, as shown in Figure 4.7. A constant infiltration rate suggests that the hydraulic gradient that causes flow is also approximately constant during this period. Given that the water level in the pond decreased from approximately 10 inches at 30 hours to less than 1 inch

at 70 hours, it appears that the water level or water pressure in the pond was not a primary component of the forces causing infiltration.

The rapid increase in infiltration during the filling portion of the test may have been caused in part by lateral flow along the sides of the ponds. This is similar to "bank storage" that occurs in stream channels. As the water level in the pond increases, flow is induced horizontally into the banks of the pond. This infiltration is in addition to the infiltration that occurs along the pond bottom. Once the water level in the pond begins to decrease, the horizontal flow is reversed and water drains into the pond along the sides and out of the pond along the bottom. This inflow, which reduces the net infiltration rate, decreases with time.

Figure 4.9 compares infiltration rates as a function of water level for the rising and falling limbs of the hydrograph. The graph shows that infiltration rates during the rising limb were significantly larger than the infiltration rates during the falling limb. In general, this is expected because the head gradient is largest for initially dry soils. However, these differences in infiltration rates could also be explained by lateral flow.

When the pond is filling up, flow in both the horizontal and vertical direction allows for more water storage in the sub-surface and thus a higher infiltration rate. When the water level in the pond decreases, the flow from the sides of the pond reverses direction.

The data shown in Figure 4.9 can be used to estimate the relative magnitude of the horizontal and vertical flows. As an example, when the depth of water in the pond is18 inches, the infiltration rate during the rising limb is approximately 1.7 in/hr while the infiltration rate during the falling limb is approximately 0.8 in/hr. During the filling

phase, the horizontal and vertical flows are both away from the pond, as shown in Figure 4.10a. Equation (4.6) describes vertical and horizontal flow from the pond during the filling phase:

$$V + H \cong 1.7 \text{ in/hr.} \tag{4.6}$$

where V is vertical flow (L/t) and H is horizontal flow (L/t).

During the draining phase, the horizontal flow is into the pond, and the vertical flow is away from the pond, as shown in Figure 4.10b. Equation (4.7) describes vertical and horizontal flow from the pond during the draining phase:

$$V - H \cong 0.8 \text{ in/hr.} \tag{4.7}$$

Equations 4.6 and 4.7 can be solved simultaneously V and H are assumed to be the same in both equations. This resulted in a horizontal flow of 0.45 in/hr and a vertical flow of 1.25 in/hr. At the water depth of 18 inches, the horizontal flow accounted for roughly 36 percent of the total infiltrating water. When the water level stopped rising, the water infiltrating vertically had the addition of the total horizontal flow volume of water that was coming back into the pond. This may explain why the net infiltration rate quickly dropped as soon as the inflow from the hydrant was shut off.

4.4.2 Balsam 7-11 Pond, Kitsap County

The basic data that were used to estimate infiltration rates at the Balsam site are shown in Table 4.1 and Figure 4.11. The flow rate into the pond during the filling stage was approximately 1000 ft^3/hr (125 gpm). The pond was filled for approximately 2 hours, and the water reached a maximum depth of approximately 31 inches. The total volume of water discharged into the pond was 2290 ft^3. Similar to the pond in Clark

County, the drainage phase can be divided into two parts. During the first part of the draining phase, the water level decreased exponentially. This occurred between hour 2 and hour 6. Between hour 6 and the end of the test, the water level declined linearly.

Figure 4.12 shows the infiltration rate averaged over 30-minute periods. The maximum infiltration rate was approximately 12 in/hr and occurred at the end of the filling phase. The infiltration rate fell to approximately 2 in/hr during the later part of the test.

The linear part of Figure 4.11 demonstrates that the infiltration rate was roughly constant after approximately 6 or 7 hours. This infers a constant gradient during the second stage of the drainage phase. The water level in the pond decreased by approximately 15 inches during the last 6 hours of the drainage stage when the infiltration rate had reached a relatively steady state. This supports the idea that the water level in the pond may have been a significant driving force for infiltration.

Figure 4.13 shows the fraction of the total inflow that had infiltrated from the pond as a function of time. Approximately 30 percent of the total inflow occurred during the filling stage of the test. Figure 4.14 compares calculated infiltration rates as a function of water level for the rising and falling limbs of the hydrograph. These calculations show that infiltration rates increased rapidly after the water level in the pond reached a depth of approximately 30 inches.

4.4.3 Krista Firs Pond, Kitsap County

The basic data that were used to estimate infiltration rates at the Krista Firs pond are shown in Table 4.1 and in Figure 4.15. The information in Table 4.1 describes the flow rates, the duration of the test, and the pond geometry. Figure 4.15 shows the depth

of water as a function of time. These depths were measured at 10-minute intervals. The flow rate into the pond was approximately 1850 ft^3/hr (230 gpm). The pond was filled for approximately 2 hours, and the water reached a maximum depth of approximately 26 inches. The total volume of water discharged into the pond was approximately 4190 ft^3.

The draining phase of the test, which lasted for approximately 70 hours, can be divided into two parts. During the first part, from hour 3 to hour 30, the water level decreased exponentially. The water level declined linearly for the next 40 hours. However, there were two jumps in the curve: one after approximately 30 hours and one after approximately 55 hours. These times correspond to October 29 and October 30, 2000. There was very little precipitation on October 29th (0.05 inches) and no precipitation on October 30th (National Oceanic and Atmospheric Administration, 2000). However, 0.30 inches and 0.13 inches of precipitation fell on October 27th and 28th, respectively. The jumps could be explained by this precipitation if the response time between precipitation and water levels was on the order of 2 days, but such a long response time is improbable.

Figure 4.16 shows the infiltration rate averaged over a 30-minute period. The maximum infiltration rate reached was approximately 13 in/hr and occurred at the end of the filling phase. The infiltration rate dropped to a relatively steady rate of approximately 0.2 in/hr after approximately 30 hours.

The estimated infiltration rate was nearly constant after approximately 20 hours, as shown in Figure 4.16. As was discussed for the Clark County test, a constant infiltration rate suggests that the hydraulic gradient that causes flow is also approximately constant during this period. Given that the water level in the pond was decreasing from

approximately 15 inches at 20 hours to approximately 5 inches hour 70 hour, it appears that the water level or water pressure in the pond was not a primary component of the forces causing infiltration.

Figure 4.17 shows the fraction of the total inflow that had infiltrated from the pond as a function of time. Approximately 20 percent of the total inflow occurred during the filling stage of the test. Figure 4.18 compares calculated infiltration rates as a function of water level for the rising and falling limbs of the hydrograph. These calculations show that infiltration rates increased rapidly after the water level in the pond reached a depth of approximately 26 inches. Figure 4.18 compares infiltration rates as a function of water level for the rising and falling limbs of the hydrograph. The graph shows that infiltration rates during the rising limb were significantly larger than the infiltration rates during the falling limb.

4.4.4 Cimarron Pond, King County

The basic data that were used to estimate infiltration rates at Cimarron pond are shown in Table 4.1 and in Figure 4.19. The information in Table 4.1 describes the flow rates, the duration of the test, and the pond geometry. Figure 4.19 shows the depth of water as a function of time. These depths were measured at 5-minute intervals. The flow rate into the pond was approximately 1220 ft^3/hr (150 gpm). The pond was filled for approximately 1.7 hours, and the water reached a maximum depth of approximately 13 inches. The total volume of water discharged into the pond was approximately 2070 ft^3. The test at the Cimarron pond was completed by placing four pressure transducers at different locations on the pond bottom. These transducers were at slightly different

elevations, as shown in Figure 4.19. The average of these four transducers was used to calculate the depth of water in the pond and the infiltration rate.

Figure 4.20 shows the infiltration rate averaged over a 30-minute period. The maximum infiltration rate was approximately 1.9 in/hr and occurred at the end of the filling phase. The infiltration rate dropped to a relatively steady rate of approximately 0.1 in/hr after approximately 2 hours. The relatively high-frequency fluctuations may have been the result of precipitation events that occurred during the drainage period. Given these higher-frequency fluctuations, the estimated average infiltration rate was nearly constant after approximately 3 hours, as shown in Figure 4.20. Again, a constant infiltration rate suggests that the hydraulic gradient that causes flow is also approximately constant during this period. Figure 4.21 compares infiltration rates as a function of water level for the rising and falling limbs of the hydrograph. The graph shows that infiltration rates during the rising limb were significantly larger than the infiltration rates during the falling limb.

4.5 Implications of the Data

Lateral or horizontal flow may have occurred during the filling phases at all four ponds. This suggests that the ponds may have had a higher infiltration rate during the initial inflow of stormwater discharge. Once a maximum water level in the pond had been reached and the water level began to decline, the infiltration rate would decrease if the horizontal flow reversed and flowed back into the pond. The infiltration rates for the ponds eventually reached a nearly constant value. The early-time and long-term infiltration rates for the four ponds included in this study are summarized in Table 4.2.

If lateral flow is consistently important, more efficient designs may require a larger ratio of side area to bottom area. This design approach would necessitate maintenance for the sides as well as the bottom of the pond. If the soil on the sides and bottom are preserved with respect to vegetation and silt build-up, the horizontal as well as the vertical flow could be an effective means of infiltrating stormwater runoff into the subsurface.

Infiltration rates based on soil texture for the three sites are included in Table 4.2. These estimates are from the WDOE *Stormwater Management Manual for Western Washington: Volume III— Hydrologic Analysis and Flow Control Design/BMPs* (2001).

The soil texture infiltration rate of sand over-estimated the actual full-scale measured rate at Krista Firs and King County. The soil texture rate for Balsam 7-11 under-estimated the actual full-scale rate, and the soil texture rate for Clark County closely estimated the actual full-scale rate. This reinforces that grain size texture alone does not include site-specific characteristics that may affect infiltration rates.

Table 4.1—Summary of data for full-scale infiltration tests.

A. Site	B. Inflow Rate (ft^3/hr)	C. Inflow Duration (hours)	D. Total Inflow (ft^3)	E. Draining Duration (hours)	F. Max. Water Depth (inches)	G. Bottom Area (ft^2)	H. Side Slope	I. Total Infiltration (ft^3)
Clark	2060	2.5	4710	67.8	21.5	1860	0.3	4820
Balsam	1000	2.2	2290	12.4	31.2	370	0.7	2260
Krista	1840	2.3	4190	78.9	26.1	1030	0.4	3960
Cimarron	1220	1.7	2070	102.9	12.9	2040	0.6	1370

Table 4.2—Summary of calculated infiltration rates.

Site	**Final (long-term) infiltration rate (in/hr)**	**Maximum (short-term) infiltration rate (in/hr)**	**Soil Texture Description**	**Estimated long-term rate from soil texture (WDOE, 2001) (in/hr)**
Clark County	0.23	2.5	Loam/Silty Loam	0.13/0.25
Balsam 7-11	2.1	13.2	Silty Loam	0.25
Krista Firs	0.33	2.8	Sand	2
Cimarron	0.1	1.9	Silty sand loam	0.25

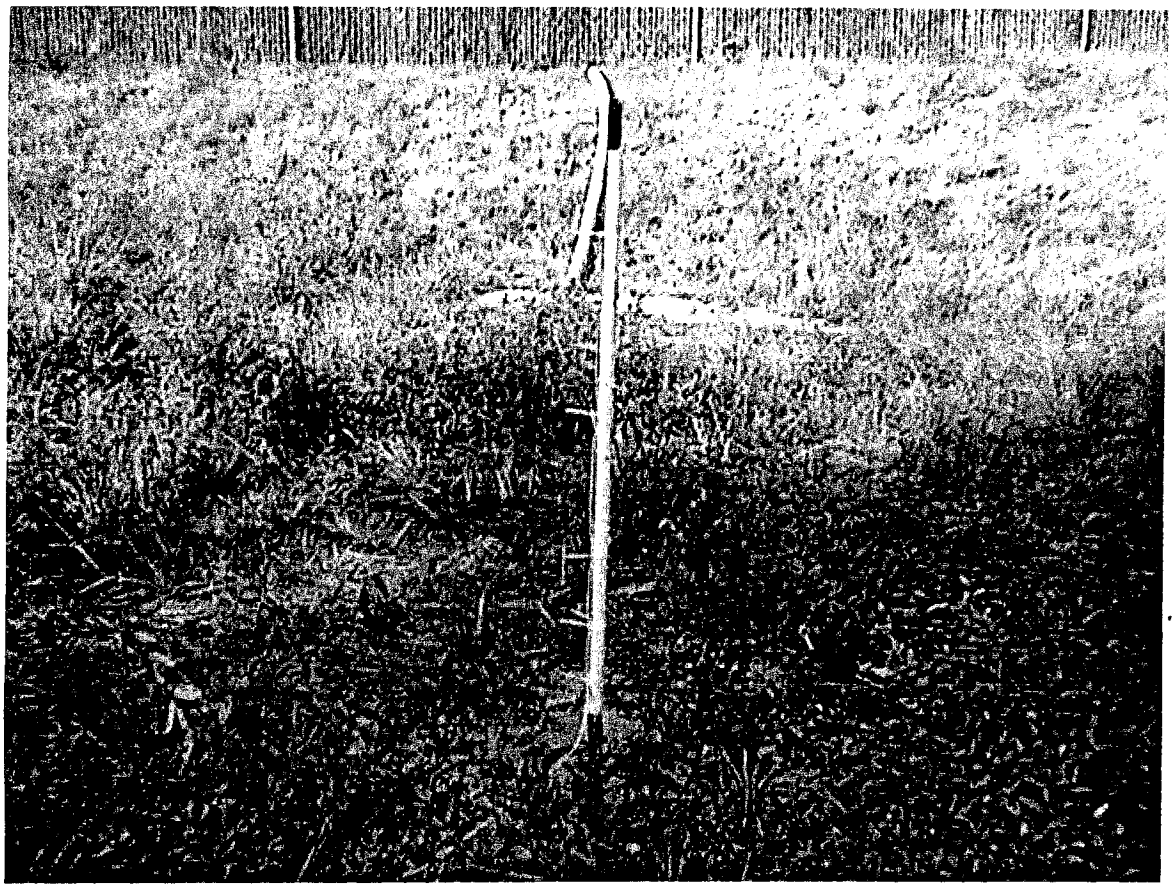

Figure 4.1—Pressure transducer installed at Krista Firs, Kitsap County.

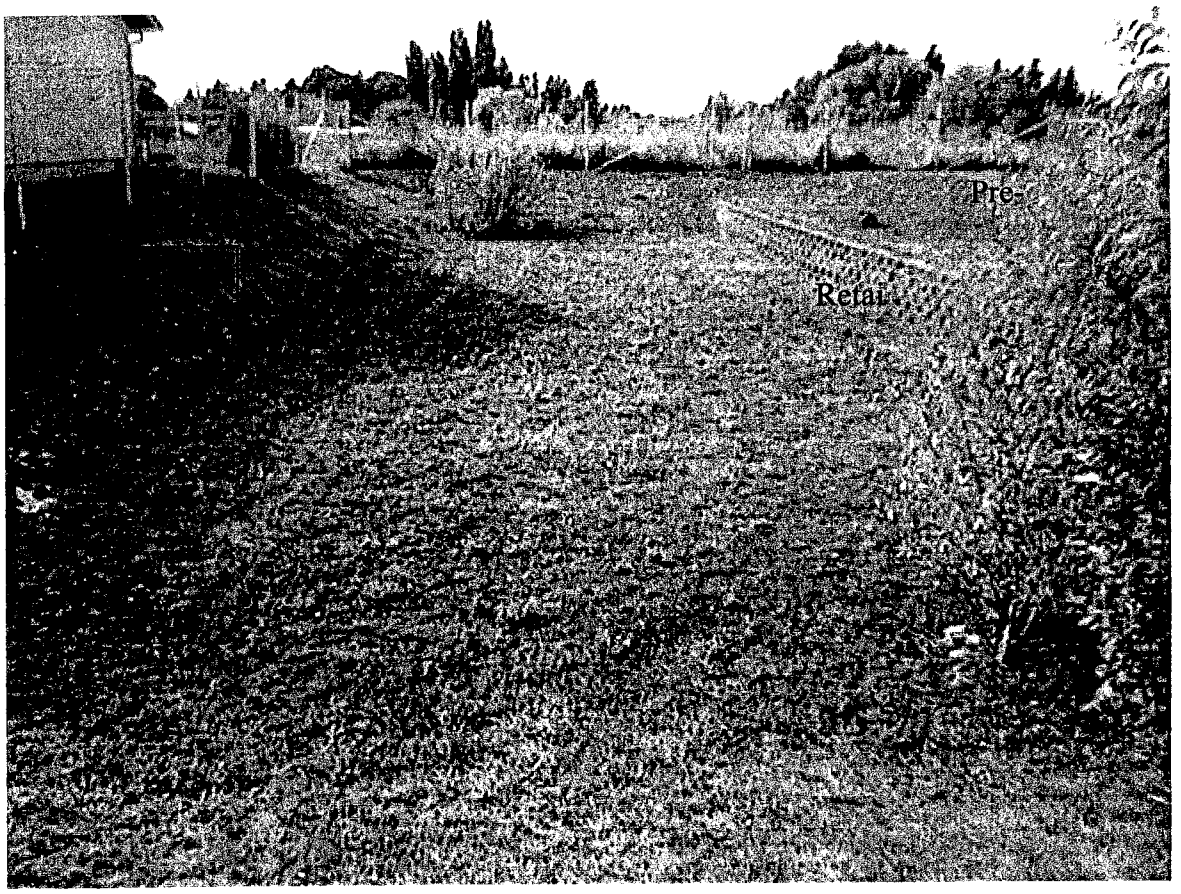

Figure 4.2—Clark County pond, Clark County, 9616 NE 59th Ave., Vancouver, Wash., 98686.

Figure 4.3—Balsam 7-11, Kitsap County, Lund Ave. SE and Jackson Ave., Port Orchard, Wash., 98366.

Figure 4.4—Krista Firs, Kitsap County, K.C. Place and Cedar Rd E., Port Orchard, Wash., 98366.

Figure 4.5—Cimarron, King County, N.E. 12th Place and 230th Avenue NE, Sammamish, Wash., 98074.

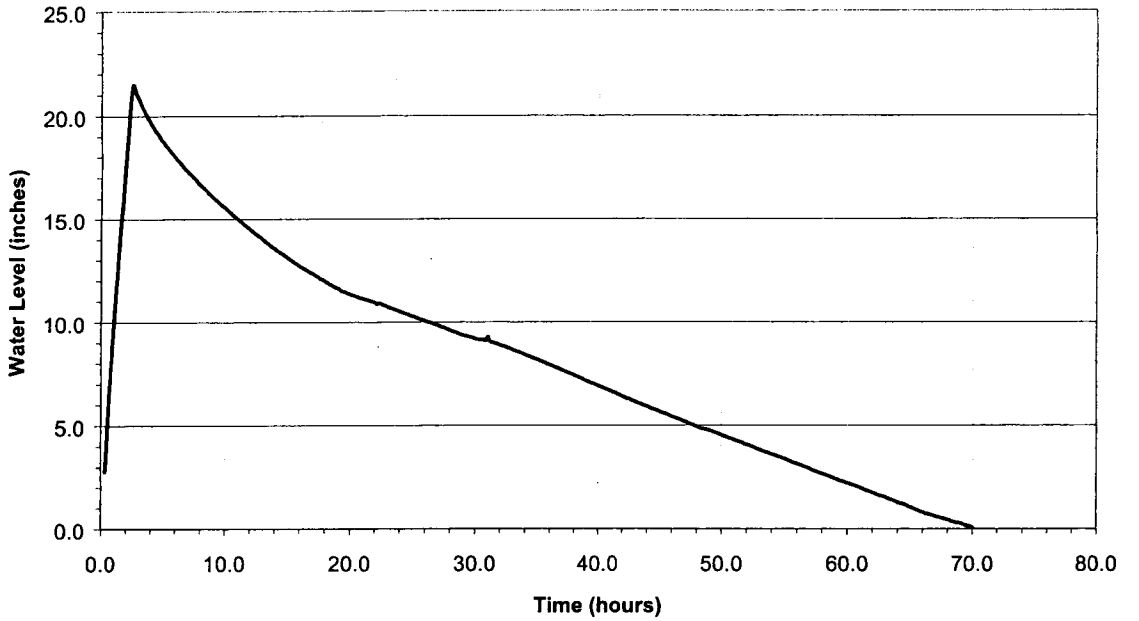

Figure 4.6—Water levels during the full-scale test at the Clark County pond.

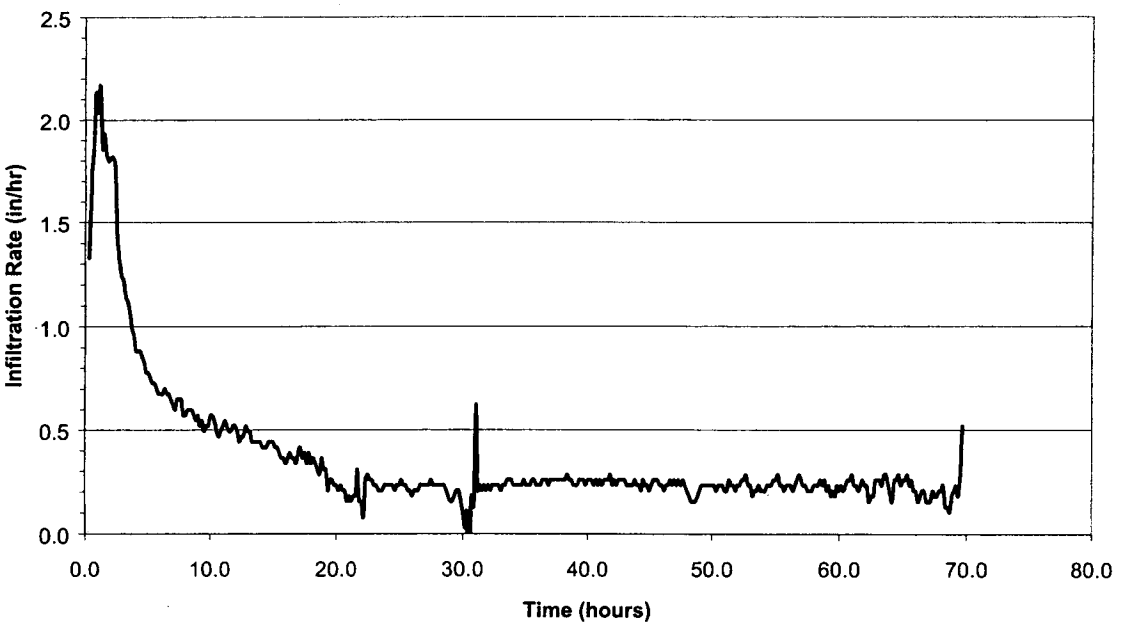

Figure 4.7—Infiltration rate for Clark County averaged over 30-minute intervals.

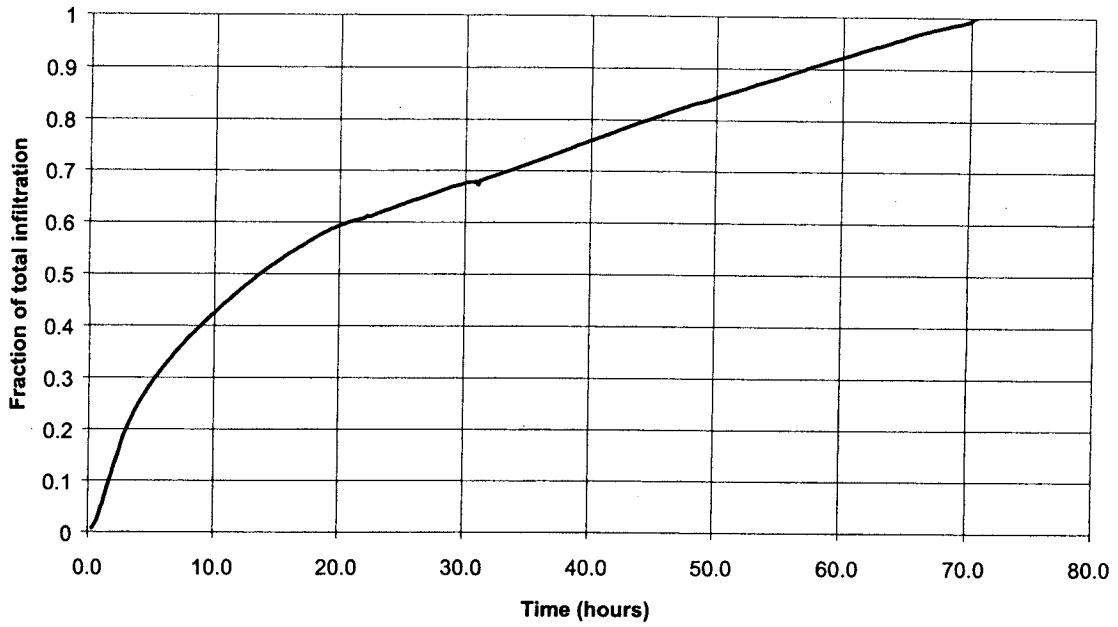

Figure 4.8—Fraction of total inflow that had infiltrated as a function of time at the Clark County pond.

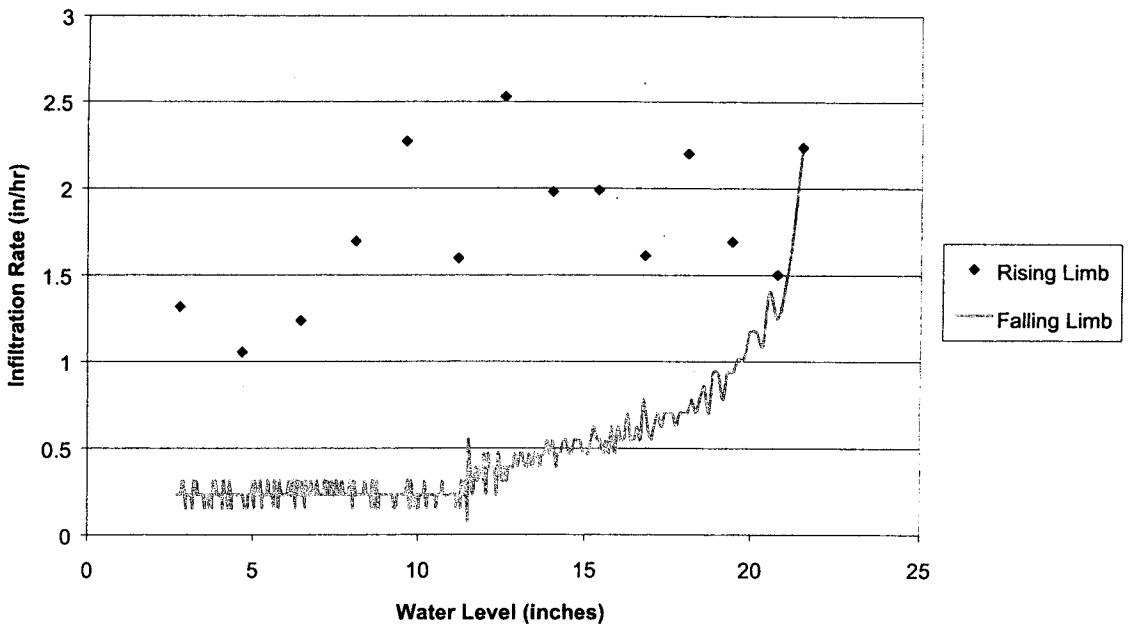

Figure 4.9—Infiltration rate versus water level for Clark County pond.

a) Filling - Equation (4.6) **b) Draining - Equation (4.7)**

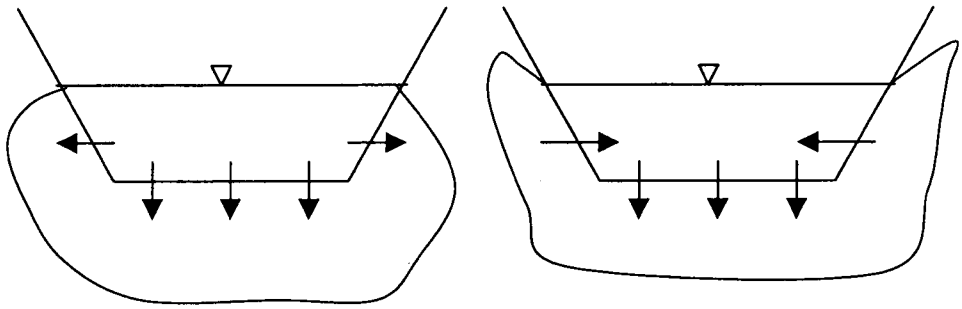

Figure 4.10—Horizontal and vertical infiltration during the filling and draining stages.

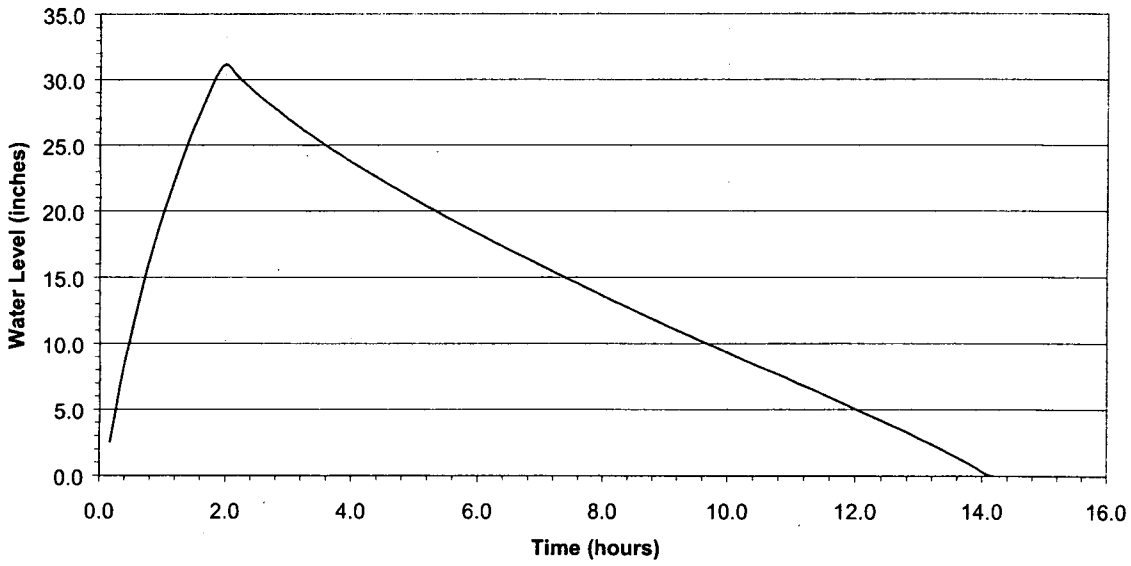

Figure 4.11—Water levels during the full-scale test at the Balsam 7-11 pond.

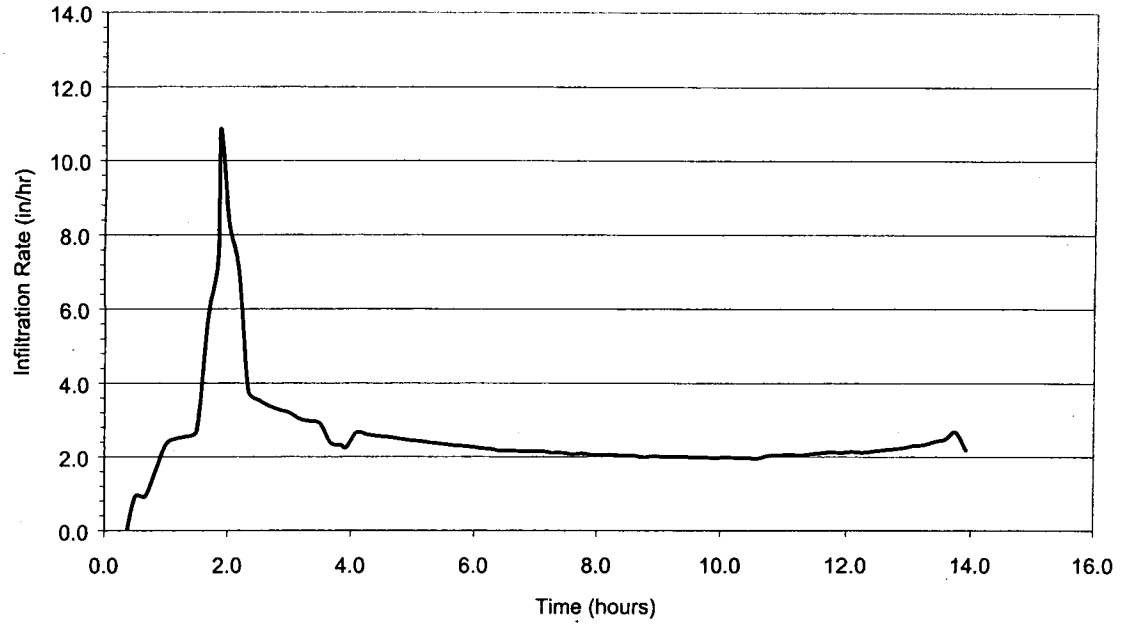

Figure 4.12—Infiltration rate for Balsam 7-11 averaged over 30-minute intervals.

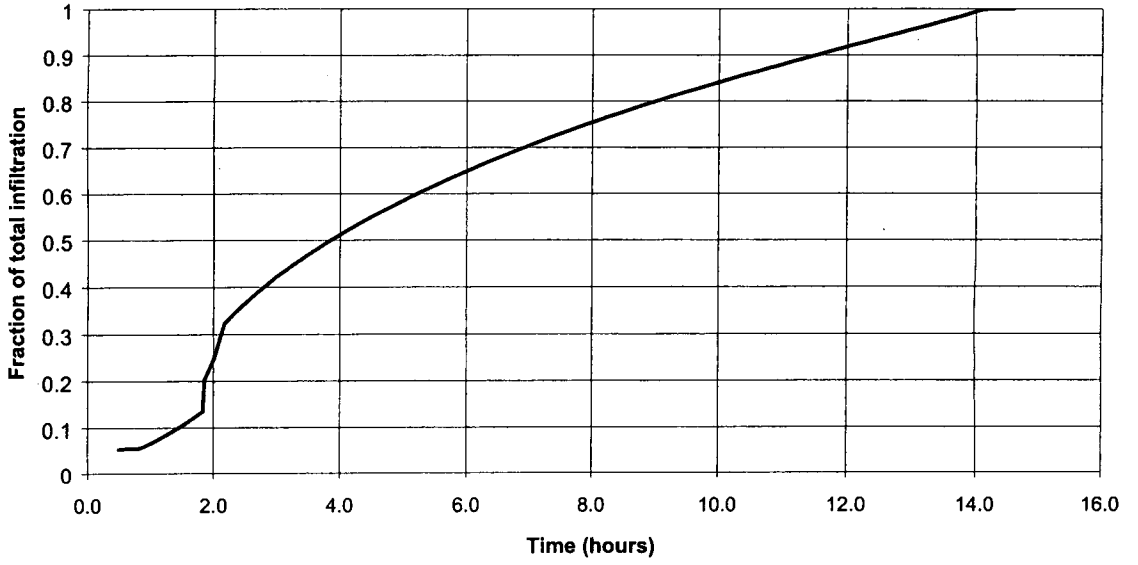

Figure 4.13—Fraction of the total flow that had infiltrated as a function of time at the Balsam 7-11 pond.

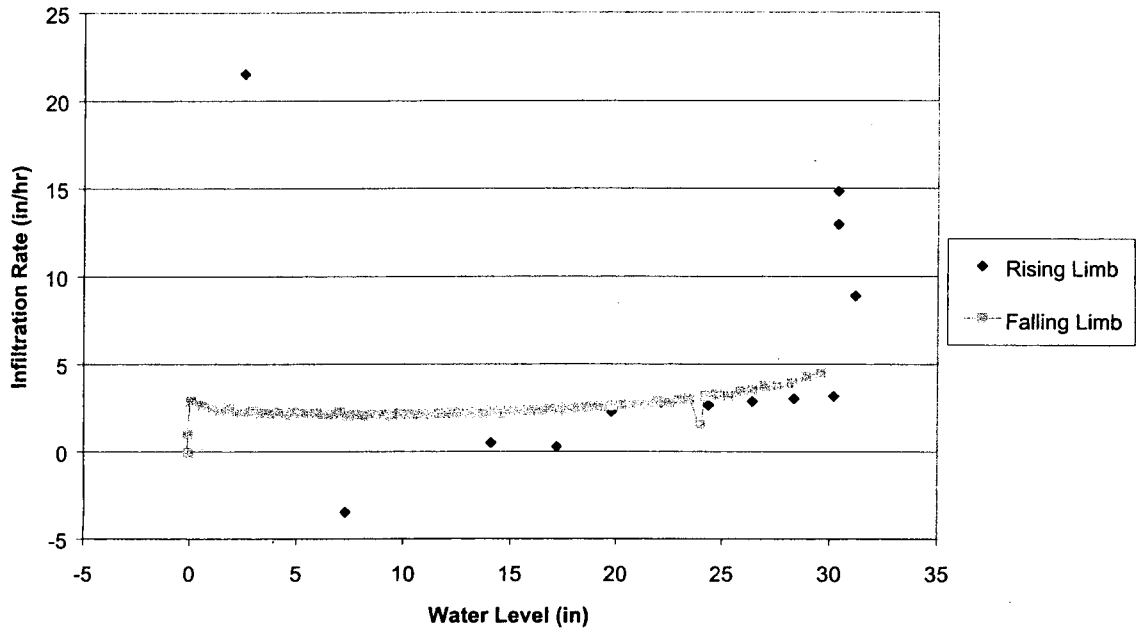

Figure 4.14—Infiltration rate versus water level for Balsam 7-11 pond.

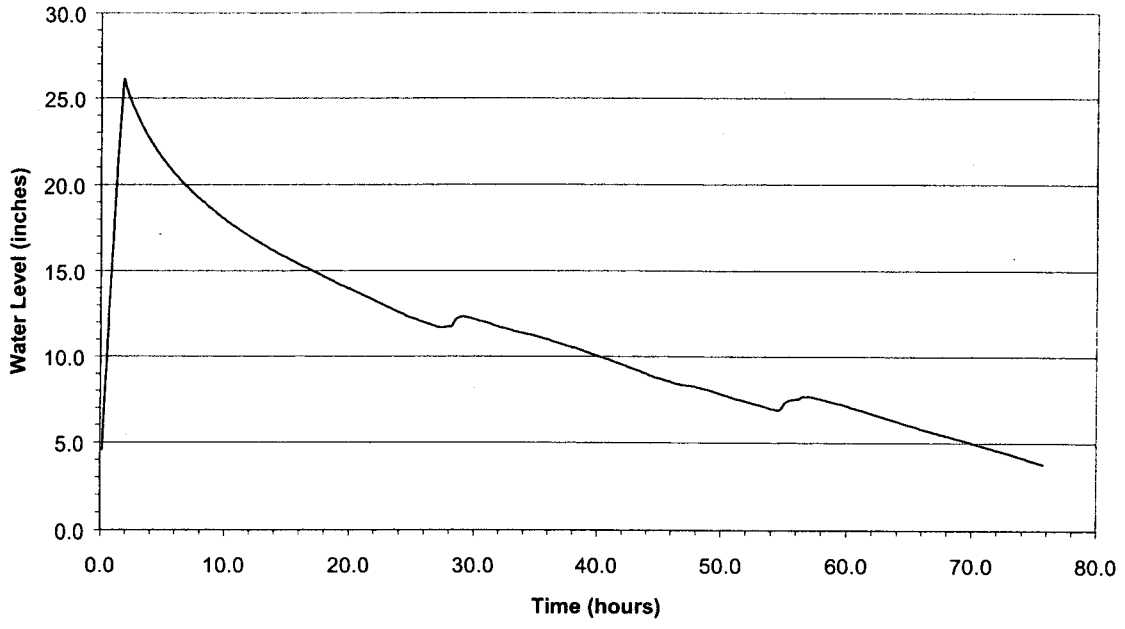

Figure 4.15—Water levels during the full-scale test at the Krista Firs pond.

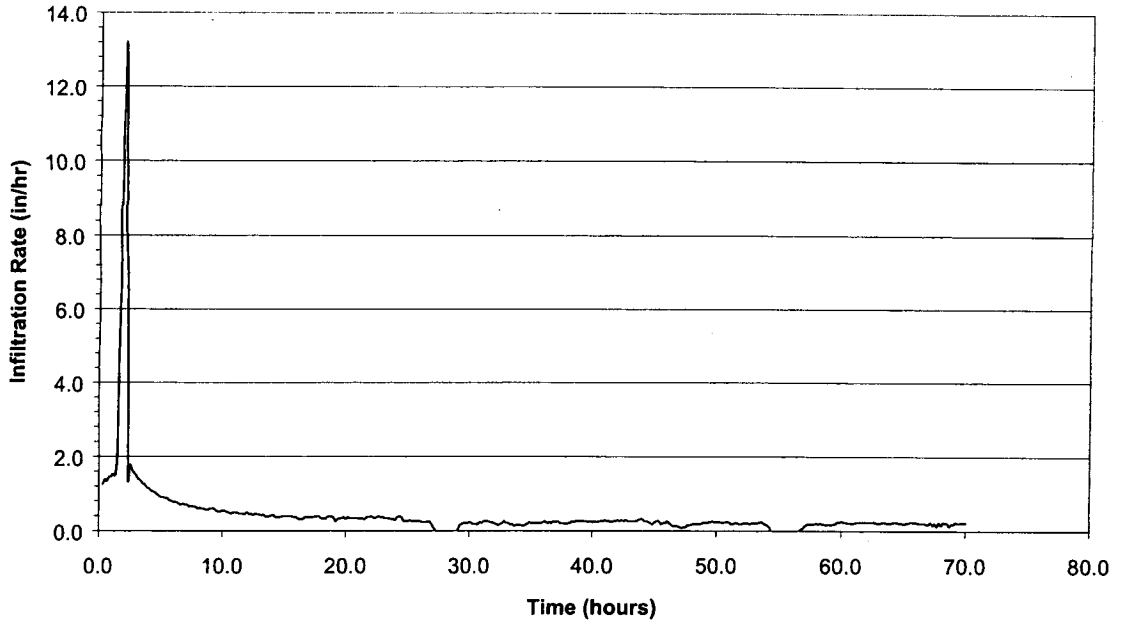

Figure 4.16—Infiltration rate for Krista Firs averaged over 30-minute intervals.

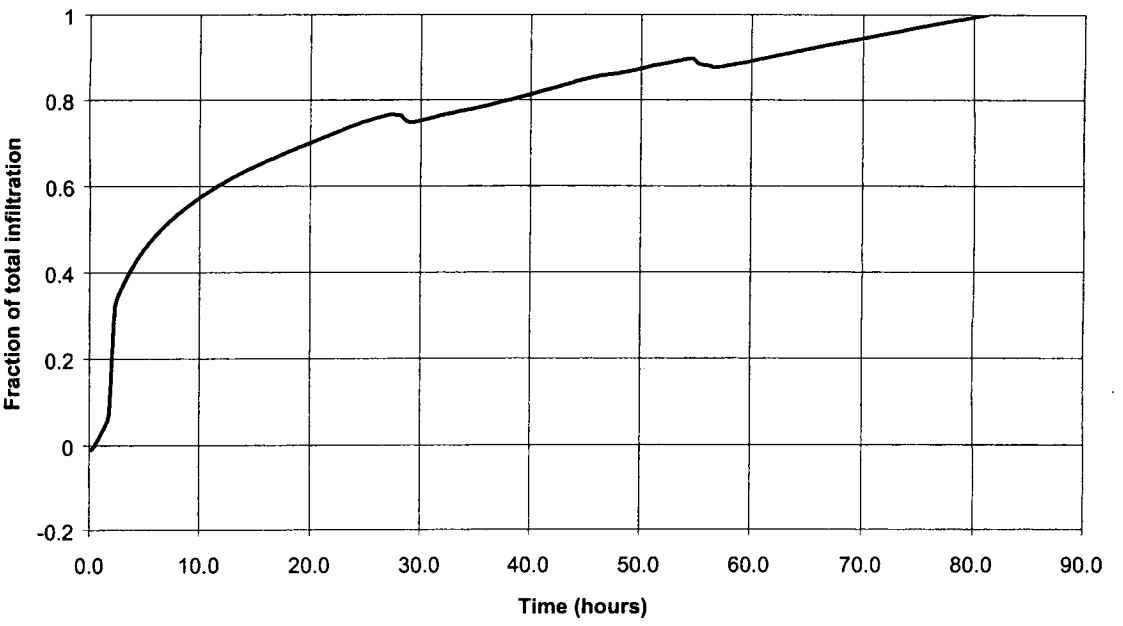

Figure 4.17—Fraction of total inflow that had infiltrated as a function of time at the Krista Firs pond.

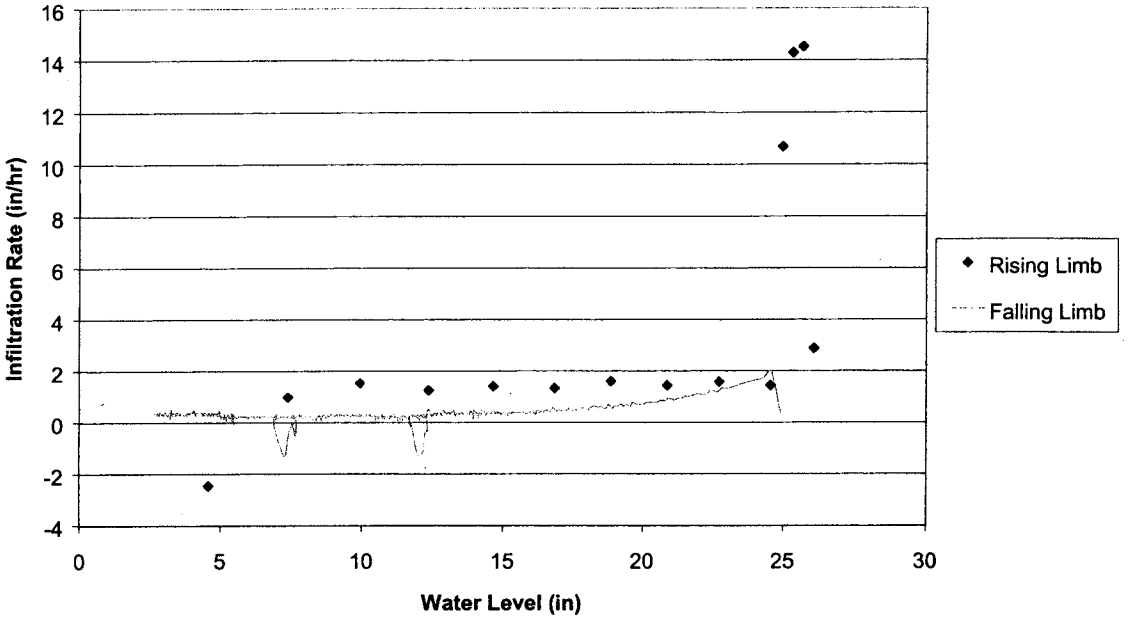

Figure 4.18—Infiltration rate versus water level for Krista Firs pond.

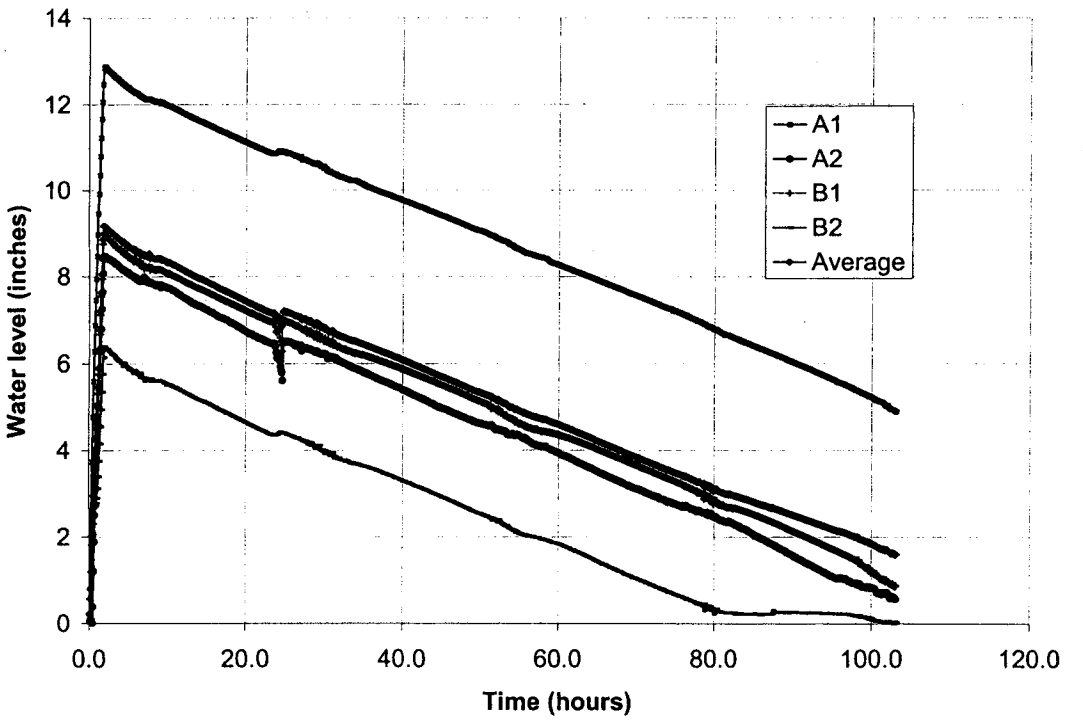

Figure 4.19—Water levels during the full-scale test at the Cimarron pond.

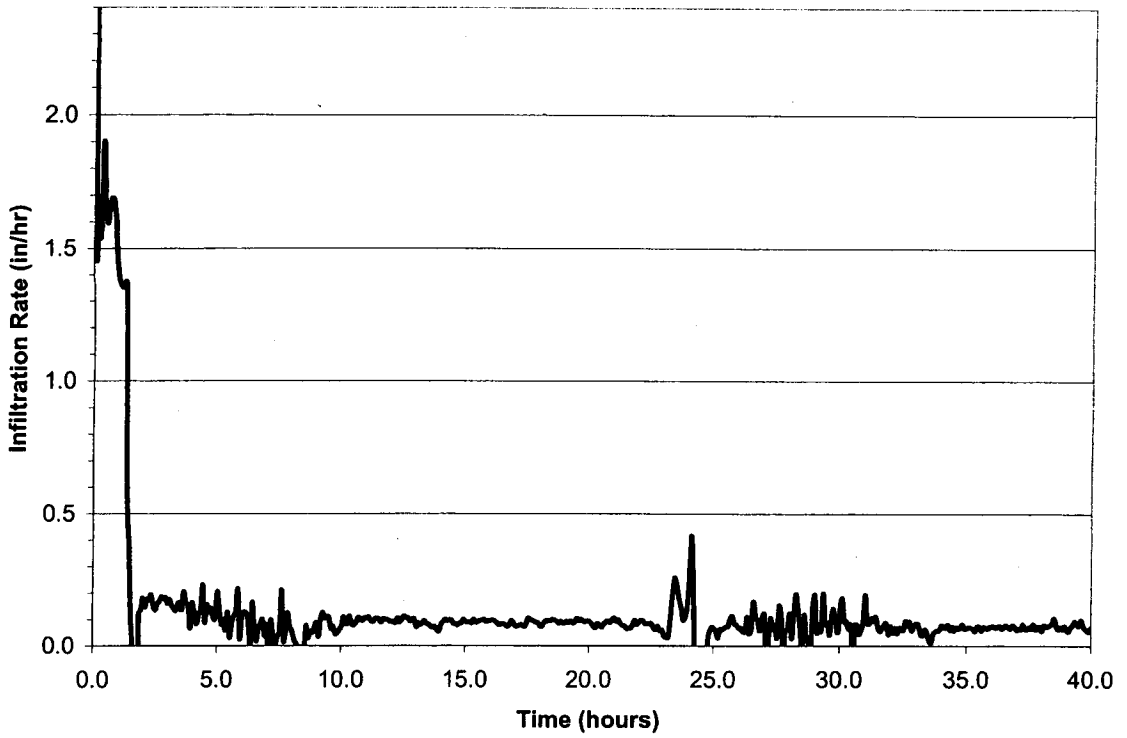

Figure 4.20—Infiltration rate for Cimarron averaged over 30-minute intervals.

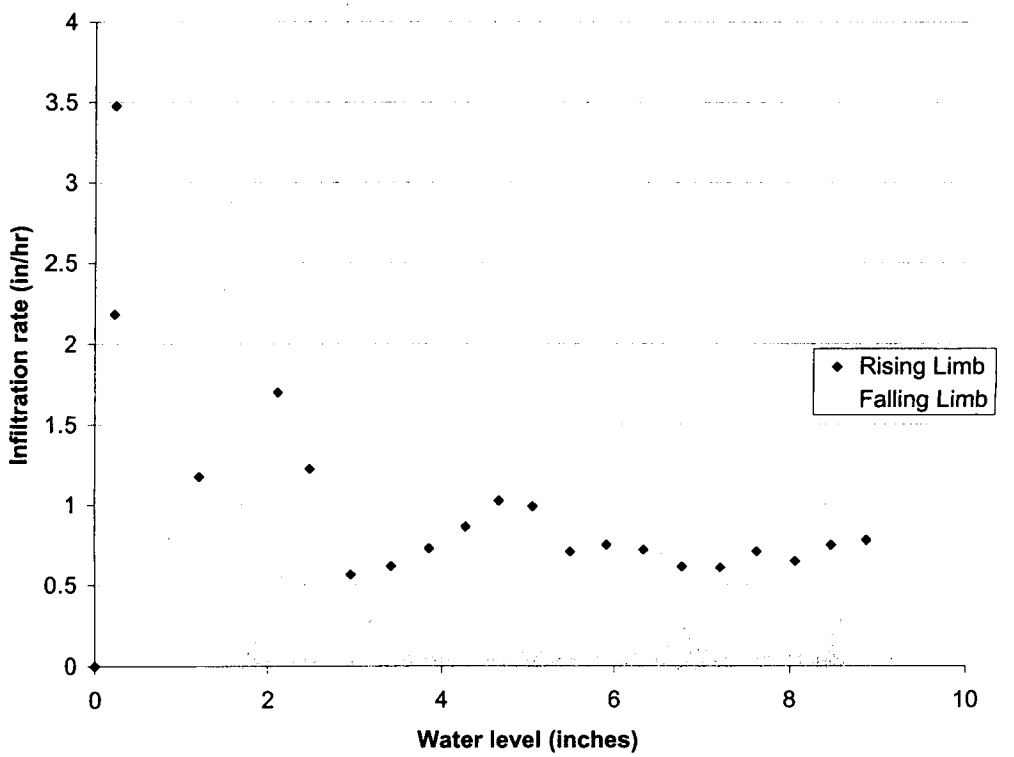

Figure 4.21—Infiltration rate versus water level for Cimarron pond.

5 COMPARISON OF FIELD-SCALE INFILTRATION RATES WITH SMALL-SCALE, SATURATED HYDRAULIC CONDUCTIVITY VALUES

Saturated hydraulic conductivity estimated from measuring air conductivity, a regression equation derived from grain size parameters, and the Hazen formula were compared to full-scale infiltration rates calculated during this study and given in literature.

5.1 Analyses of Estimated Saturated Hydraulic Conductivity and Measured Full-Scale Infiltration Rates

Table 5.1 summarizes the measured full-scale infiltration rates and estimated saturated hydraulic conductivity rates for 15 sites. Full-scale infiltration tests were calculated for three of the sites during this study. Full-scale monitored rates for the other 12 sites were taken from literature. The 15 sites are described more fully in Appendix D.

The estimated saturated hydraulic conductivity values for columns B, C, and D in Table 5.1 are derived as an equivalent K_s value. Hydraulic conductivity values vary in heterogeneous geological formations (Freeze and Cherry, 1979). Therefore, an estimated K_s value was determined for each homogeneous soil layer, and the equivalent vertical K_s value was calculated using equation 5.1 (Freeze and Cherry, 1979):

$$K_{equiv} = \left(\frac{d}{\sum \frac{d_i}{K_i}} \right) \qquad (5.1)$$

where d is the total length of the soil column, d_i is the length of a homogenous layer in the soil column, and K_i is the saturated hydraulic conductivity of the homogenous layer in the

soil column. Measured K_s rates for each soil layer and the calculated K_{equiv} for each method in Table 5.1 are given in Appendix E.

Table 5.2 provides a ratio of the estimated saturated hydraulic conductivity and the long-term infiltration rate for the 15 ponds. The most conservative derived regression equation is $0.87d_{10}^2$. The estimated saturated hydraulic conductivity rates measured with the air permeameter method ("Lab K_s") over-predicted the monitored infiltration rates for all 15 ponds. The estimated K_s rates were off by a greater factor than the rates estimated from the Hazen or regression equation (Table 5.2), with the exceptions of Beaverdam, Airdustrial, and Sweetbriar. The air permeability method showed the same trend as the other two equations—finer sands produce lower estimates than coarse sands..

5.2 Limitations to Each Approach

The use of the air permeameter approach in a laboratory setting to estimate field-scale saturated hydraulic conductivity is limited by the disturbance of soil samples. The structure of the soil as it exists in the field is difficult, if not impossible, to reproduce for laboratory samples.

Non-uniform soil samples can result in voids in the air permeameter cylinder. These voids allow preferential pathways for the air to flow through and thus produce higher air conductivity estimates. In general, the shortcomings of this type of testing procedure arise from disturbed soil samples and non-uniform soil structure. Density, porosity, soil structure, and packing play a significant role in both water and air conductivity. When these parameters are mechanically altered, small-scale effects are lost..

There are limitations in determining infiltration based on soil texture as well. Although soil texture can provide good insight into the potential infiltration rate of a soil type, site-specific characteristics also influence the actual infiltration rate. Specific site characteristics that should be considered when infiltration potential is estimated include flow direction, heterogeneity of the soil formation, depth from the bottom of the pond to the water table, and impermeable surfaces in the subsoil. Soil texture alone does not incorporate these other factors. Another consideration is that infiltration rates of soils with the same textural classification can still differ because of structure and packing.

Table 5.1—Comparison of estimated saturated hydraulic conductivity and long-term full-scale infiltration rates.

Site	A. Long-term Full-scale (in/hr)	B. K_{equiv} Hazen (in/hr)	C. K_{equiv} Regression (in/hr)	D. K_{equiv} Lab K_s (in/hr)
Clark County Pond	0.23	0.01	0.01	20
Beaverdam, King County	1.9	403	351	183
Balsam 7-11, Kitsap County	2.1	0.03	0.04	17
Krista Firs, Kitsap County	0.33	41	36	204
Airdustrial, Thurston County	0.92	24	35	81
Bush, Thurston County	9.8	122	106	232
Echo Glen, Thurston County	13.5	428	372	a
Lacey Lid, Thurston County	0.33	21	23	60
Margaret McKenny, Thurston County	1.64	59	43	145
Ridgeview, Thurston County	4.0	787	571	a
Springfield, Thurston County	3.0	10	9	14
State Farm, Thurston County	4.26	52	45	83
Sweetbriar, Thurston County	0.26	34	37	28
Westwood Baptist, Thurston County	0.5	b	b	30
Wood Glen, Thurston County	1.28	51	56	104

"a"—soil texture was too coarse to measure using the air permeameter method
"b"—the soil was too fine to determine a d_{10} value.

Table 5.2—Ratio of estimated *s* versus long-term infiltration rates (I).

Hazen:I	Regression:I	Lab K_s:I
0.04	0.04	87
212	185	96
0.01	0.02	8
124	109	618
26	38	88
12	11	24
32	28	n/a
64	70	182
36	26	88
197	143	n/a
3	3	5
12	11	19
131	142	108
n/a	n/a	60
40	44	81

6 VALIDATION OF BASE MODEL ASSUMPTIONS

Results from a steady-state saturated flow model were compared to results from a transient unsaturated model to evaluate errors that are introduced when a simplified, steady-state, saturated model is used to simulate flow from infiltration ponds. Sections 6.1 and 6.2 describe the two model types used in the comparison, and sections 6.3 and 6.4 quantify and discuss the error introduced by steady-state, saturated flow assumptions.

6.1 Description of Saturated and Unsaturated Flow Models

6.1.1 Saturated Flow Model

The groundwater flow model MODFLOW was used for the steady-state saturated flow simulations (McDonald and Harbaugh, 1988). This finite difference model simulates saturated flow in three dimensions. Because the unsaturated transient model described below was a 2-dimensional model, the third dimension in MODFLOW was not used. Figure 6.1 is a cross-sectional view of the model domain and the applied boundary conditions for the simplified infiltration facility used in the comparison study. The geometry of the facility was similar to a trench in terms of width (1 meter). This geometry was necessary because of limitations on spatial resolution associated with the unsaturated model, as described below. However, this geometry also emphasized the differences between the saturated and unsaturated flow models, which was the goal of the simulations described in this section. The trench or pond was located in the upper left-hand corner to take advantage of symmetry. To simplify the comparison, the water level in the pond was set to 0.5 meters above the pond bottom by specifying a constant head boundary condition within the pond. The boundary conditions are shown in Figure 6.1.

The left boundary acted as a no-flow boundary because of symmetry. Because rainfall was neglected and the bottom was assumed to be impervious, both the top and the bottom of the model were also no-flow boundaries. Outflow from the domain was allowed along the right hand boundary below the water table. As of result of the boundary conditions, water that left the pond flowed down to the water table and out below the water table. The depth to the water table from the pond floor was 3 meters, typical for infiltration ponds in Western Washington.

Table 6.1 lists all of the model parameters used for the saturated model. Three values for saturated hydraulic conductivity were used in the evaluations to represent a range of values typically found beneath infiltration ponds. The model output gave water table location and the flow exiting the pond. The infiltration rate for the pond was solved for by dividing the flow by the wetted perimeter of the pond.

6.1.2 Unsaturated Flow Model

The 2-dimensional saturated-unsaturated finite-difference model VS2DH 3.0 was used for the transient unsaturated flow model simulations (Hsieh et al., 2000). The unsaturated hydraulic characteristics were represented by the Van Genuchten equation (Van Genuchten, 1980). Figure 6.2 is a cross-section view of the model domain and applied boundary conditions. Table 6.2 lists the parameters used in the Van Genuchten equation. Hydrostatic equilibrium was assumed for the initial condition. The initial condition was a flat water table with dry soil above the water table and around the pond (as shown in Figure 6.2). The transient simulations were run for 30 hours. As an example of the model output, Figure 6.3 shows the advance of the wetting front in a medium sand at three different times.

The transient unsaturated flow model is more complicated to use than the steady-state saturated flow model. The unsaturated forms of the governing equations are highly nonlinear and are difficult to solve numerically (Anderson and Woessner, 1992). Also, the additional relationships that must be specified in unsaturated flow modeling, such as between hydraulic conductivity and pressure head, are very sensitive to small changes in moisture content. This sensitivity causes instabilities to develop during the numerical solution. Using small nodal spacing (on the order of centimeters) and small times steps (on the order of seconds) can minimize these instabilities but requires long computational times. VS2D only allows 85,000 nodes, which prohibits modeling a large region when centimeter-scale grid spacing is required.

6.2 Comparison of Infiltration Rates

The evaluation of the steady-state, saturated flow assumption is separated into two distinct discussions. The first discussion considers errors in assuming that the infiltration exiting the pond has reached steady-state. The second discussion considers the assumption of saturated flow. In evaluating these assumptions, the two numerical models presented above were used to compare calculated infiltration rates exiting the infiltration pond in both models. For each unique situation, both models simulated flow using the same boundary conditions, hydraulic parameters, and model dimensions.

6.2.1 Steady-State vs. Transient

Two scenarios were developed to examine how quickly the flow from an infiltration pond will reach steady-state and how the infiltration rate depends on the proximity of the constant head boundary condition to the pond. The *length* from the center of the pond to the outer edge of the constant head boundary was set to 10 and 50

meters for the first and second scenarios, respectively. Figures 6.4 and 6.5 show the infiltration rate versus time for both models when the hydraulic conductivity of the soil was 0.024 cm/s. The main difference between these two results was the decrease in the steady-state saturated flow infiltration rate as the boundary was moved farther away from the pond. However, in the transient simulation, the wetting front did not migrate fast enough with low permeable soils for the boundary condition to affect the infiltration rate within the time assumed in the analysis.

In scenario 1, the transient model reached a steady infiltration rate after approximately 5 hours. This quick response occurred because the wetting front reached the boundary condition, which set the gradient. When the boundaries were extended to a distance of 50 meters in the second scenario, the infiltration rates decreased to a value close to a different steady-state infiltration rate. This trend would continue as the distance to the boundary was increased, until the boundary conditions were distant enough that they would not affect the wetting front migration in the transient simulation.

Figures 6.6 through 6.9 show the infiltration rate versus time in both scenarios for two additional hydraulic conductivities. For these lower permeable units, the transient simulations were identical for both scenarios since the water did not flow fast enough to be influenced by the boundary conditions within the 30-hour time period. The steady-state saturated simulations, however, produced different infiltration rates because the location of the boundary will always affect the infiltration rate at steady-state.

A small kink in the curve develops at around 3 hours in both figures 6.6 and 6.7. At this time, the wetting front reached the water table and caused the infiltration rate to drop at a quicker rate. If the water table had been farther from the bottom of the

infiltration pond, the infiltration rate would not have shown this sudden decrease. The same kink can also be seen in figures 6.8 and 6.9 after 9 hours of infiltration. It is also present in figures 6.4 and 6.5; however, because the wetting front moved through the subsurface so quickly, it occurs before only 1 hour of infiltration.

6.2.2 Saturated vs. Unsaturated

In addition to modeling under the assumption of steady-state flow, the assumption of saturated flow instead of unsaturated flow must be evaluated. In Figure 6.4, it is clear that the transient simulation had reached a steady infiltration rate after 5 hours because there were no changes in the rate for over 25 hours. Therefore, the differences between the infiltration rates of the saturated and unsaturated models had to all be due to differences in modeling the two types of flow. To quantify the difference in infiltration rates that occur when a saturated flow model versus an unsaturated flow model is used, additional simulations were run. The previous simulations (figures 6.6 to 6.9) could not be used because a steady infiltration rate was not attained. Two additional simulations were performed to determine the difference present at the lower hydraulic conductivity values of 0.0024 cm/s and 0.00081 cm/s. In these additional simulations, the distance to the constant-head boundary was reduced to 4 meters to allow the transient models to reach a steady infiltration rate. Figures 6.10 and 6.11 give the results of using the smaller model domain. In both cases, a steady infiltration rate was achieved within the time period modeled. The differences between the two values resulted from modeling a saturated or unsaturated flow model. The difference between the saturated and unsaturated flow models was lowest in highly permeable soils and increased as the hydraulic conductivity of the soil decreased. Table 6.3 shows that the error in the final

steady-state infiltration rate varied from 19 to 36 percent over a range of hydraulic conductivities typically found beneath infiltration ponds in Western Washington.

6.3 Validity of the Steady-State Saturated Flow Assumption

The results of the model comparison suggest that, under certain hydraulic conditions, the errors introduced by assuming steady-state saturated flow may be acceptable for simulating flow from infiltration ponds. In permeable materials, the system will reach steady-state within a relatively short amount of time, and differences between saturated flow and unsaturated flow will be low. Conversely, when a lower permeable unit is below the pond, the errors in the steady-state saturated flow model results may be large. It is important to note, however, that the results from the steady-state saturated flow simulations always give conservative infiltration rate estimates because infiltration rates calculated under these assumptions are always less than transient unsaturated flow infiltration rate estimates. Additionally, the relative relationships that are established in the evaluation that follows will still hold true. The absolute values of infiltration will have large errors for systems with low permeable soils.

Errors in the steady-state saturated assumptions should be considered relative to errors introduced by characterization and generalization of aquifer properties and by the enforcement of boundary conditions. There is significant uncertainty in any hydraulic conductivity estimate, which can vary over an order of magnitude from one point to another. Also, treating the boundary conditions for the models as constant head introduces error because uncertainty is associated with the water table level.

Table 6.1—Modeling parameters

Texture Class	Total Porosity*	Residual Moisture Content (θ_r)*	Saturated Hydraulic Conductivity (cm/s)
Medium Sand	0.375	0.02	2.4×10^{-2}
Fine Sand	0.377	0.075	2.4×10^{-3}
Sandy Loam	0.496	0.15	8.1×10^{-4}

* Parameters only necessary in unsaturated model

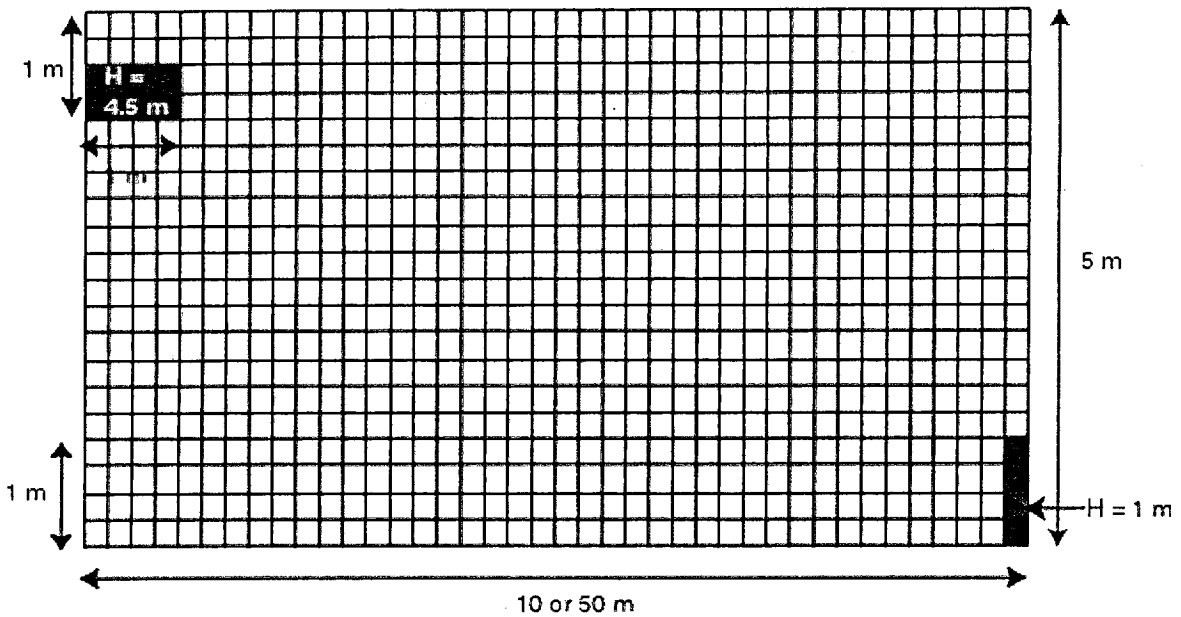

Figure 6.1—Cross-section view of steady-state saturated flow model used in comparison study

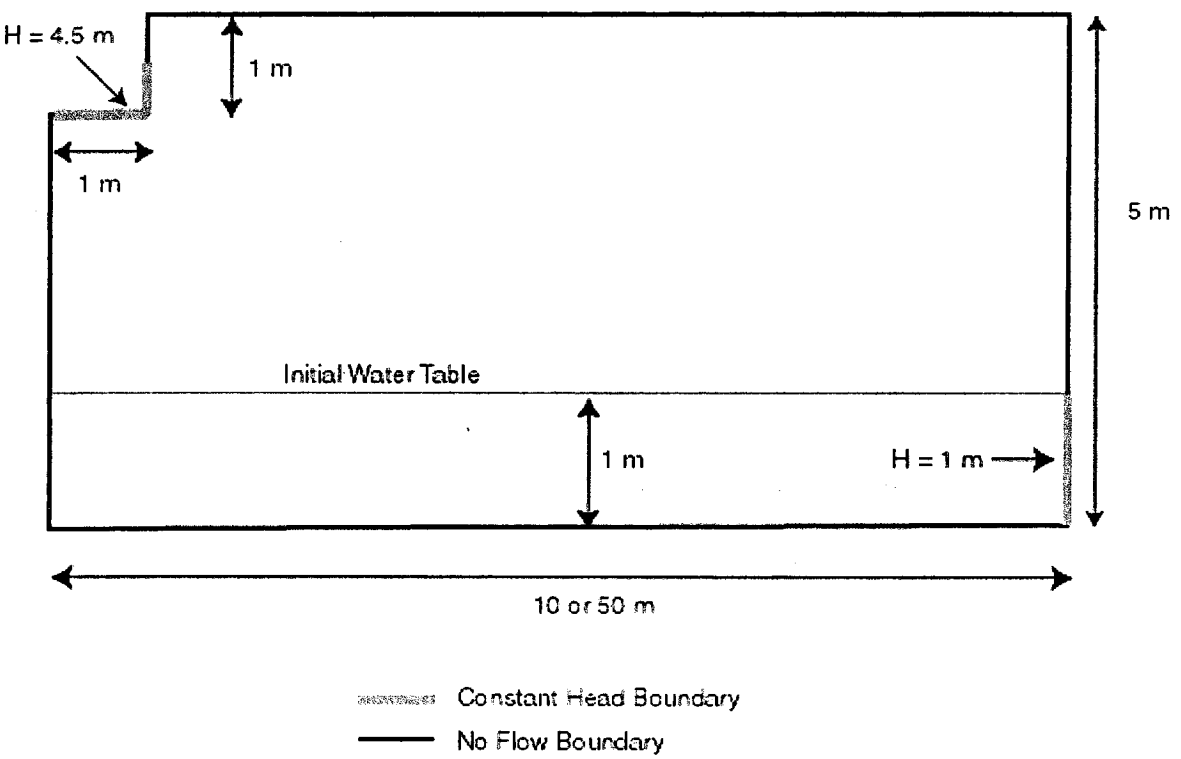

Figure 6.2—Cross-section view of transient unsaturated flow model used in comparison study

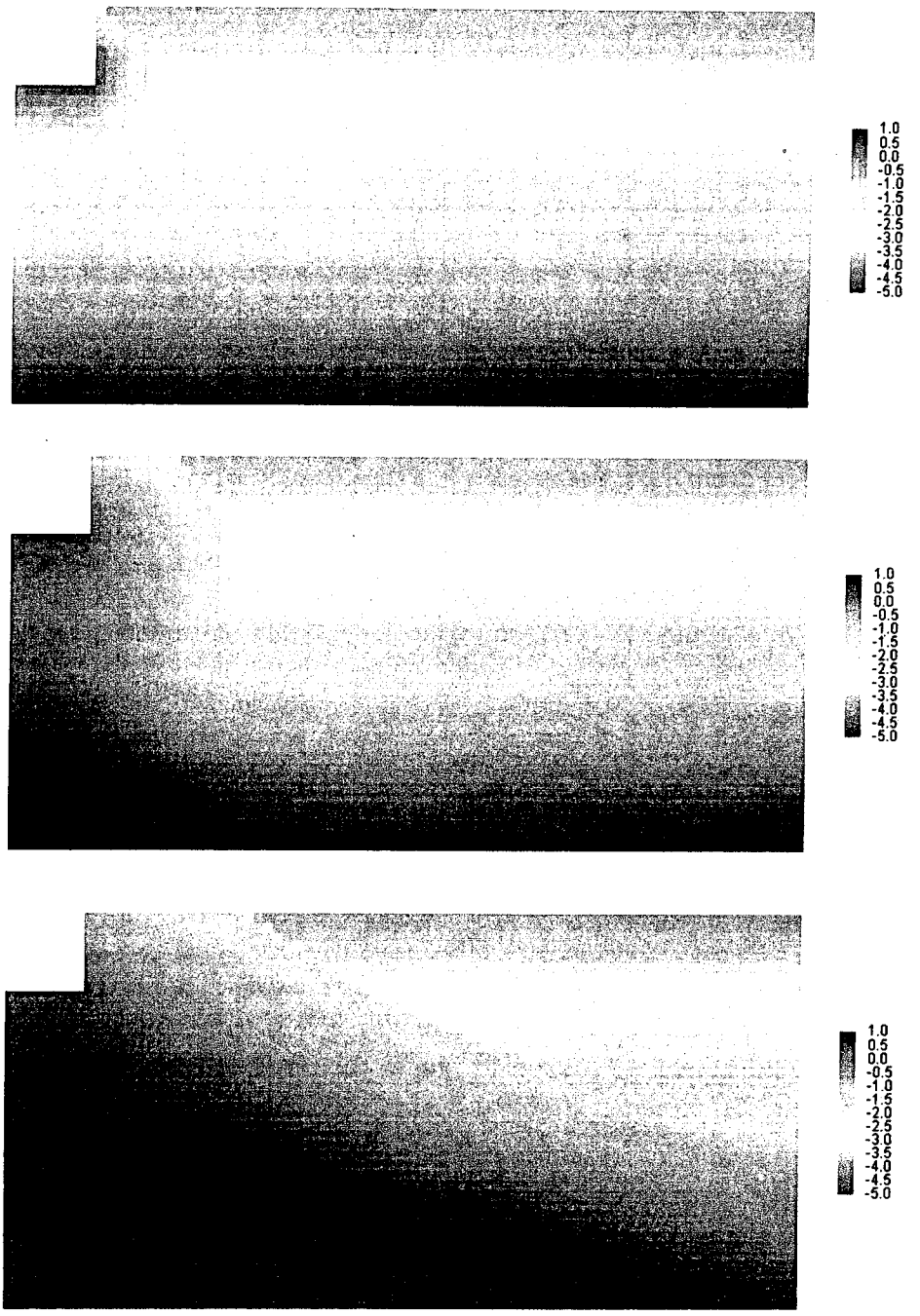

Figure 6.3—Pressure head contour map showing the advance of the wetting front at t = 0.024, 0.4, and 2.3 hours (legend units in meters)

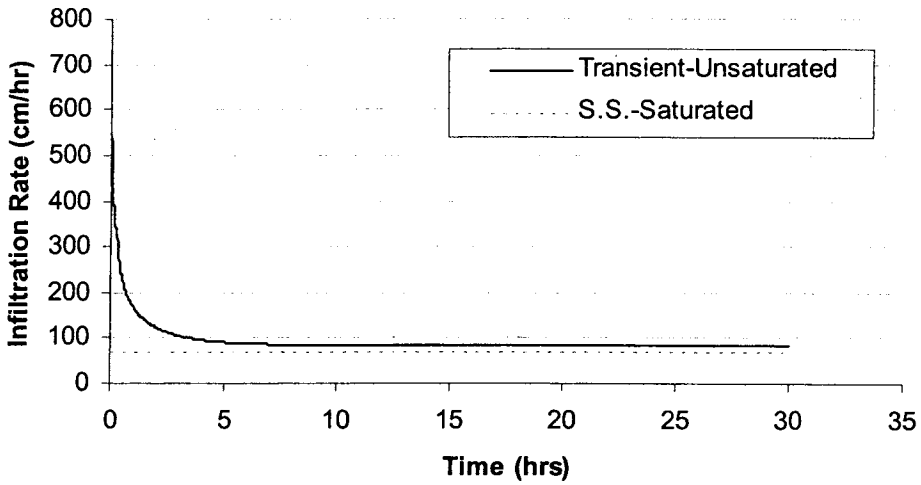

Figure 6.4—Infiltration rate versus time for K = 0.024 cm/s in Scenario 1

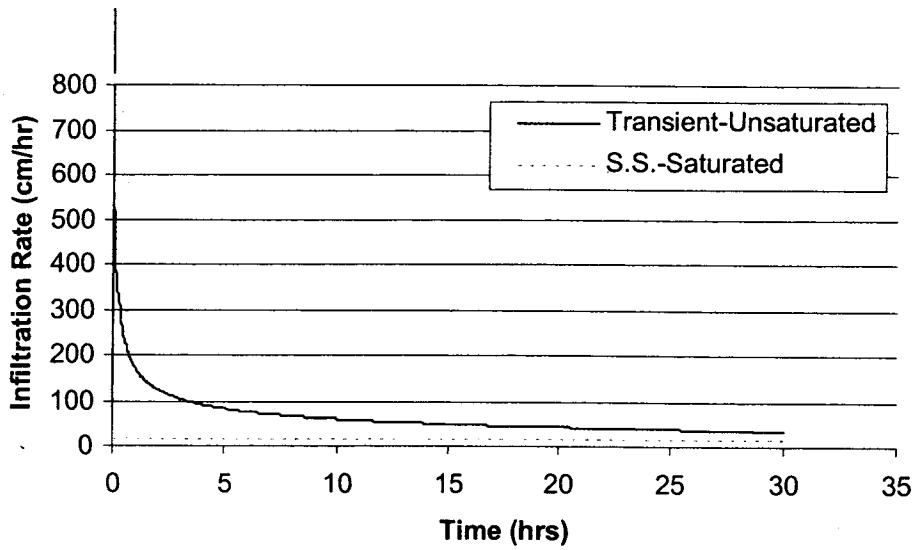

Figure 6.5—Infiltration rate versus time for K = 0.024 cm/s in Scenario 2

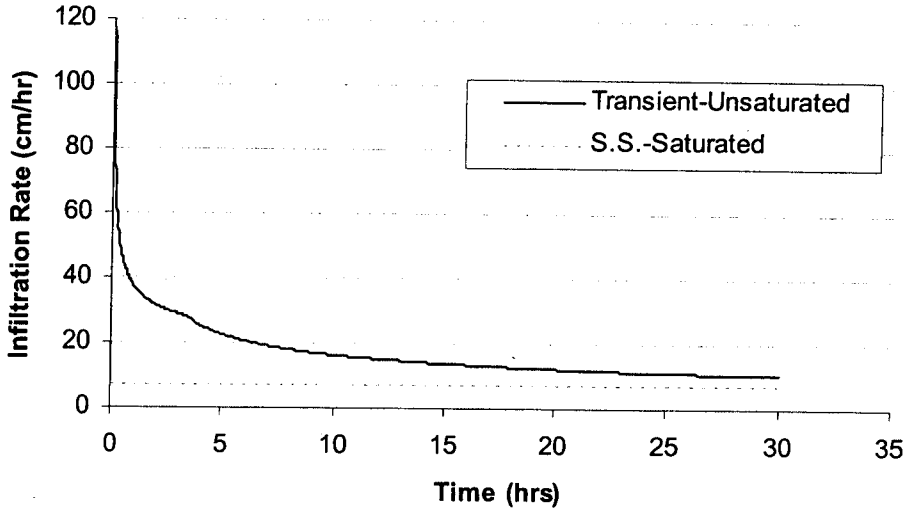

Figure 6.6—Infiltration rate versus time for K = 0.0024 cm/s in Scenario 1

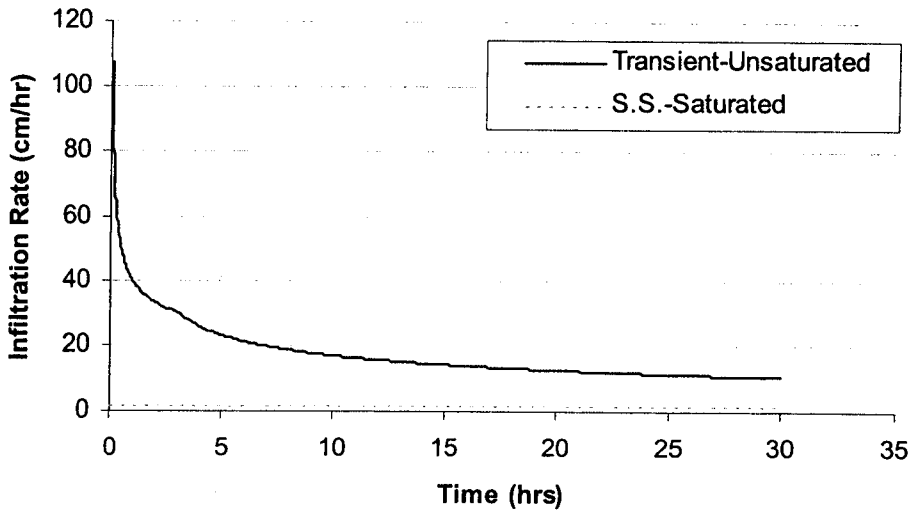

Figure 6.7—Infiltration rate versus time for K = 0.0024 cm/s in Scenario 2

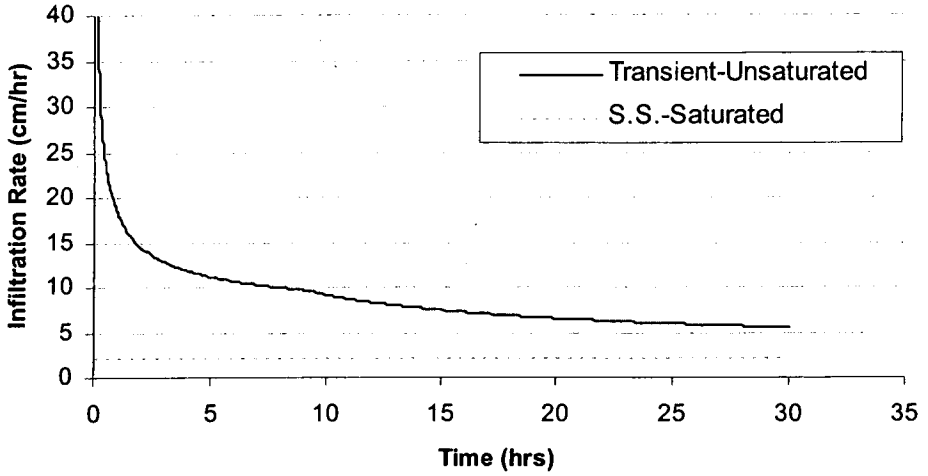

Figure 6.8—Infiltration rate versus time for K = 0.00081 cm/s in Scenario 1

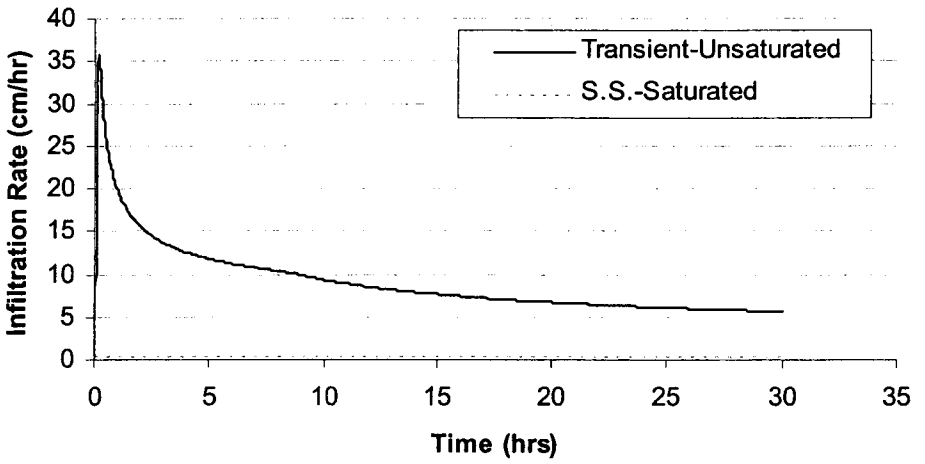

Figure 6.9—Infiltration rate versus time for K = 0.00081 cm/s in Scenario 2

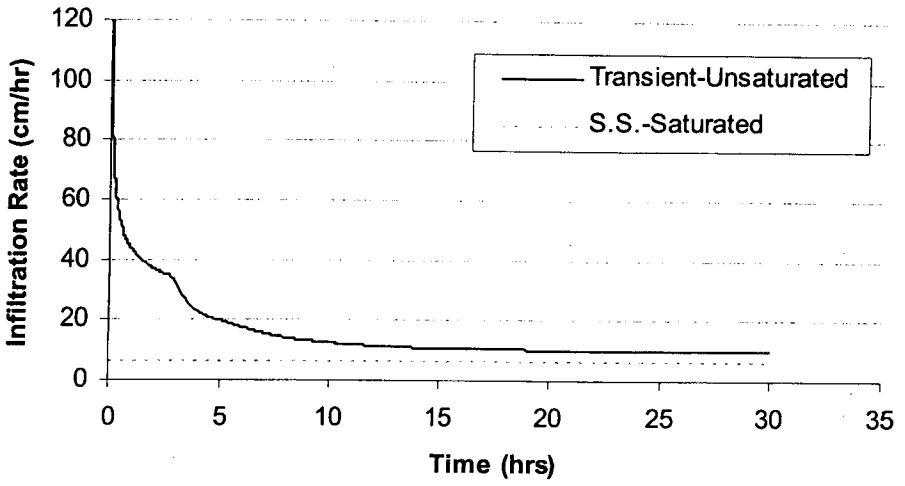

Figure 6.10—Infiltration rate versus time for K = 0.0024 in small model

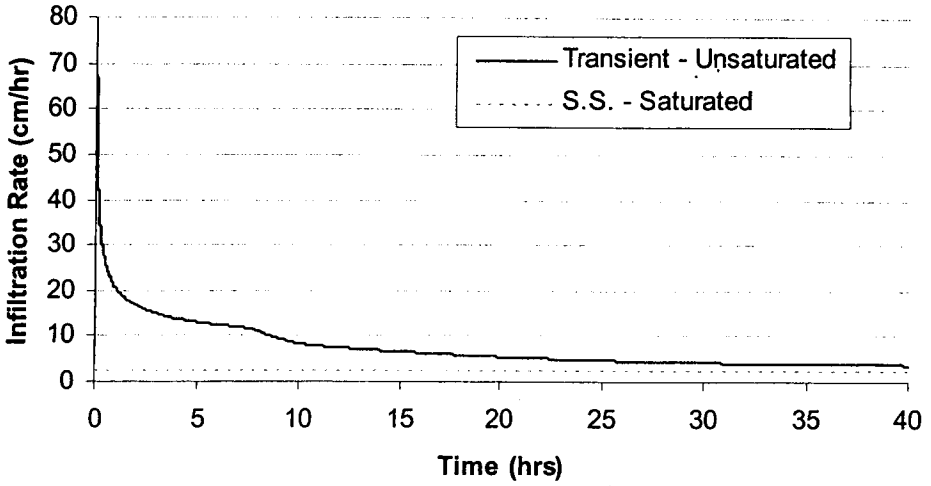

Figure 6.11—Infiltration rate versus time for K = 0.00081 cm/s in small model

7 EVALUATION OF INFILTRATION POND PERFORMANCE

In this section, 3-dimensional, steady-state, saturated flow model simulations are used to examine the influence of different parameters on the overall effectiveness of infiltration ponds. A base model of the Lacey-Lid infiltration pond in Thurston County, Washington, is presented; the effect of site-specific parameters on infiltration rates are examined; and the benefits of possible design modifications are considered. Finally, model simulations are used to examine hydraulic gradients beneath infiltration ponds.

7.1 Thurston County Base Model Description

A base model of a "typical" pond was developed in MODFLOW to evaluate different design alternatives. This model was loosely based on the geometry and observed geology beneath the Lacey-Lid infiltration pond in Thurston County, Wash. (see Figure 7.1) as described in the *Water Resources Investigations Report 92-4109* (Drost et al., 1999). The 3-dimensional grid representing the pond covered an area of 1555 meters by 1524 meters. The pond was located in the center of the model domain, had an area of 36.6 by 73.2-meters, and was 1.5 meters deep. The elevation at the bottom of the model was set at 0 meters, and the top of the model was set at 44.2 meters.

The model is divided into five fields that represent regions with distinct hydrogeologic properties. Table 7.1 describes the hydraulic parameters used in the base model. Figure 7.2 is a cross-section view through the center of the pond showing the location of each field.

The hydraulic parameters in these fields were changed to test the sensitivity of the pond to different conditions. For example, when a gravel bed beneath the pond was

simulated, the hydraulic conductivity of field 5 was increased to a value consistent with gravel.

7.1.1 Boundary-Conditions

A no-flow boundary was enforced along the perimeter of the layers above the regional water table. The layers beneath the water table had a constant head boundary equal to the elevation of the water table. The confining unit (layer 30) had a no-flow boundary along the perimeter. The perimeter around the bottom layer had a constant head boundary that was equal to 0.91 meters less than the water table elevation. The water level in the pond was set to 1.5 meters above the pond bottom by specifying a constant head of 44.2 meters. The hydraulic gradient between the upper unconfined unit and the lower confined unit remained for all of the simulations. A recharge rate of 30.5 cm/yr was applied to the surface of the entire model to reduce the effects of the boundary conditions to the flow field.

7.1.2 Grid

The model contained 86 rows, 86 columns, and 31 layers. The dimensions of the rows and columns ranged from 0.6 meters to 45.7 meters. The finest row and column spacing existed around the perimeter of the infiltration pond and was required to accurately simulate lateral flow. The grid spacing gradually increased away from the pond to a maximum value of 45.7 meters. The rows and columns along the model perimeter had a dimension of 9.1 meters. Figure 7.3 shows a plan view of the grid spacing with a blow-up around the edge of the infiltration pond. The layers were most thin beneath the pond and above the water table. The top 25 layers were each 0.3-meters

thick. The next three layers were 0.6-meters thick. The lowest three layers had thicknesses of 12.2, 9.2, and 15.2 meters, respectively.

7.2 Factors in Pond Performance

7.2.1 Water Table Elevation and Lateral Flow

A series of simulations were performed to quantify the change in the infiltration rate that occurs from water table fluctuation and to determine the amount of lateral flow from infiltration ponds. Figure 7.4 is a cross-section view of the model through the pond, giving an example of the model output. Table 7.2 gives the model infiltration rates and percentage of water leaving the sides and bottom of the pond for pairs of water table elevations and hydraulic conductivities. Model simulations were run with water table elevations of between 36.6 meters and 39.6 meters to represent conservative seasonal variations in Western Washington. The values of 0.018, 0.035, and 0.11 cm/s correspond to a typical range of saturated hydraulic conductivities for outwash sand deposits (Fetter, 1994). Figure 7.5 is a plot of the hydraulic conductivity versus the infiltration rate and shows the linear relationship between infiltration rate and hydraulic conductivity that is expected from Darcy's law.

The substantial decrease in infiltration rate that occurs when the water levels rise emphasizes the importance of understanding regional water table variations at a proposed infiltration pond site. If, for example, a PIT is performed in the summer when regional water table elevations are low, the measured infiltration rate could be twice the rate that would be observed in the winter when the water table levels rise.

Changes in water table elevation have little effect on the percentage of the flow that occurs through the sides of the infiltration pond. Under all the conditions modeled,

there was a slight increase in the lateral flow as the water table approached the pond bottom, but nearly one-third of the flow from the infiltration pond left through the sides.

7.2.2 Confining Unit

Table 7.3 summarizes the changes in infiltration rate due to variations in the hydraulic conductivity of the confining unit (Field 2). The percentage of change in infiltration rate was calculated between the base model case and the values listed in Table 7.3. These changes were the greatest when the hydraulic conductivity was reduced from the base value of 0.0035 cm/s to 3.5×10^{-5} cm/s. Figure 7.6 shows that as the hydraulic conductivity increased past 0.004 cm/s, the infiltration rates started to level off. These results also illustrate that differences in the hydraulic conductivity of the confining unit result in similar percentage changes regardless of the water table elevation.

7.2.3 Pond Geometry

Table 7.4 shows infiltration rate variations resulting from changes in the pond geometry. For all the ponds the area of the footprint, the depth of the pond, and the water level in the pond were the same. Figure 7.7 is a plot of the infiltration rate versus pond perimeters. It illustrates how the infiltration rate increases linearly as a pond becomes more elongate. The increase in the infiltration rate can be attributed to the increase in the lateral flow that occurs as the pond perimeter increases.

7.2.4 Water Level in the Pond

The sensitivity to the water level in the pond was investigated by changing the constant head boundary in Field 3 (the inside of the pond) to represent lower levels of water in the pond. The results of Table 7.5 suggest that the decrease in the total infiltration rate that accompanies lowering the water level in a pond is a result of a

decrease in the amount of lateral flow. The amount of water that exited the bottom of the pond was similar for all pond depths.

7.2.5 Anisotropy

The effects that anisotropy have on the infiltration rate are shown in Table 7.6. Simulations were done under isotropic conditions and then compared to systems that had ratios of 3:1 and 10:1 between the horizontal and vertical hydraulic conductivity. These ratios of anisotropy are typical of natural systems. The hydraulic conductivity in the horizontal remained the same, and the vertical value was reduced to obtain the appropriate ratio. These results show that, as expected, decreasing the vertical hydraulic conductivity will reduce the infiltration rate out the bottom of the pond dramatically. The increase in the amount of water exiting the sides of the pond is not enough to maintain previous levels of infiltration, which causes a decrease in the overall infiltration out of the pond.

7.2.6 Design Alternatives

7.2.6.1 Gravel Base

A series of simulations were run to quantify changes in infiltration rate due to replacement of the natural soil beneath a pond with a gravel material. Table 7.7 summarizes the changes in infiltration rates that resulted from the addition of 0.9 meters of highly permeable material beneath the footprint of the infiltration pond. The range of hydraulic conductivity tested represented typical values for gravel material (Fetter, 1994).

The increase in the total infiltration rate ranged from 0.8 percent to 1.8 percent for all the water table elevations considered. While the amount of flow out the bottom of the

pond increased substantially, this was counteracted by a decrease in the amount of lateral flow, which resulted in an insignificant increase in total infiltration rate.

7.2.6.2 Gravel Column Modification

A gravel column with a high hydraulic conductivity was simulated from the pond bottom down to an elevation of 35.4 meters (1.2 meters below the regional groundwater elevation). The column was 3 by 3 meters in area and had a hydraulic conductivity of 35.3 cm/s. The addition of the column increased the infiltration rate from 17.69 cm/hr to 17.72 cm/hr. This insignificant change indicates that adding a gravel column will not affect a pond's performance during steady-state saturated conditions. The small effect is due to the hydraulic gradient term. Adding a gravel chimney has little impact if no significant hydraulic gradient exists to drive groundwater flow.

The major caveat to these results is that they were determined under the assumption of steady-state saturated flow. Results reported in Section 6.3 demonstrated that the error in these assumptions varies according to the subsurface properties, but in general they are small in comparison to errors introduced in the characterization and generalization of subsurface aquifer parameters and enforcement of boundary conditions.

7.3 Evaluations of Hydraulic Gradients Beneath Infiltration Ponds

7.3.1 Importance of Hydraulic Gradients in Infiltration Pond Performance

As discussed in Section 1, the design of an infiltration pond requires an accurate estimation of the hydraulic gradient. Some design approaches found in the literature (Ferguson, 1994; Stahre and Urbonas, 1990) recommend using a constant vertical hydraulic gradient of 1.0. This assumption makes the infiltration rate equal to the hydraulic conductivity of the subsurface material. Unfortunately, this simplified method,

which is common practice, does not account for the possibility of hydraulic gradients being less than 1.0. If a hydraulic gradient of 1.0 is used in the design process, the pond size may be undersized. Prolonged gradients of less than 1.0 will cause flooding from the infiltration pond since the pond will only have been designed to store all the water from the appropriate design storm. Conversely, a cost is also associated with underestimating the hydraulic gradient. This will result in land being used for an infiltration pond that could have been used for other purposes.

7.3.2 Gradient Changes in Transient Unsaturated Flow Model

The transient unsaturated flow model introduced in section 6.2 was used to monitor the time evolution of the hydraulic gradient beneath an infiltration pond for different soil types during a 30-hour recharge period. Darcy's law was used to solve for the hydraulic gradient at each time step. Since the flow leaving the pond at each time step is known, the hydraulic gradient can be solved for:

$$i = \frac{Q}{A \cdot K}, \qquad 7.1$$

where i is the hydraulic gradient (L/L), A is the area of the wetted perimeter (L), and K is the hydraulic conductivity of the material beneath the pond (L/T).

Figure 7.8 is a graph of the hydraulic gradients beneath a pond over time for a sandy soil ($K=2.4 \times 10^{-2}$ cm/s) and shows how the hydraulic gradient decreases to below 1.0 after only 2 hours of infiltration. Figures 7.9 and 7.10 show the same time series for a fine sand and sandy loam with hydraulic conductivities of 2.4×10^{-3} cm/s and 8.1×10^{-4} cm/s, respectively. The hydraulic gradient of the pond in Figure 7.9 decreases to below one after 17 hours, whereas the hydraulic gradient in Figure 7.10 remains greater than 1.0 within the 30-hour period.

These results demonstrate that, in highly permeable soils, assuming a hydraulic gradient of 1.0 is not conservative. Conversely, in low permeable soils, assuming a hydraulic gradient of 1.0 may be conservative.

7.3.3 Gradient Variations Caused by Differences in Hydraulic Conductivity and Water Table Elevation

The steady-state saturated flow model of the Lacey-Lid infiltration pond was used to establish differences in hydraulic gradients for different hydraulic conductivity values and depths to the water table. All model parameters (i.e., recharge rate, confining unit hydraulic conductivity) were the same as in the base model presented in section 7.1. Figure 7.11 shows how the flow out of the pond changed according to depth to the water table and hydraulic conductivity of the soil. Figure 7.12 shows the variation in hydraulic gradient for different hydraulic conductivity values and depths to groundwater. The hydraulic conductivity values chosen for this evaluation only represented permeable soils such as well-sorted sands, since it had been shown previously that a steady-state is not reached and the hydraulic gradient does not decrease below 1.0 within 30 hours for less permeable soils.

The linear relationship between the depth to the water table and the hydraulic gradient was expected since the gradient was equal to the change in head over the change in length. Because the model applied a fixed recharge to the upper surface of the entire model domain, the hydraulic gradient was not a fixed value for all hydraulic conductivities. Instead, as Figure 7.12 illustrates, variations in the gradient occurred, depending on the hydraulic conductivity of the soil surrounding the pond.

Table 7.1—Descriptions and hydraulic parameters for each field

Field	Description	Hydraulic Conductivity (cm/s)	Porosity
1	Region around and below the infiltration pond, but above the confining unit	0.035	0.21
2	Simulates a confining unit between the upper unconfined aquifer and the lower confined aquifer	0.0035	0.21
3	The inside of the pond that simulates no aquifer matrix; The depth is 5 feet and it cuts across 5 layers.	35.	1
4	Simulates a confined aquifer	0.035	0.21
5	3 feet directly beneath the footprint of the infiltration pond	0.035	0.21

Table 7.2—Infiltration rates for different water table elevations

Elevation of Water Table (m)	Hydraulic Conductivity in Field 1 (cm/s)	Infiltration Rate (cm/hr)	Percent of Total	
			Bottom	Sides
*36.6	0.018	9.2	69	31
	0.035*	17.7		
	0.11	49.4		
38.1	0.018	7.6	68	32
	0.035	14.7		
	0.11	41.2		
39.6	0.018	5.9	67	33
	0.035	11.5		
	0.11	32.4		
41.2	0.018	4.1	66	34
	0.035	8.1		
	0.11	23.1		
42.7	0.018	2.3	66	34
	0.035	4.54		
	0.11	13.1		

* Base Model Case

Table 7.3—Effect of confining unit on infiltration rate

Elevation of Water Table (m)	Hydraulic Conductivity in Field 2 (cm/s)	Infiltration Rate (cm/hr)	Percent Change in Infiltration Rate		
			Total	Bottom	Sides
120	3.5E-5	12.2	-45	-53	-24
	0.0011	16.2	-9	-11	-10
	0.0035	17.7	--	--	--
	0.011	19.2	+8	+10	+4
125	3.53-5	10.2	-44	-51	-24
	0.0035	13.5	-9	-11	-5
	0.011	15.9	+8	+10	+4
130	3.5E-5	8.0	-44	-50	-24
	0.0035	10.6	-9	-10	-5
	0.011	12.5	+8	+9	+4

* Base Model Case

Table 7.4—Infiltration rates for different pond perimeters

Pond Perimeter (m)	Pond Dimensions (m x m)	Water Table Elevation (m)	Infiltration Rate (cm/hr)	% Sides
207	51.7 x 51.7	36.6	17.4	30.7
219.5	36.6 x 73.2	36.6	17.7	31.4
329.3	146.3 x 18.3	36.6	20.2	35.5

Table 7.5—Changes in infiltration rates caused by varying water depths in pond

Depth of Water in Pond (ft)	Percent Change in Infiltration Rate		
	Total	Bottom	Sides
1.5	--	--	--
1.2	-8	-0.78	-22
0.9	-11	-0.84	-30
0.6	-17	-1.78	-43

Table 7.6—Changes in infiltration rates caused by anisotropy

Ratio of Horizontal to Vertical Hydraulic Conductivity	Percent Change in Infiltration Rate		
	Total	Bottom	Sides
1:1	--	--	--
3:1	-23	-26	+14
10:1	-74	-86	+34

Table 7.7—Infiltration rate changes due to addition of gravel base

Elevation of Water Table (m)	Hydraulic Conductivity of Field 5 (cm/s)	Percent Change in Infiltration Rate		
		Total	Bottom	Sides
36.6	0.088	+0.8	+5.7	-10.8
	0.35	+1.5	+12.7	-27.0
	0.88	+1.8	+15.7	-34.7
38.1	0.088	+0.8	+5.8	-10.6
	0.35	+1.5	+13.0	-26.9
	0.88	+1.8	+16.0	-34.7
39.6	0.088	+0.8	+5.9	-10.6
	0.35	+1.4	+13.2	-26.7
	0.88	+1.7	+16.3	-34.3

Figure 7.1—Lacey-Lid infiltration pond in Thurston County, Wash.

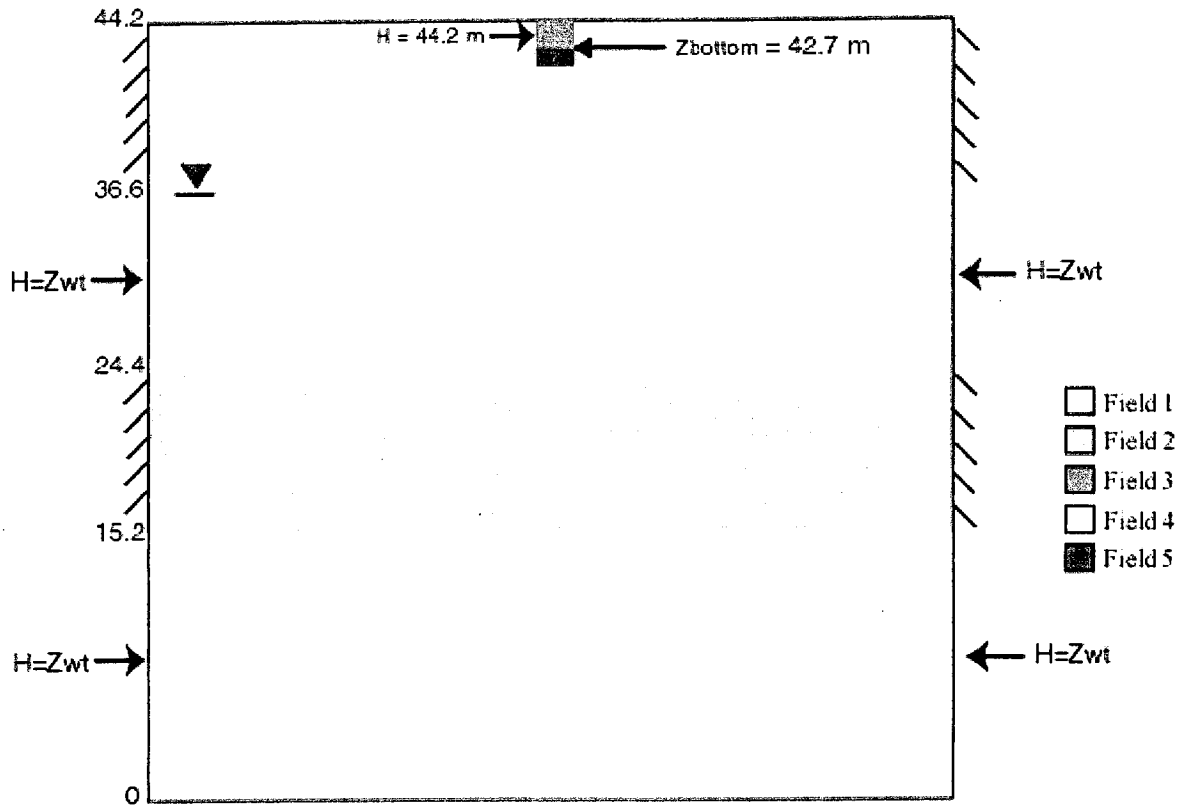

Figure 7.2—Cross-section view of modeled domain showing locations of five fields

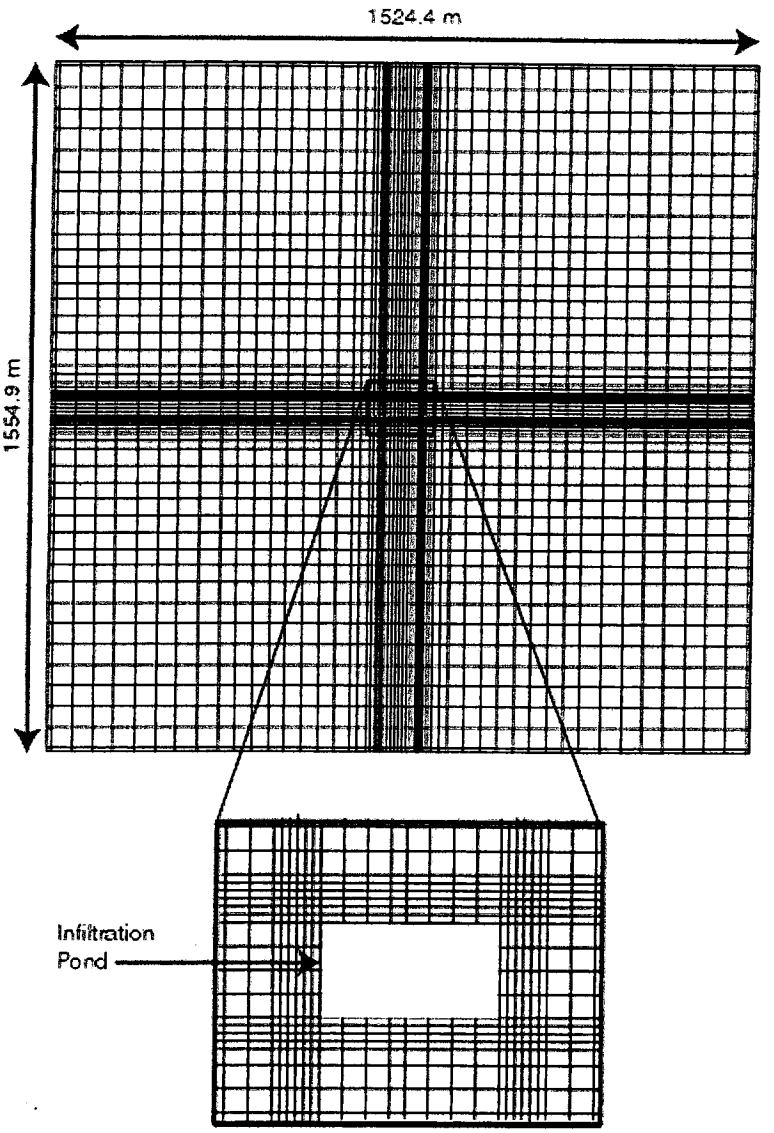

Figure 7.3—Plan view of row and column spacing

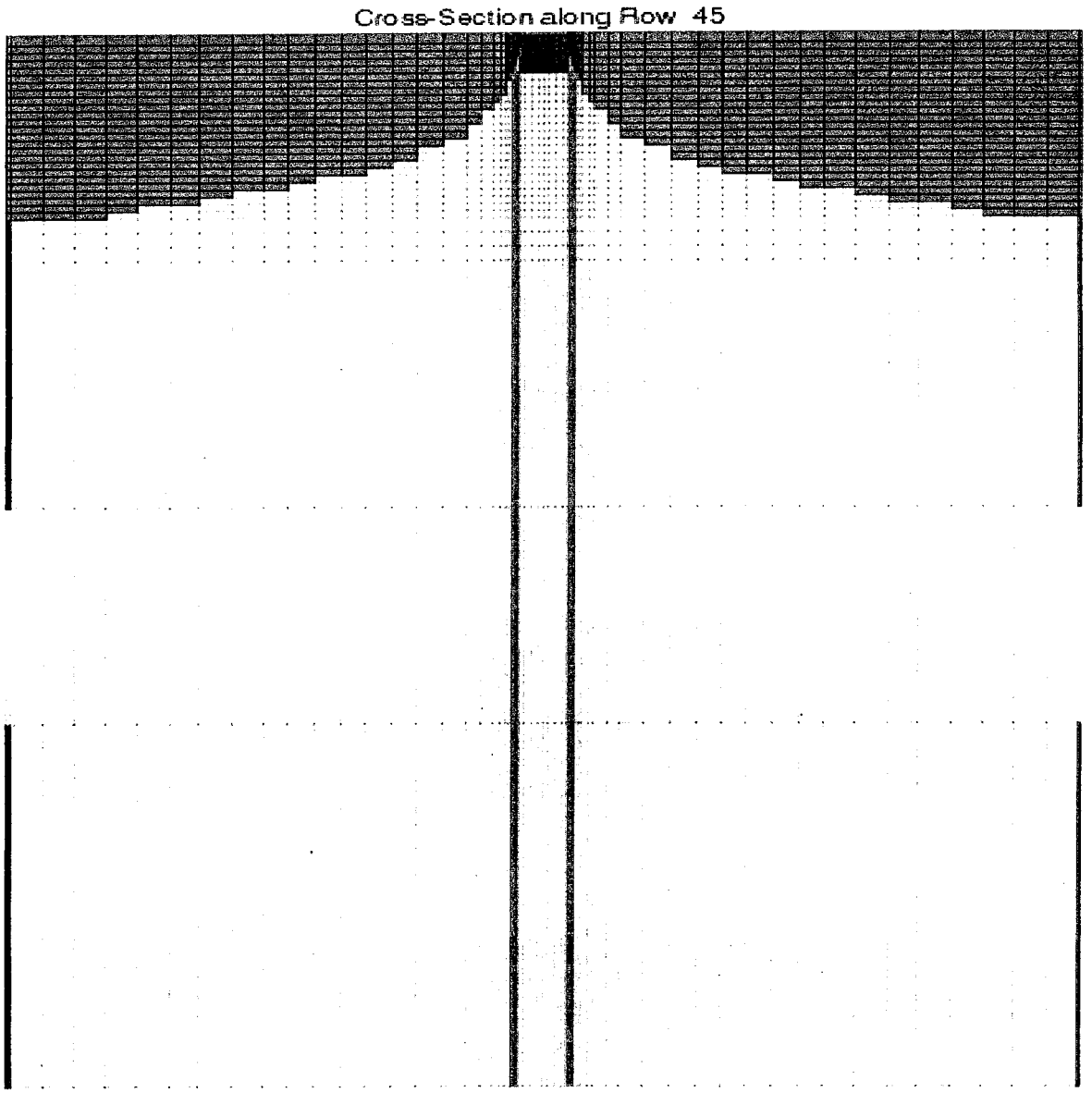

Figure 7.4—Cross-section view of flow from Lacey-Lid infiltration pond

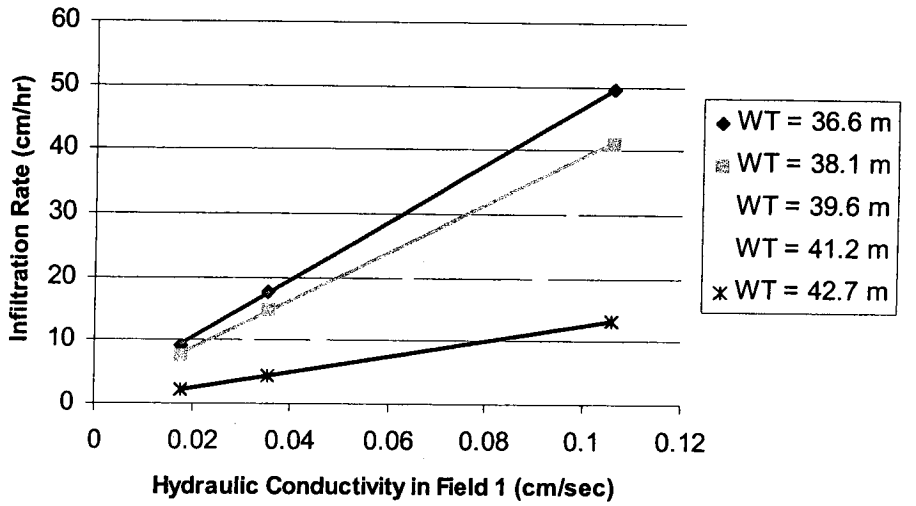

Figure 7.5—Infiltration rate versus hydraulic conductivity in field 1

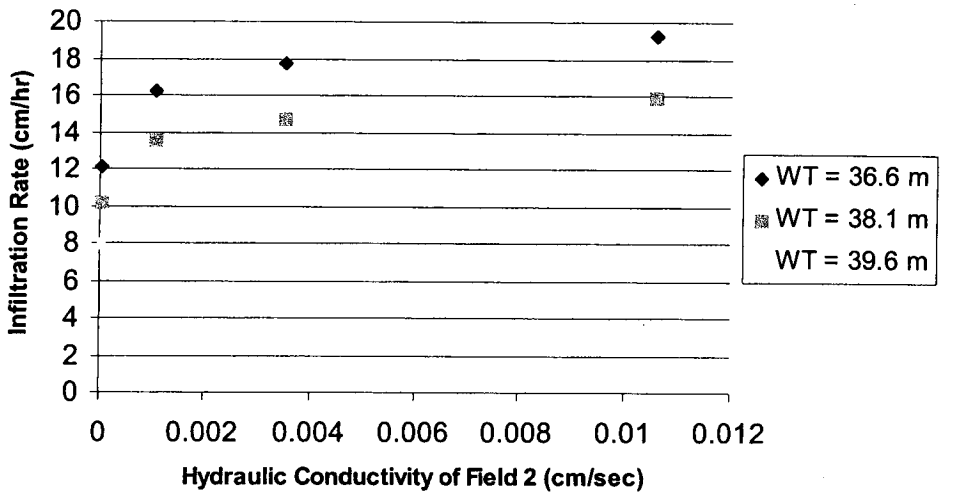

Figure 7.6—Infiltration rate versus hydraulic conductivity in field 2

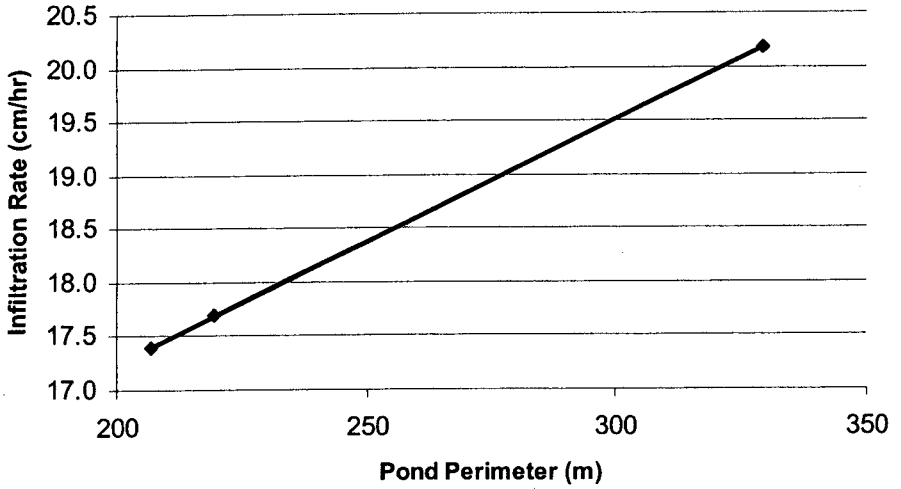

Figure 7.7—Infiltration rate versus pond perimeter

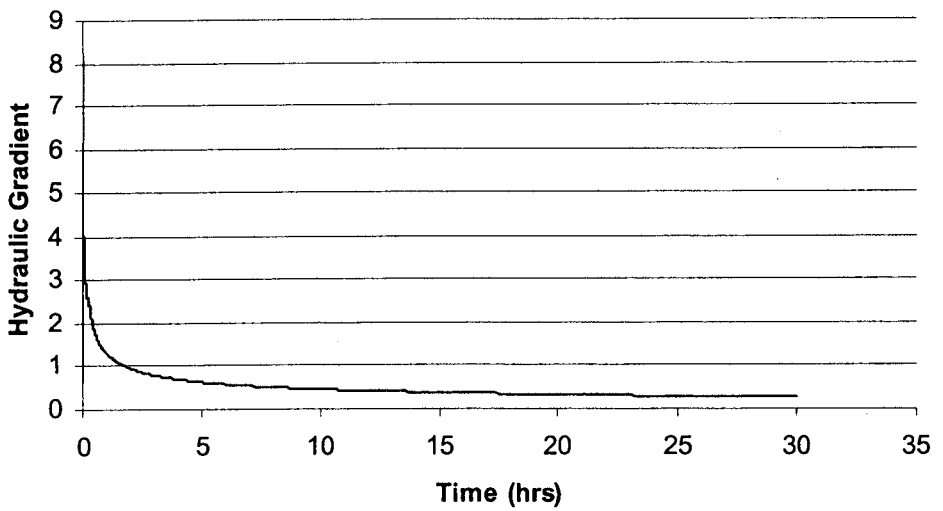

Figure 7.8—Hydraulic gradient versus time for $K = 2.4 \times 10^{-2}$ cm/s

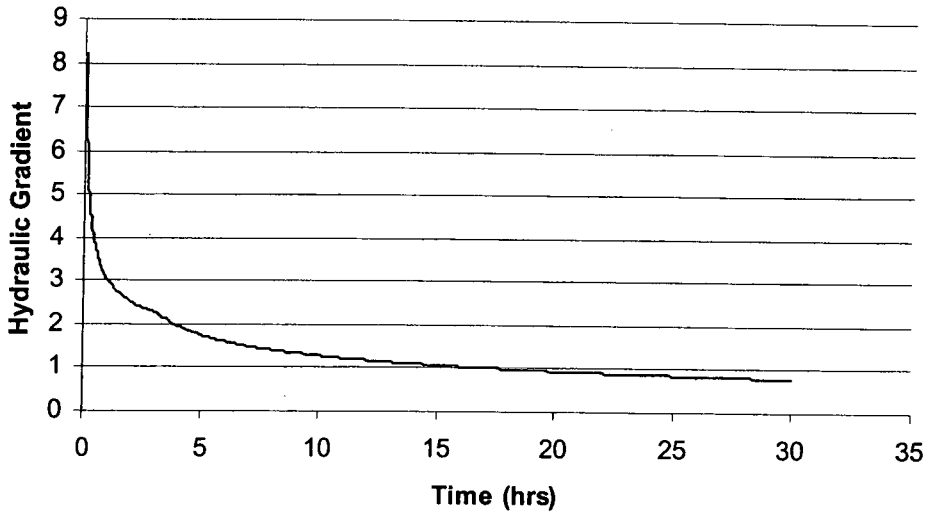

Figure 7.9—Hydraulic gradient versus time for K = 2.4×10^{-3} cm/s

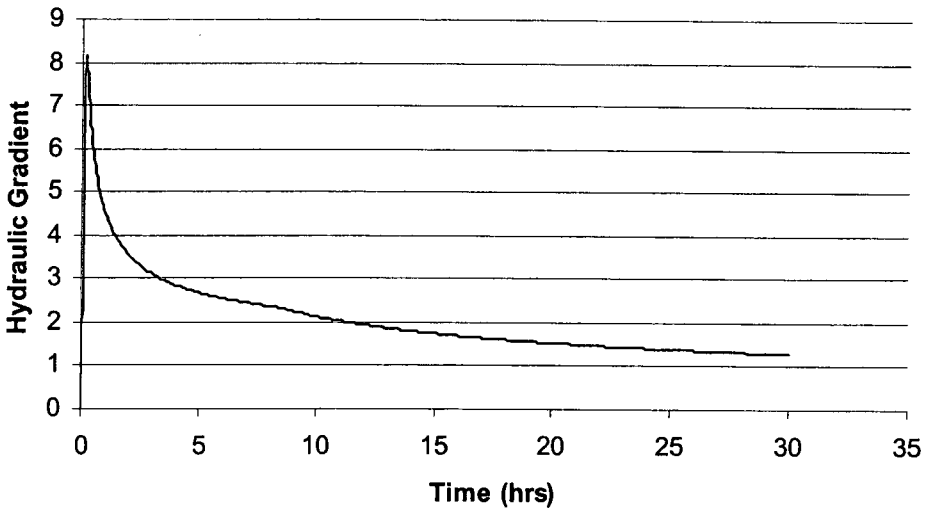

Figure 7.10—Hydraulic gradient versus time for K = 8.1×10^{-4} cm/s

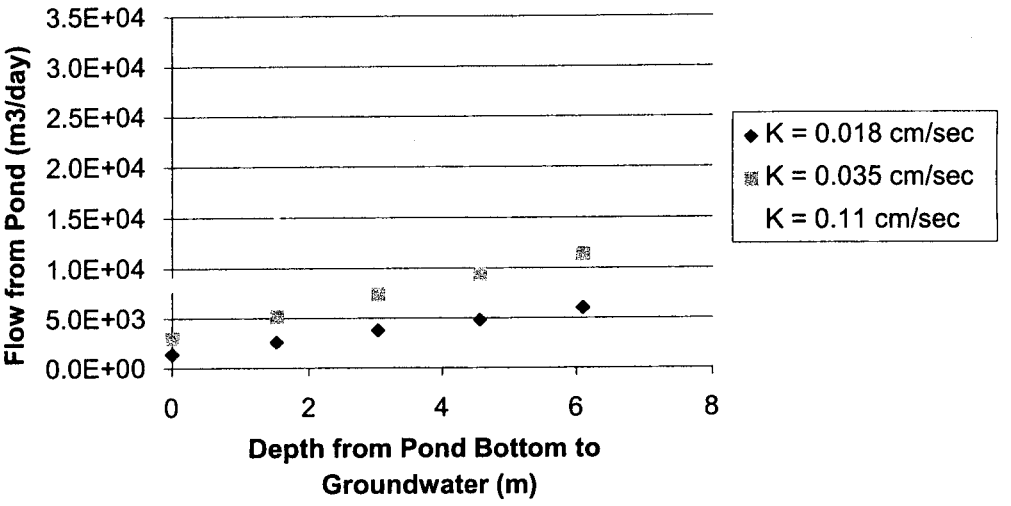

Figure 7.11—Flow exiting Lacey-Lid pond for different groundwater depths and hydraulic conductivities

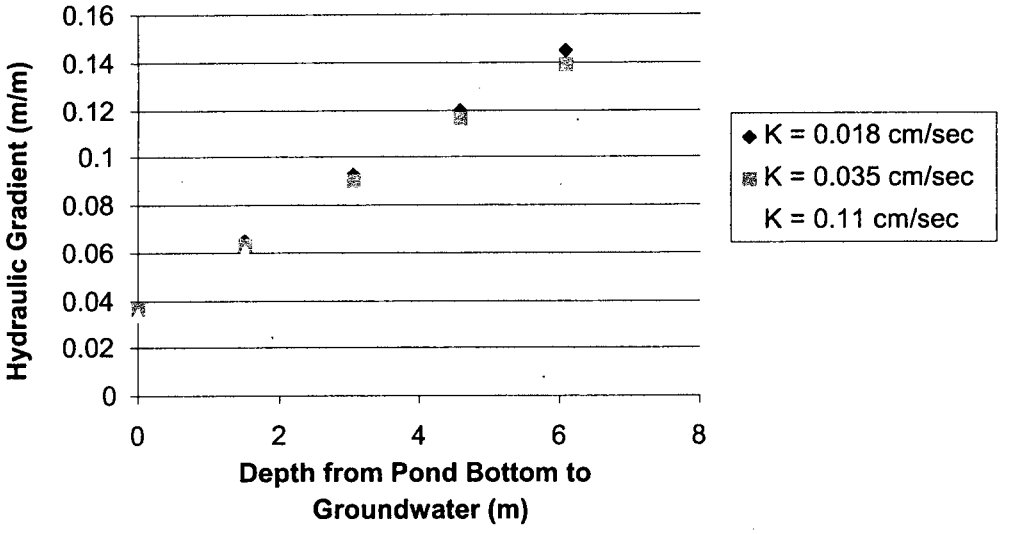

Figure 7.12—Hydraulic gradient values for different groundwater depths and hydraulic conductivities (for Lacey-Lid infiltration pond)

8 CONCLUSIONS AND DESIGN RECOMMENDATIONS

The following conclusions and design recommendations were developed from the results of the studies described in this report.

8.1. Effects of Hydraulic Gradient

- Short-term infiltration tests will tend to over-estimate long-term infiltration rates, as shown by the Green-Ampt approximation. The initial infiltration rate is significantly larger than the saturated hydraulic conductivity because the hydraulic gradient term is larger than 1.0. As more water infiltrates, the gradient approaches a value of 1.0, and the infiltration rate approaches the saturated hydraulic conductivity.
- If recharge or infiltration is sufficient to cause the wetting front to reach a regional or perched water table, the hydraulic gradient may drop to a value significantly less than 1.0, and the infiltration rate may be much less than the saturated hydraulic conductivity. This is a very important concept and one that is overlooked in design approaches in which infiltration rates are estimated solely on the basis of soil types or saturated hydraulic conductivity estimates.
- A transient, unsaturated flow model was used to monitor the time evolution of the hydraulic gradient beneath an infiltration pond for different soil types during a 30-hour recharge period. The results demonstrated that, in highly permeable soils, assuming a hydraulic gradient of 1.0 is not conservative. Conversely, in low permeable soils, assuming a hydraulic gradient of 1.0 may be conservative.

8.2 Regressions for Saturated Hydraulic Conductivity

- Equation C-8, shown in Table 8.1, produces estimates of hydraulic conductivity that have a sum of mean square errors that is approximately 35 percent smaller than the mean square errors produced by the Hazen equation for the set of synthetic and natural soils used in this study. This polynomial equation uses data that are readily available from grain size analyses and should be considered an alternative for the Hazen equation, especially for more coarse-grained soils with a hydraulic conductivity larger than approximately 0.05 cm/s.

8.3 Full-Scale Infiltration Tests

- Full-scale infiltration tests conducted at four sites in western Washington showed that the infiltration rate increases with time during the filling portion of the test. After the discharge to the pond is stopped, the infiltration rate quickly decreases to a rate that may be several times smaller than the initial rate. The rapid increase in infiltration during the filling portion of the test may be caused in part by lateral flow along the sides of the ponds. This is similar to "bank storage" that occurs in stream channels. As the water level in the pond increases, flow is induced horizontally into the banks of the pond. This infiltration is in addition to the infiltration that occurs along the pond bottom. Once the water level in the pond begins to decrease, the horizontal flow is reversed and water drains into the pond along the sides and out of the pond along the bottom. This inflow, which reduces the net infiltration rate, decreases with time.
- Infiltration rates based on soil texture for four sites are included in Table 8.2. These estimates are from the WDOE *Stormwater Management Manual for the*

Puget Sound Basin (2001). The infiltration rates based on soil textures over-estimated the actual full-scale measured rate at Krista Firs (Kitsap County) and at Cimarron (King County). The soil texture rate for Balsam 7-11 (Kitsap County) under-estimated the actual full-scale rate, and the soil texture rate for Clark County closely estimated the actual full-scale rate.

- Saturated hydraulic conductivity values estimated from measuring air conductivity and from regression equations derived from grain size parameters were compared to full-scale infiltration rates calculated during this study and given in literature. The estimated saturated hydraulic conductivity values were up to two orders-of-magnitude larger that the full-scale infiltration rates for some sites and were two orders-of-magnitude smaller in other cases. This reinforces that grain size texture alone does not include site-specific characteristics that may affect infiltration rate

8.4 Comparison of Modeling Approaches

- Results from a steady-state saturated flow model were compared to results from a transient unsaturated model to evaluate errors that are introduced when the simplified model is used to simulate flow from infiltration ponds. These results show that the steady-state assumption may significantly under-estimate infiltration rates and that the amount of this under-estimation is dependent upon site-specific hydrologic information.
- Computer simulations were used to quantify the difference in estimated infiltration rates that occur when a saturated flow model is used versus an unsaturated flow model. The difference between the saturated and unsaturated

flow models is lowest in highly permeable soils and increases as the hydraulic conductivity of the soil decreases. The modeling results suggest that the error in the final steady-state infiltration rate varies from 20 to 40 percent over a range of hydraulic conductivities typically found beneath infiltration ponds in Western Washington.

8.5 Design Alternatives from Computer Simulations

- The results of computer simulations suggest the infiltration rate increases linearly as a pond becomes more elongate. The increase in the infiltration rate can be attributed to the increase in the lateral flow that occurs as the pond perimeter increases.
- A gravel column with a high hydraulic conductivity was simulated from the pond bottom down to the regional groundwater table. The addition of the column increased the infiltration rate by less than 1 percent. This insignificant change indicates that adding a gravel column will not affect the pond's performance during steady-state saturated conditions. The small effect is due to the hydraulic gradient term. Adding a gravel chimney has little impact if no significant hydraulic gradient exists to drive groundwater
- If lateral flow is consistently important, more efficient designs may require a larger ratio of side area to bottom area. This design approach would necessitate maintenance for the sides as well as the bottom of the pond. If the soil on the sides and bottom are preserved with respect to vegetation and silt build-up, the horizontal as well as the vertical flow could be an effective means of infiltrating storm-water runoff into the subsurface.

Table 8.1—Sum of mean square error of synthetic and natural soils for selected equations.

	Regression Equation	Sum of mean square error
C.1	$0.87 d_{10}^2$	5.43
C.6	$0.0029 + 1.0 d_{10} - 0.014 d_{60} - 0.0011 d_{90}$ $- 0.19 d_{10}^2 + 3.1(10^{-4}) d_{60}^2 - 2.5 (10^{-5}) d_{90}^2$	3.45
C.8	$0.019 + 0.82 d_{10} + 2.8(10^{-5}) d_{60}^2 - 0.0045 d_{90}$	3.50

Table 8.2—Summary of calculated infiltration rates.

Site	Long-term infiltration rate (in/hr)	Short-term infiltration rate (in/hr)	Soil Texture Description	Estimated long-term rate from soil texture (WDOE, 2001) (in/hr)
Clark County	0.23	2.5	Loam/Silty Loam	0.13/0.25
Balsam 7-11	2.1	13.2	Silty Loam	0.25
Krista Firs	0.33	2.8	Sand	2
Cimarron	0.1	1.9	Silty sand loam	0.25

ACKNOWLEDGMENTS

The authors wish to acknowledge the generous help and support provided during the study by Tony Allen and Keith Anderson at the Washington State Department of Transportation. Steve Foley at King County, Jerry Anderson at Kitsap County, Ed McMillan at Clark County, and Scott Lindblum at Thurston County were especially helpful. Each provided access to stormwater facilities in their jurisdictions, freely offered data and information related to these facilities, and shared their considerable experiences and insights.

REFERENCES

Anderson, J., *personal interview*, Surface and Storm Water Management Department, Kitsap County, January, 2001.

Anderson M.P. and W.W. Woessner, *Applied groundwater modeling : simulation of flow and advective transport,* Academic Press, San Diego, 1992.

Bouwer, H., *Groundwater Hydrology*, McGraw-Hill Book Company, 1978.

Bouwer, H. and R.C. Rice, Effect of water depth in groundwater recharge basins on infiltration, *ASCE Journal of Irrigation and Drainage Engineering,* Vol. 115(4), pp. 556-567, 1989.

Butchart, C.D., *Using Air Conductivity and Soil Texture as Indicators of Infiltration Rates for Stormwater Infiltration Ponds*, M.S. Thesis, Department of Civil and Environmental Engineering, University of Washington, 2001.

Carsel, R.F. and R.S., Parrish, Developing joint probability distributions of soil water retention characteristics, *Water Resources Research*, 24(5), pp. 755-769, 1988.

Chin, D.A., *Water Resources Engineering*, Prentice Hall, 2000.

Chow, V.T., D.R. Maidment and L.W. Mays, *Applied Hydrology*, McGraw-Hill Book Company, 1988.

Corey, A.T., Methods of Soil Analysis, Part 1, *American Society of Agronomy - Soil Science Society of America*, 1986.

Danielson, R.E. and P.L. Sutherland, Porosity, Methods of Soil Analysis, Part 1, *American Society of Agronomy - Soil Science Society of America*, 1986.

Davis, S.N. and R.J.M. DeWiest, *Hydrogeology*, John Wiley & Sons, Inc., 1966.

Davis, J.M., J.L. Wilson and F.M. Phillips, A portable air-minipermeameter for rapid in-situ field measurements, *Ground Water*, Vol 32, No. 2, pp. 258-266, 1994.

Drost, B.W. et al., Hydrology and quality of ground water in northern Thurston County, Washington, *Water Resources Investigations Report 92-4109,* U.S. Geological Survey; Denver, CO, 1999.

Duchene, M., E.A. McBean, and N.R. Thomson, Modeling of Infiltration from Trenches for Storm-water Contro, ASCE Journal of Water Resources Planning and Management, Vol. 120(3), pp. 276-293, 1992.

Ferguson, B.K., *Stormwater Infiltration*, CRC Press, Inc., 1994.

Fetter, C.W., *Applied Hydrogeology*, Prentice-Hall, Inc., 1994.

Foley, S. *personal interview*, Department of Natural Resources, Water and Land Resources Division, King County, August, 2000.

Freeze A. and J. Cherry, *Groundwate*r, Prentice-Hall, Inc., 1979.

Hsieh, P.A., W. Wingle, and R.W. Healy, A graphical software package for simulating fluid flow and solute or energy transport in variably saturated porous media: *U.S. Geological Survey Water-Resources Investigations* Report 99-4130, 2000

Janna, W.S., *Introduction to Fluid Mechanics*, PWS-Kent Publishing Company, 1993.

King County, *King County Surface Water Design Manual*, Seattle, Washington, 1998.

Loll P., P. Moldrup, P. Schjonning, and H. Riley, Predicting saturated hydraulic conductivity from air permeability: Application in stochastic water infiltration modeling, *Water Resource Resources*, Vol. 35, No. 8, pp. 2387-2400, 1999.

Maryland Department of Natural Resources, Water Resources Administration, Stormwater Management Division, *Standards and Specifications for Infiltration Practices*, Maryland Department of Natural Resources, Annapolis, Maryland, 1984.

Maryland Department of the Environment and Center for Watershed Protection, *2000 Maryland Stormwater Design Manual, Volumes I and II*, Maryland Department of the Environment, Baltimore, Maryland, 2000.

Massmann, J.W., Applying groundwater flow models in vapor extraction system design, *ASCE Journal of Environmental Engineering*, Vol. 115, pp. 129-149, 1989.

Massmann, J.W. and L. Johnson, A set of exercises illustrating flow in porous media, *Ground Water*, Volume 34(4), July-August, pp. 499-503, 2001.

Mays, L.W., *Water Resources Handbook*, McGraw-Hill, 1996.

McDonald M.G. and A.W. Harbaugh, A modular three-dimensional finite-difference ground-water flow model, *Techniques of Water-Resources Investigations of the United States Geological Survey. Book 6, Modeling techniques ; chapter A1*, U.S. Geological Survey, 1988.

Meyer, P.D., M.L. Rockhold, and G.W. Gee, *Uncertainty Analyses of Infiltration and Subsurface Flow and Transport for SDMP Sites*, Pacific Northwest National Laboratory, 1997.

National Oceanic and Atmospheric Administration, 2000
http://www.seawfo.noaa.gov/climate/olympia/2000/OCT2000/103100.cli

Rawls, W.J., and D.L. Brakensiek, *Prediction of Soil Water Properties for Hydrologic Modeling*, Watershed Management in the Eighties, ASCE, 1985.

Rawls, W.J., D.L. Brakensiek and K.E. Saxton, *Estimation of Soil Water Properties*, Transations of the ASAE, 1982.

Salvucci, G.D. and D. Entekhabi, Explicit expressions for Green-Ampt (delta function diffusivity) infiltration rate and cumulative storage, *Water Resources Research*, Vol. 30, No. 9, pp. 2661-2663, 1994.

Schuh, W.M., Seasonal Variation of Clogging of an Artificial Recharge Basin in a Northern Climate, *Journal of Hydrology* 120 (1-4): pp 193-215, 1990

Springer, D.S., H.A. Loaiciga, S.J. Cullen, and L.G. Everett, Air permeability of porous materials under controlled laboratory conditions, *Ground Water*, Vol. 36, No. 4, pp. 558-565, 1998.

Stahre P. and B. Urbonas, *Stormwater detention for drainage, water quality, and CSO management*, Prentice Hall Englewood Cliffs, N.J, 1990.

Stolar, S., M.S. Evaluation of Factors Affecting Infiltration Pond Performance, MS Thesis, Department of Civil and Environmental Engineering, University of Washington, 2001.

Stonestrom, D.A. and J. Rubin, *Air permeability and trapped-air content in two soils*, Water Resource. Resources., Vol. 25, No. 9, pp. 1959-1969, 1989.

Van Genuchten, M.T., A closed-form equation for predicting the hydraulic conductivity of unsaturated soils, *Soil Science Society of America Journal*, Vol. 44 (5), pp. 892-898, 1980.

Ward, A.D. and W.J. Elliot, *Environmental Hydrology*, Lewis Publishers, 1995.

Washington Department of Ecology, *Stormwater Management Manual for Western Washington: Volume III -- Hydrologic Analysis and Flow Control Design/BMPs*, Publication 99-13, August, 2001.

Water Environment Federation, *WEF Manual of Practice #23, Urban Runoff Quality Management*, Water Environment Federation & ASCE, 1998.

Wiltsie, E., *Stormwater Facilities Performance Study, Infiltration Pond Testing and Data Evaluation, Thurston County, Washington*, August 10, 1998.

Appendix A—Data Used in Regressions for Synthetic Soil Samples

	Soil Texture Mixture								
Sample	% 16	% 50	% 125	% Flour	K_{air} (cm/s)	D10	D60	D90	K_{sat} (cm/s)
1a	100	0	0	0	6.50E-02	0.88	1.2	1.6	9.75E-01
1b	95	0	0	5	3.50E-02	0.82	1.2	1.6	5.25E-01
1c	90	0	0	10	2.20E-02	0.42	1.2	1.6	3.30E-01
1d	85	0	0	15	1.10E-02	0.025	1.1	1.6	1.65E-01
1e	80	0	0	20	4.30E-03	0.014	1.1	1.6	6.45E-02
2a	0	100	0	0	2.70E-03	0.19	0.32	0.38	4.05E-02
2b	0	95	0	5	1.10E-03	0.17	0.31	0.38	1.65E-02
2c	0	90	0	10	3.50E-04	0.1	0.3	0.38	5.25E-03
2d	0	85	0	15	9.90E-05	0.025	0.29	0.38	1.49E-03
2e	0	80	0	20	4.20E-05	0.014	0.28	0.38	6.30E-04
3a	0	0	100	0	3.80E-04	0.034	0.08	0.1	5.70E-03
3b	0	0	95	5	2.50E-04	0.03	0.08	0.1	3.75E-03
3c	0	0	90	10	1.60E-04	0.022	0.078	0.1	2.40E-03
3d	0	0	85	15	1.20E-04	0.014	0.073	0.097	1.80E-03
3e	0	0	80	20	7.50E-05	0.009	0.07	0.096	1.13E-03
4a	40	20	40	0	3.70E-03	0.046	0.42	1.3	5.55E-02
4b	38	19	38	5	2.10E-03	0.038	0.38	1.3	3.15E-02
4c	36	18	36	10	1.00E-04	0.031	0.35	1.3	1.50E-03
4d	34	17	34	15	4.50E-05	0.02	0.31	1.2	6.75E-04
4e	32	16	32	20	2.70E-05	0.012	0.29	1.2	4.05E-04
5a	20	60	20	0	2.20E-03	0.07	0.32	1	3.30E-02
5b	19	57	19	5	2.40E-04	0.05	0.31	1	3.60E-03

5c	18	54	18	10	1.30E-04	0.035	0.3	1	1.95E-03
5d	17	51	17	15	4.90E-05	0.024	0.28	1	7.35E-04
5e	16	48	16	20	3.30E-05	0.014	0.28	1	4.95E-04
6a	20	40	40	0	1.40E-03	0.046	0.28	1.1	2.10E-02
6b	19	38	38	5	2.30E-04	0.04	0.27	1.1	3.45E-03
6c	18	36	36	10	1.00E-04	0.032	0.26	1.1	1.50E-03
6d	17	34	34	15	6.30E-05	0.02	0.25	1.1	9.45E-04
6e	16	32	32	20	4.30E-05	0.012	0.24	1	6.45E-04
7a	20	20	60	0	4.80E-04	0.04	0.17	1	7.20E-03
7b	19	19	57	5	2.80E-04	0.035	0.1	1	4.20E-03
7c	18	18	54	10	1.64E-04	0.03	0.1	1	2.46E-03
7d	17	17	51	15	1.00E-04	0.017	0.096	1	1.50E-03
7e	16	16	48	20	4.80E-05	0.01	0.095	1	7.20E-04
8a	60	20	20	0	1.30E-02	0.07	1	1.5	1.95E-01
8b	57	19	19	5	9.40E-03	0.05	1	1.5	1.41E-01
8c	54	18	18	10	6.40E-03	0.036	0.95	1.4	9.60E-02
8d	51	17	17	15	1.50E-04	0.024	0.9	1.3	2.25E-03
8e	48	16	16	20	1.20E-04	0.014	0.9	1.3	1.80E-03
9a	40	40	20	0	1.50E-02	0.07	0.43	1.2	2.25E-01
9b	38	38	19	5	1.50E-03	0.05	4	1.2	2.25E-02
9c	36	36	18	10	7.50E-05	0.035	0.35	1.2	1.13E-03
9d	34	34	17	15	3.50E-03	0.023	0.34	1.1	5.25E-02
9e	32	32	16	20	4.30E-05	0.014	0.33	1.1	6.45E-04
10a	33	33	33	0	9.90E-04	0.05	0.36	1.2	1.49E-02
10b	32	32	32	4	2.00E-04	0.042	0.35	1.2	3.00E-03
10c	30	30	30	10	5.70E-05	0.032	0.32	1.1	8.55E-04
10d	28	28	28	16	5.30E-05	0.019	0.3	1.1	7.95E-04
10e	27	27	27	19	3.10E-05	0.014	0.3	1.1	4.65E-04
11a	0	25	75	0	4.00E-04	0.035	0.093	0.3	6.00E-03

11b	0	75	25	0	9.50E-04	0.06	0.28	0.37	1.43E-02
11c	25	0	75	0	2.40E-04	0.035	0.093	1.1	3.60E-03
11d	75	0	25	0	5.00E-03	0.06	1	1.5	7.50E-02
11e	25	75	0	0	2.10E-03	0.2	0.35	1.1	3.15E-02
11f	75	25	0	0	1.50E-03	0.26	1	1.5	2.25E-02
12a	50	50	0	0	4.60E-03	0.23	0.94	1.2	6.90E-02
12b	0	50	50	0	3.70E-04	0.04	0.23	0.35	5.55E-03
12c	50	0	50	0	7.00E-04	0.04	0.94	1.2	1.05E-02
13a	80	20	0	0	1.50E-02	0.3	1	1.5	2.25E-01
13b	85	10	5	0	3.00E-02	0.3	1	1.5	4.50E-01
13c	85	10	0	5	2.10E-02	0.3	1	1.5	3.15E-01
13d	90	10	0	0	4.50E-02	0.43	0.95	1.5	6.75E-01
13e	95	5	0	0	5.20E-02	0.83	0.95	1.5	7.80E-01
14a	95	0	5	0	3.90E-02	0.83	1	1.4	5.85E-01
14b	95	0	0	5	3.50E-02	0.83	1	1.4	5.25E-01
14c	75	15	10	0	2.00E-02	0.11	1	1.4	3.00E-01
14d	80	10	10	0	2.00E-02	0.11	1	1.4	3.00E-01
14e	80	10	0	10	1.20E-02	0.075	1	1.4	1.80E-01
15a	85	5	5	5	2.00E-02	0.11	1	1.6	3.00E-01
15b	85	15	0	0	4.00E-02	0.31	1	1.6	6.00E-01

Appendix B — Measured Air Conductivity and the Corresponding Saturated Hydraulic Conductivity for Soil Samples Collected at Field Sites

Site	Test Pit# layer (#) depth"	K_{air} (cm/s)	K_{air} (cm/hr)	K_{equiv} (cm/hr)	$K_{average}$ (cm/hr)	K_w (cm/hr)
Clark County	TH1 (1) 14"	1.00E-03	3.60E+00			
	TH2 (1) 10"	9.20E-04	3.31E+00			
	TH3 (1) 9"	5.50E+04	1.98E+08			
	TH4 (1) 6"	1.30E-03	4.68E+00	5	5	55
Beaverdam, King County	TH1 (1) 4"	7.00E-02	2.52E+02			
	TH1 (2) 6"	5.90E-03	2.12E+01			
	TH1 (3) 3"	6.00E-02	2.16E+02	42		
	TH2 (1) 4"	2.50E-03	9.00E+00			
	TH2 (2) 4"	7.30E-02	2.63E+02			
	TH2 (3) 4"	6.50E-02	2.34E+02	25		
	TH3 (1) 4"	2.50E-03	9.00E+00			
	TH3 (2) 12"	6.60E-02	2.38E+02	32		
	TH4 (1) 4"	2.50E-03	9.00E+00			
	TH4 (2) 8"	5.90E-02	2.12E+02	25	31	357
Balsam 7-11, Kitsap Co.	TH1 (1) 10"	2.90E-03	1.04E+01			
	TH1 (2) 18"	5.00E-05	1.80E-01	0		
	TH2 (1) 7"	5.40E-04	1.94E+00			
	TH2 (2) 14"	3.90E-03	1.40E+01			
	TH2 (3) 24"	2.70E-03	9.72E+00	6	3	38
Krista Firs, Kitsap Co.	TH1 (1) 13"	6.20E-03	2.23E+01	22		
	TH1 (2) 14"	Too fast to measure.				
	TH2 (1) 27"	3.80E-03	1.37E+01			
	TH2 (2) 30"	2.00E-03	7.20E+00	9		
	TH3 (1) 10"	1.40E-02	5.04E+01	50	27	314
Airdustrial, Th. Co.	TH1 (1) 67"	5.10E-03	1.84E+01	18		
	TH2 (1) 48"	2.50E-03	9.00E+00	9	14	157
Bush, Th. Co.	TH1 (1) 20"	7.50E-03	2.70E+01			
	TH1 (2) 20"	7.50E-03	2.70E+01			
	TH1 (3) 35"	1.90E-02	6.84E+01	38		
	TH2 (1) 33"	1.50E-02	5.40E+01			
	TH2 (2) 30"	9.00E-03	3.24E+01	43	40	463
Echo Glen, Th. Co.	TH1 (2) 7"	1.10E-02	3.96E+01			
	TH1 (3) 14"	Too fast to measure.				
	TH1 (4) 12"	Too fast to measure.				
	TH1 (5) 7"	4.00E-02	1.44E+02	62	62	714
Lacey Lid, Th. Co.	TH1 (1) 69"	2.00E-03	7.20E+00	7		
	TH2 (1) 50"	3.60E-03	1.30E+01	13	10	116
Margaret McKenny, Th. Co.	TH1 (1) 22"	5.90E-03	2.12E+01			
	TH1 (2) 20"	9.20E-03	3.31E+01			
	TH1 (3) 12"	6.00E-03	2.16E+01	25	25	283

Ridgeview, Th. Co.	TH1 (1) 32"	Too fast to measure.				
	TH1 (2) 5"	3.40E-02	1.22E+02			
	TH1 (3) 11"	Too fast to measure.				
	TH1 (4) 15"	5.70E-03	2.05E+01			
	TH2 (1) 35"	Too fast to measure.				
	TH2 (2) 12"	Too fast to measure.				
	TH2 (3) 15"	Too fast to measure.				
	TH3 (1) 60"	Too fast to measure.		26	26	298
Springfield, Th. Co.	TH1 (1) 13"	3.40E-04	1.22E+00			
	TH1 (2) 8"	1.10E-03	3.96E+00			
	TH1 (3) 10"	3.20E-03	1.15E+01	2		
	TH2 (1) 9"	3.50E-04	1.26E+00			
	TH2 (2) 6"	2.00E-03	7.20E+00			
	TH2 (3) 17"	2.20E-03	7.92E+00	3		
	TH3 (1) 14"	2.50E-04	9.00E-01			
	TH3 (2) 8"	1.00E-02	3.60E+01			
	TH3 (3) 7"	7.80E-03	2.81E+01	2		
	TH4 (1) 18"	4.00E-04	1.44E+00			
	TH4 (2) 8"	7.40E-03	2.66E+01	2	2	27
State Farm, Th. Co.	TH1 (1) 38"	5.40E-03	1.94E+01			
	TH1 (2) 27"	2.80E-03	1.01E+01	14	14	161
Sweetbriar, Th. Co.	TH1 (1) 36"	1.40E-03	5.04E+00			
	TH1 (2) 9"	3.80E-04	1.37E+00			
	TH1 (3) 24"	3.00E-02	1.08E+02	5		
	TH2 (1) 36"	1.10E-03	3.96E+00			
	TH2 (2) 30"	1.40E-03	5.04E+00	4	5	54
Westwood Baptist, Th. Co.	TH1 (1) 11"	5.10E-04	1.84E+00			
	TH1 (2) 10"	4.40E-04	1.58E+00			
	TH1 (3) 6"	4.00E-03	1.44E+01	2		
	TH2 (1) 15"	1.30E-04	4.68E-01			
	TH2 (2) 6"	1.20E-03	4.32E+00			
	TH2 (3) 5"	1.20E-02	4.32E+01	1		
	TH3 (1) 6"	1.70E-04	6.12E-01			
	TH3 (2) 6"	8.50E-03	3.06E+01			
	TH3 (3) 16"	1.50E-03	5.40E+00	2		
	TH4 (1) 10"	2.20E-03	7.92E+00			
	TH4 (2) 10"	2.80E-04	1.01E+00			
	TH4 (3) 11"	6.50E-04	2.34E+00	2		
	TH5 (1) 4"	2.20E-04	7.92E-01			
	TH5 (2) 14"	3.40E-03	1.22E+01	3		
	TH6 (1) 6"	5.70E-04	2.05E+00	2	2	23
Woodard Glen, Th. Co.	TH1 (1) 15"	1.40E-02	5.04E+01			
	TH1 (2) 28"	5.80E-03	2.09E+01	26		
	TH2 (1) 36"	2.70E-03	9.72E+00			
	TH2 (2) 6"	1.80E-03	6.48E+00	9	18	203

Appendix C—Grain Size Curves for Synthetic and Natural Soils

C.1 Grain Size Curves for Synthetic Soil Samples

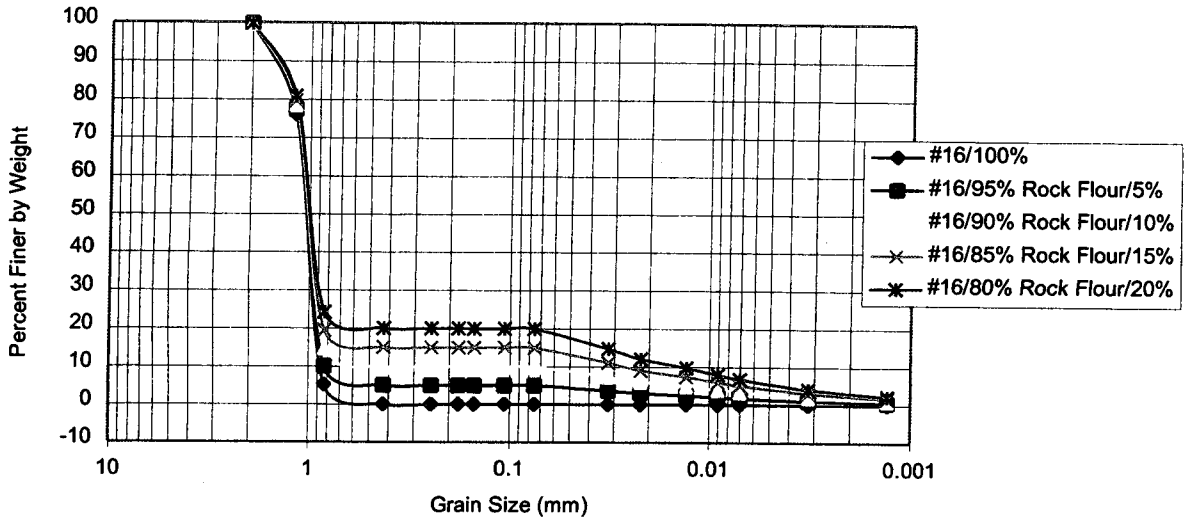

Figure C.1 – Grain size distribution for #16 synthetic soil

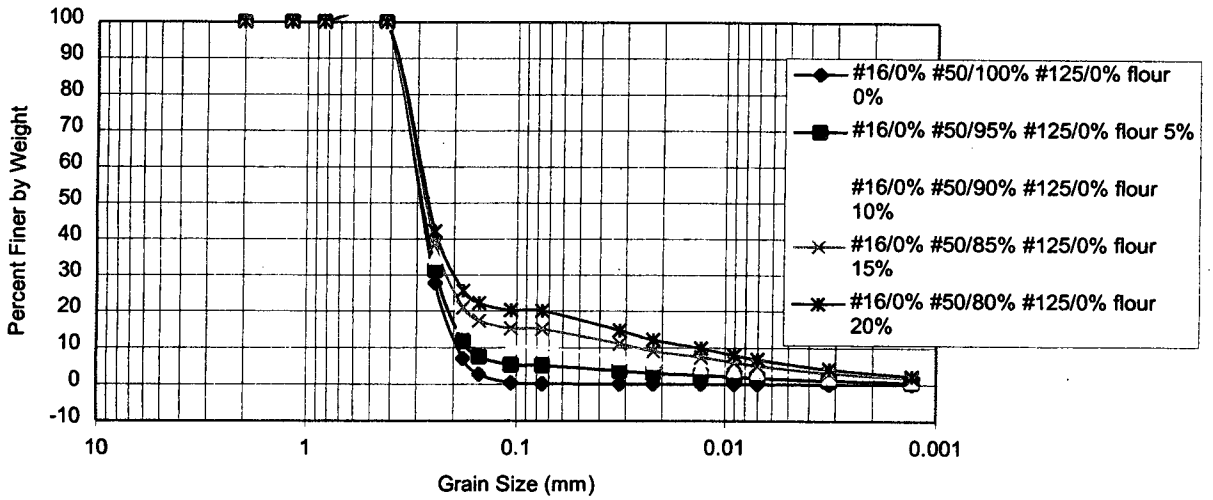

Figure C.2 – Grain size distribution for #50 synthetic soil

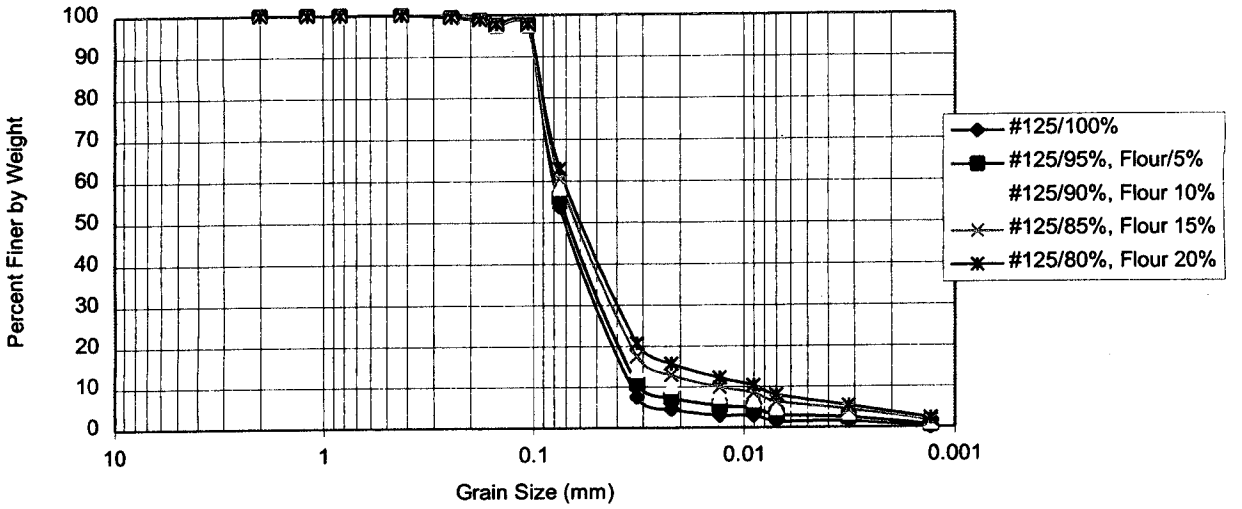

Figure C.3 – Grain size distribution for #125 synthetic soil

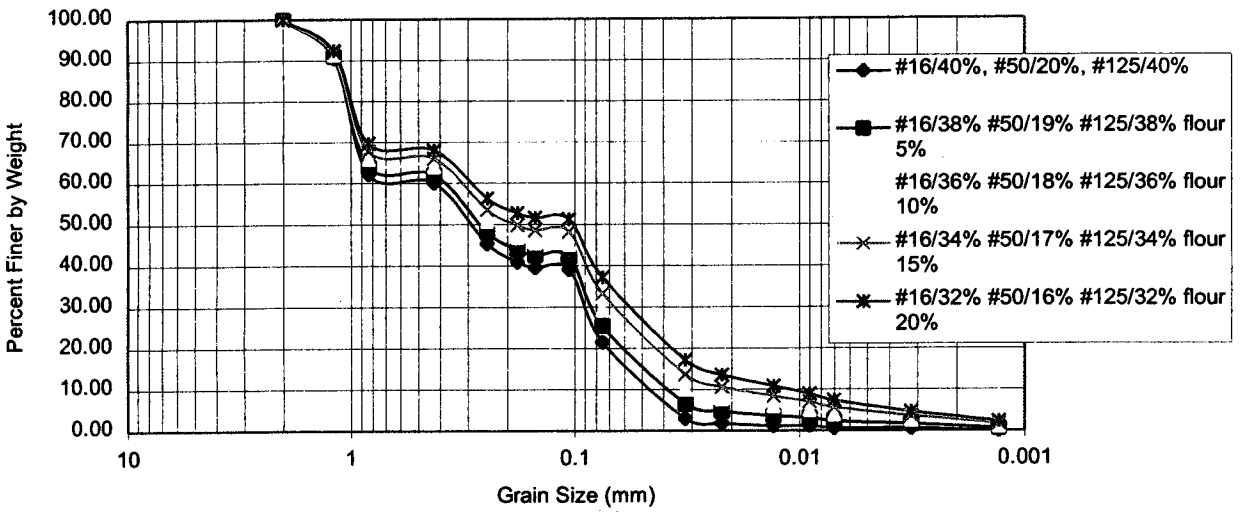

Figure C.4 – Grain size distribution for #16/40% #50/20% #125/40% synthetic soil

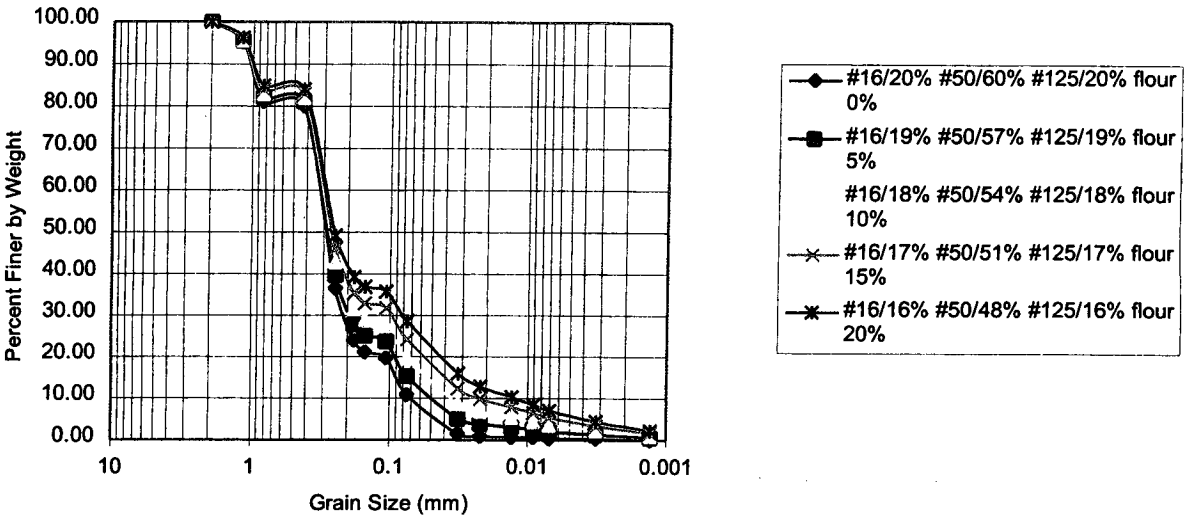

Figure C.5 – Grain size distribution for #16/20% #50/60% #125/20% synthetic soil

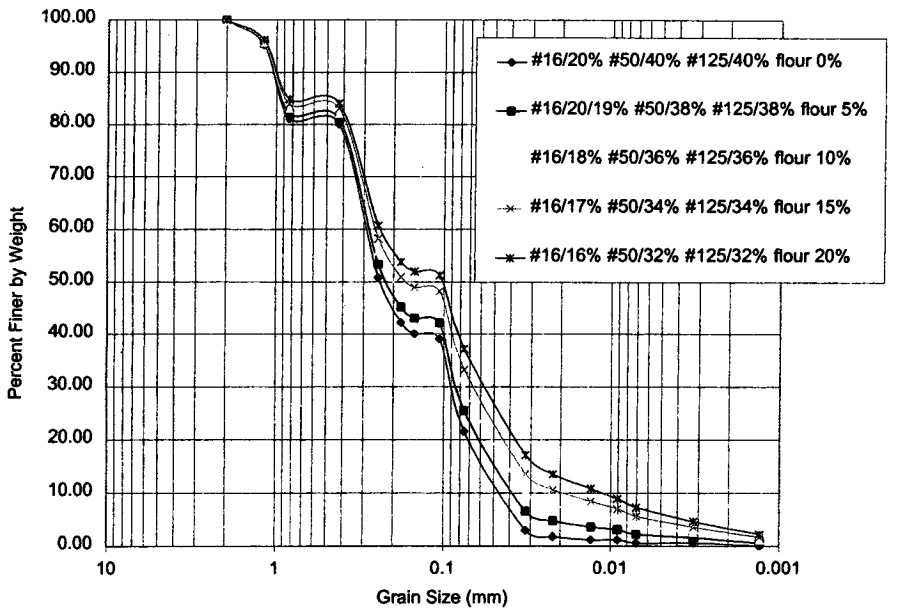

Figure C.6 – Grain size distribution for #16/20% #50/40% #125/40% synthetic soil

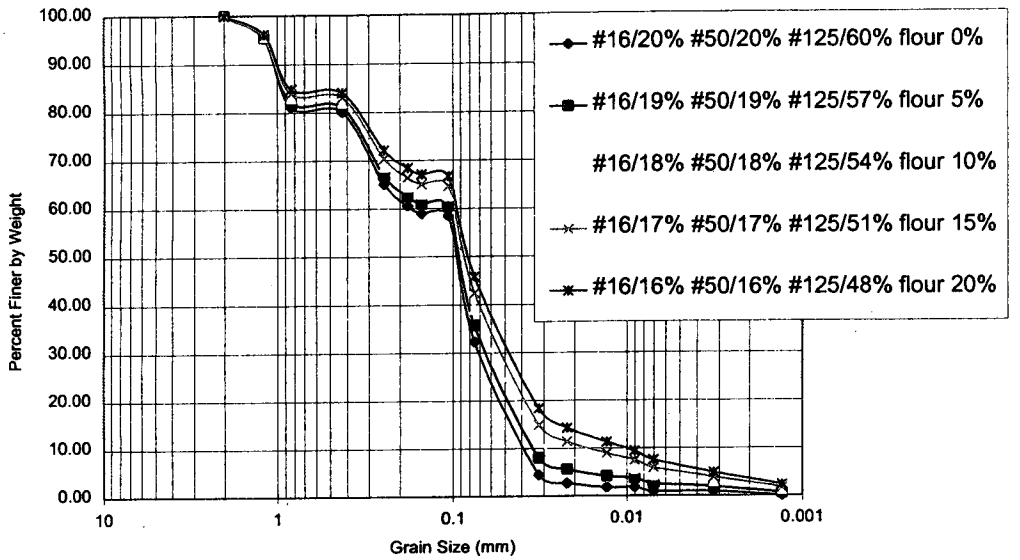

Figure C.7 – Grain size distribution for #16/20% #50/20% #125/60% synthetic soil

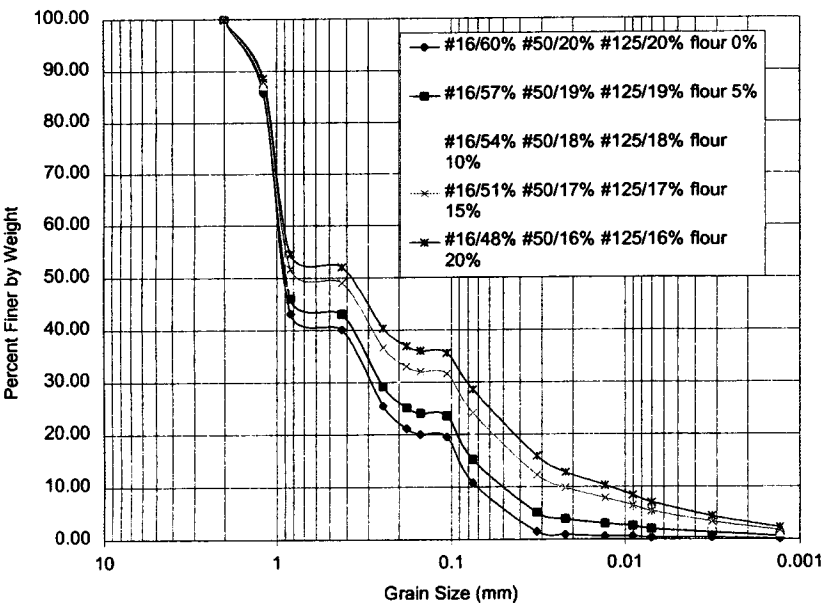

Figure C.8 – Grain size distribution for #16/60% #50/20% #125/20% synthetic soil

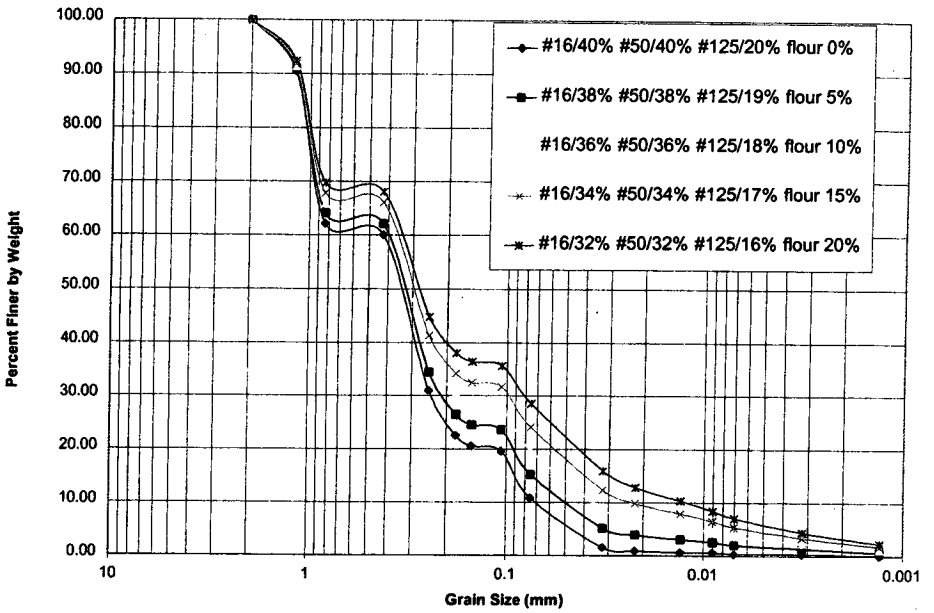

Figure C.9 – Grain size distribution for #16/40% #50/40% #125/20% synthetic soil

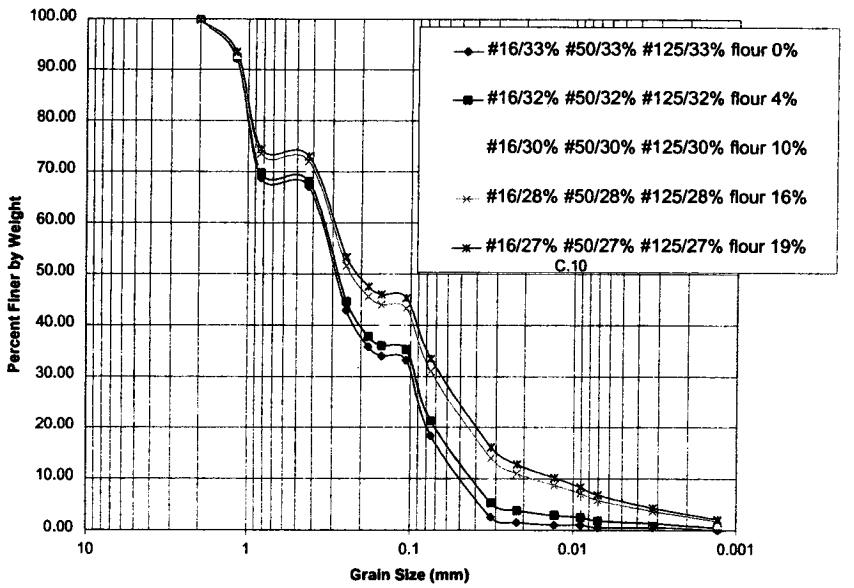

Figure C.10 – Grain size distribution for #16/33% #50/33% #125/33% synthetic soil

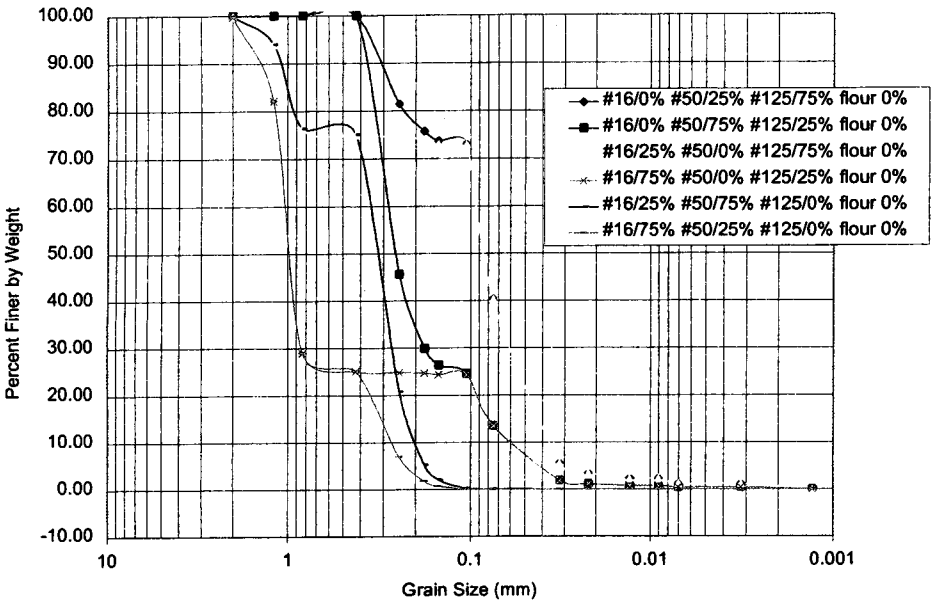

Figure C.11 – Grain size distribution for 25%-75% synthetic soil

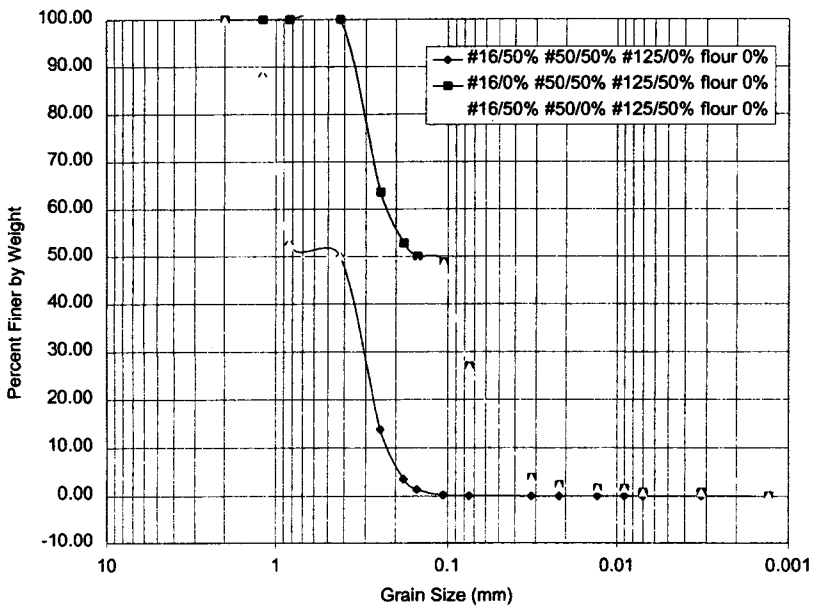

Figure C.12 – Grain size distribution for 50%-50% synthetic soil

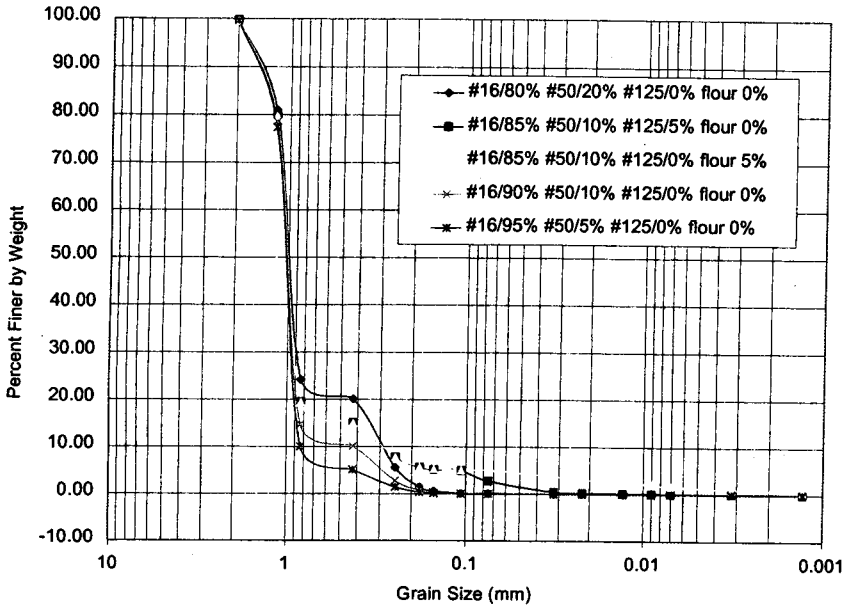

Figure C.13 – Grain size distribution for Mixed Synthetic Samples synthetic soil

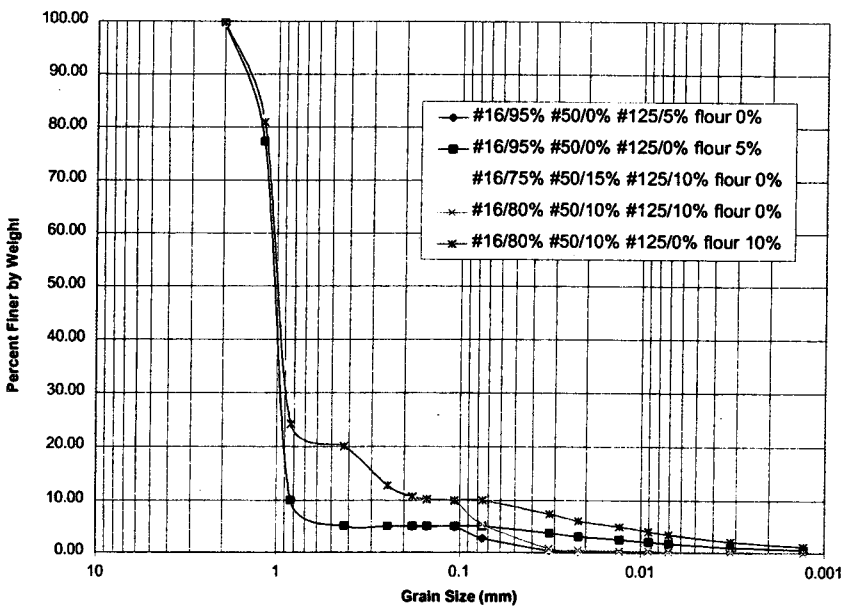

Figure C.14 – Grain size distribution for Mixed Synthetic Samples synthetic soil

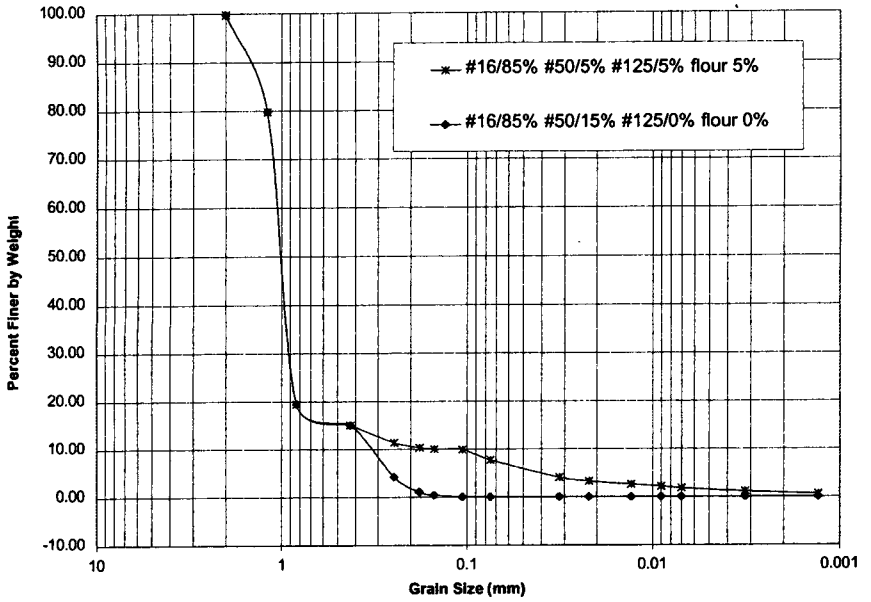

Figure C.15 – Grain size distribution for Mixed Synthetic Samples synthetic soil

C.2 Grain Size Curves for Natural Samples

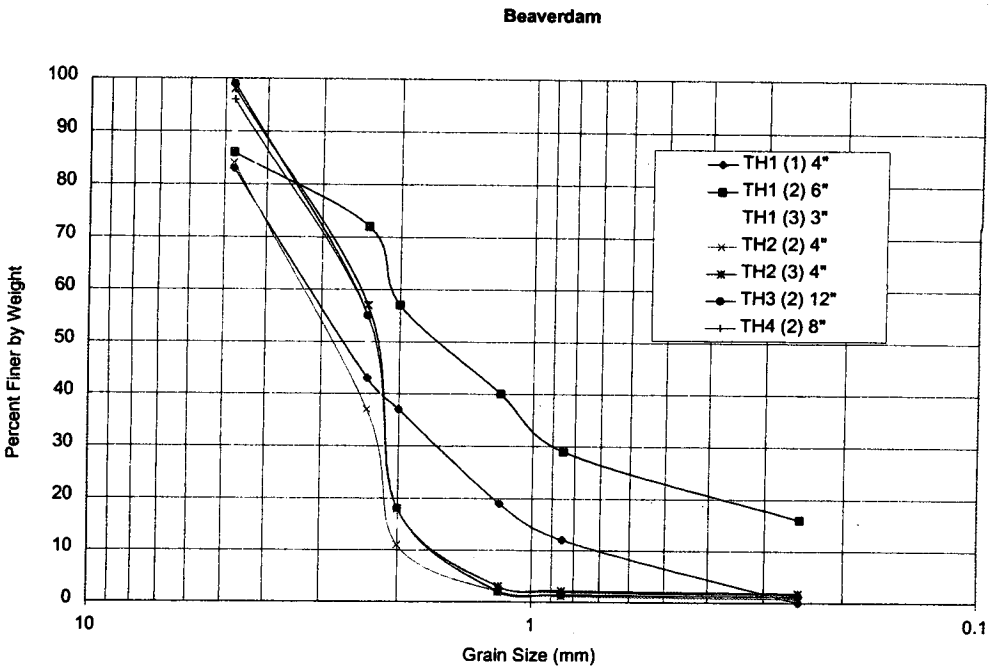

Figure C.16 – Grain size distribution for Beaverdam, King County pond

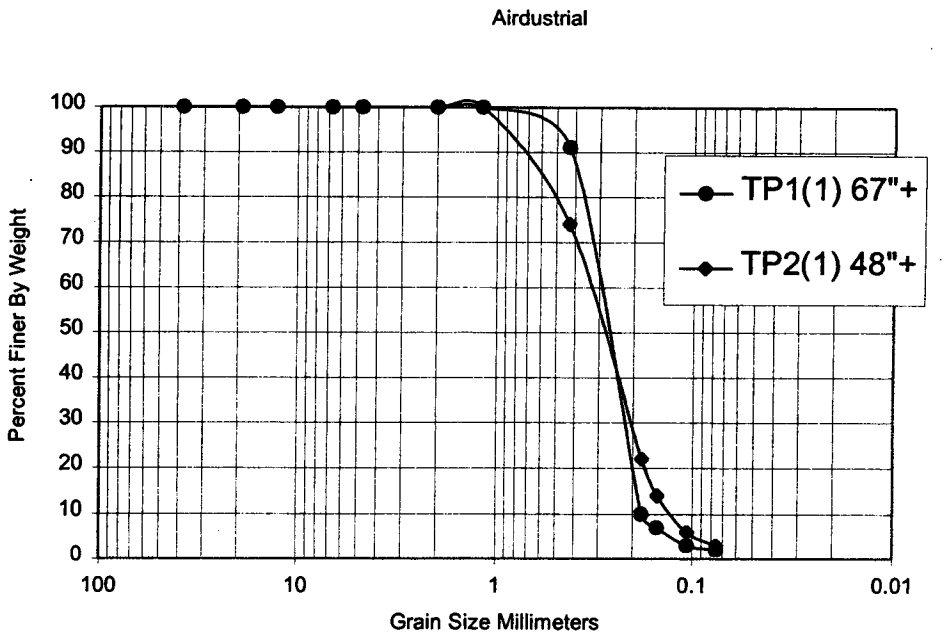

Figure C.17 – Grain size distribution for Airdustrial, Thurston County infiltration pond

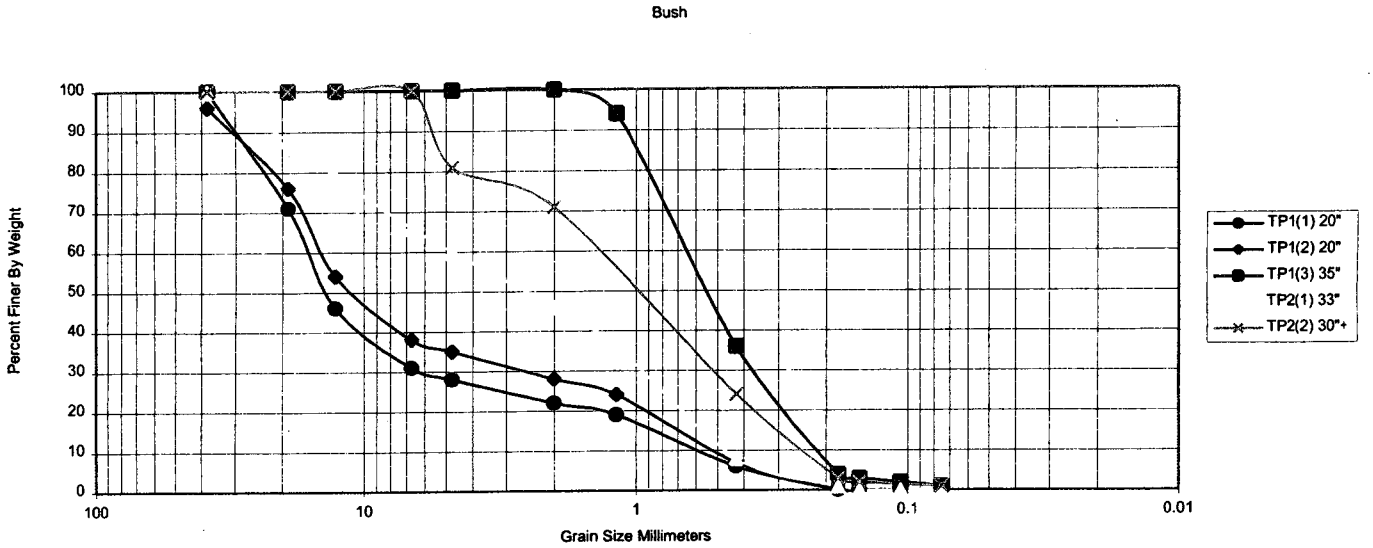

Figure C.18 – Grain size distribution for Bush, Thurston County infiltration pond

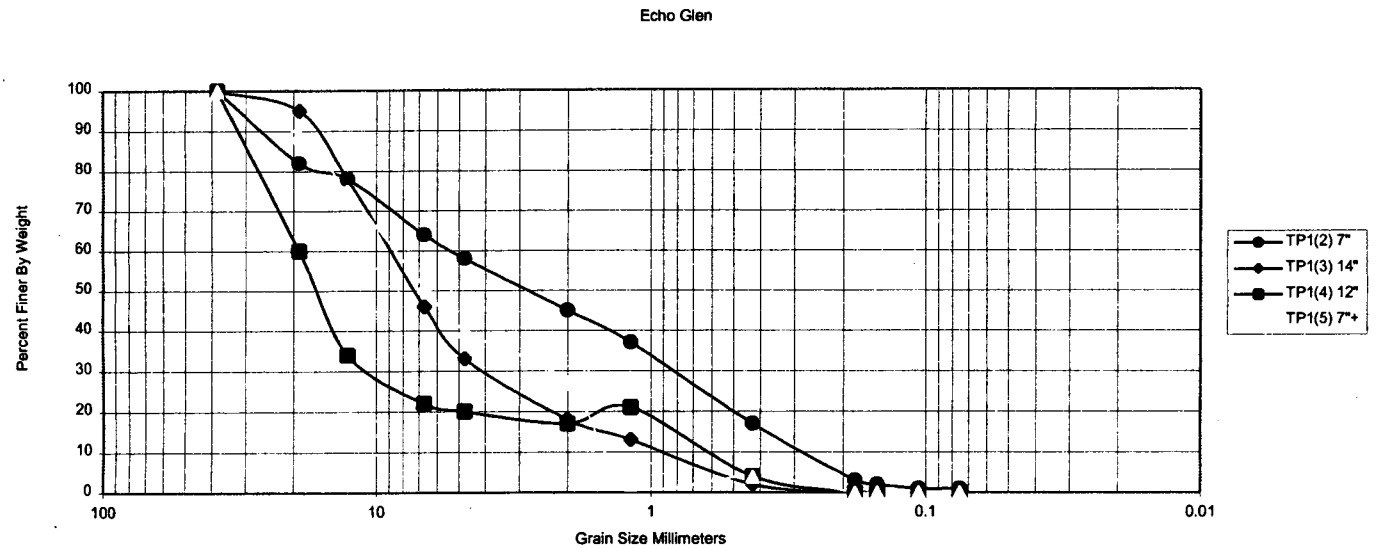

Figure C.19 – Grain size distribution for Echo Glen, Thurston County infiltration pond

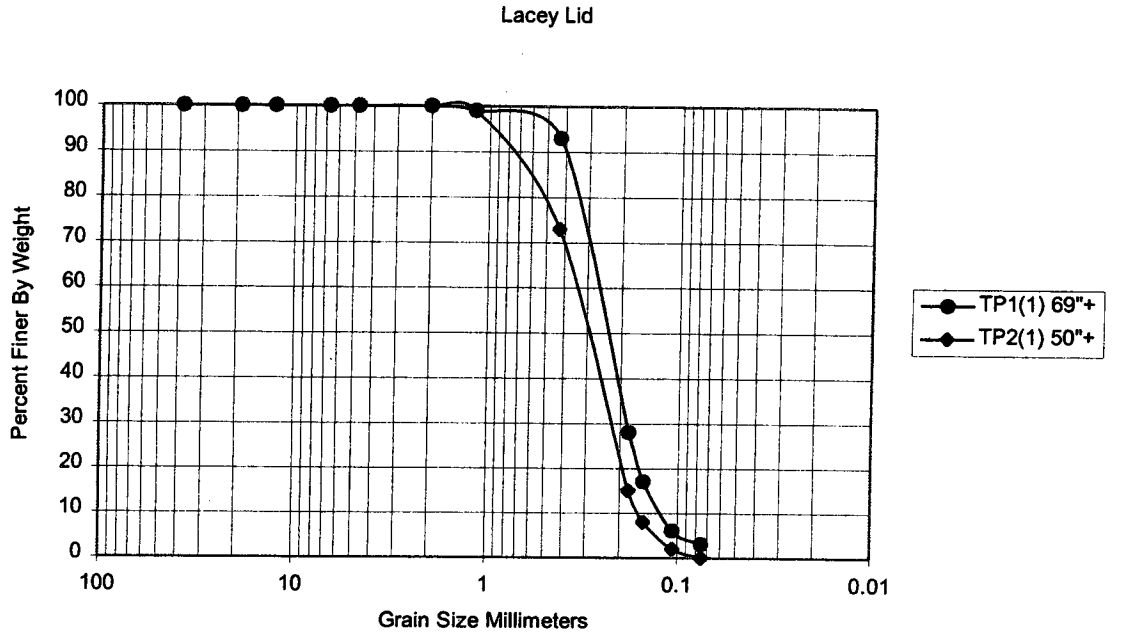

Figure C.20 – Grain size distribution for Lacy Lid, Thurston County infiltration pond

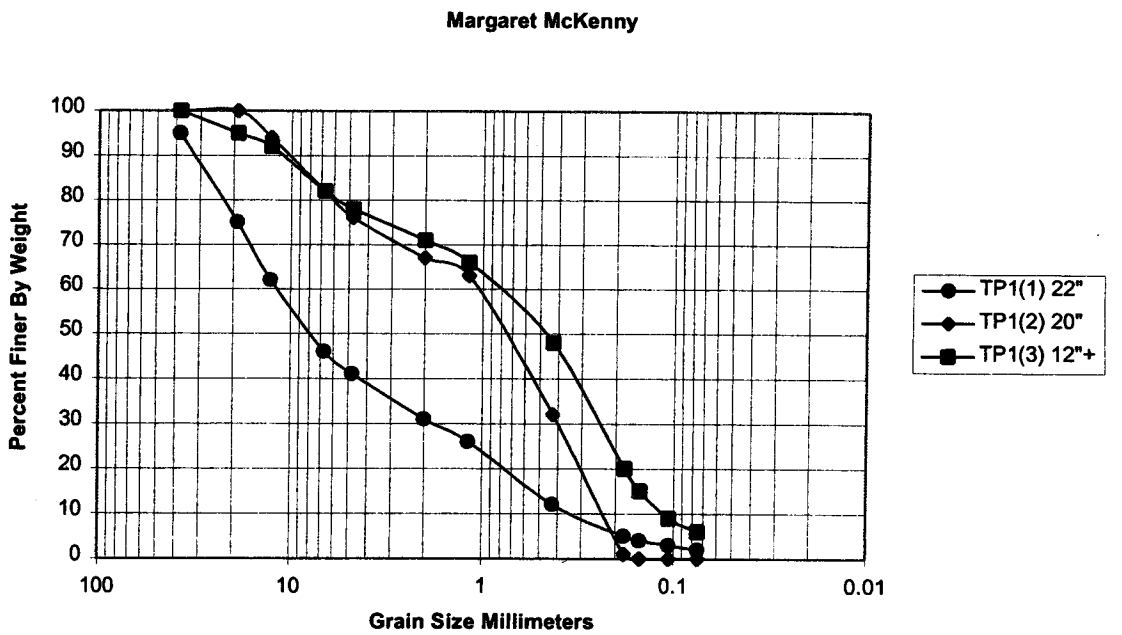

Figure C.21 – Grain size distribution for Margaret McKenny, Thurston County infiltration pond

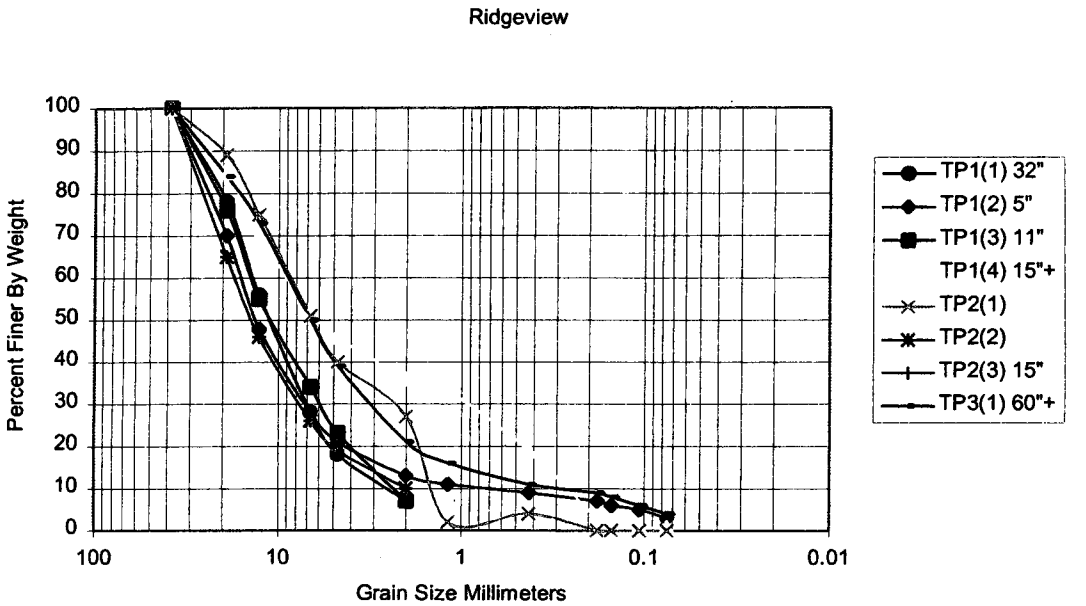

Figure C.22 – Grain size distribution for Ridgeview, Thurston County infiltration pond

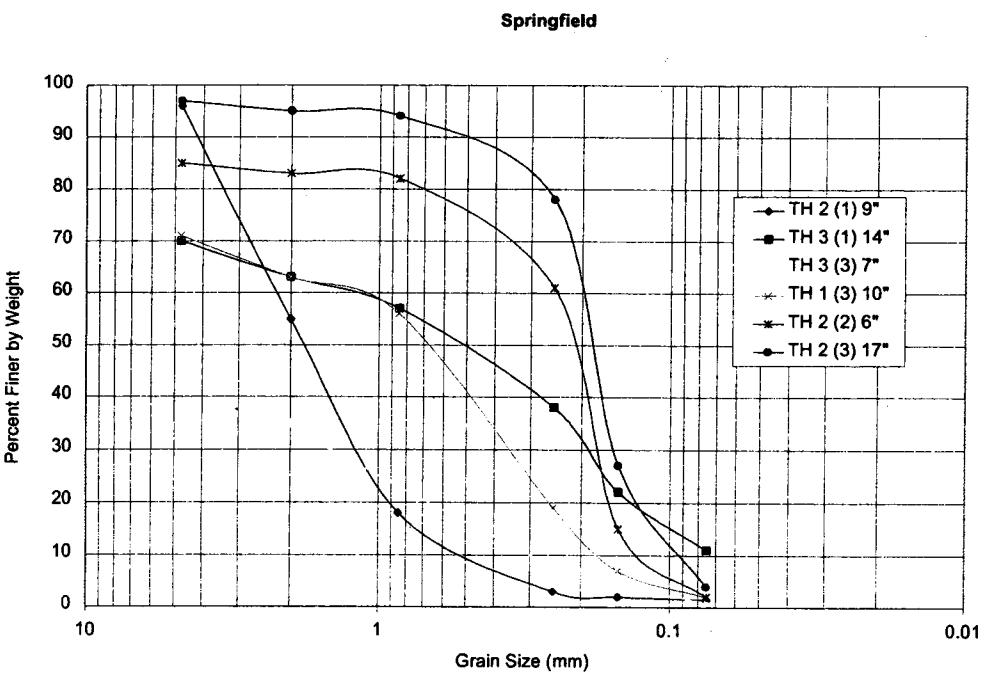

Figure C.23 – Grain size distribution for Springfield, Thurston County infiltration pond

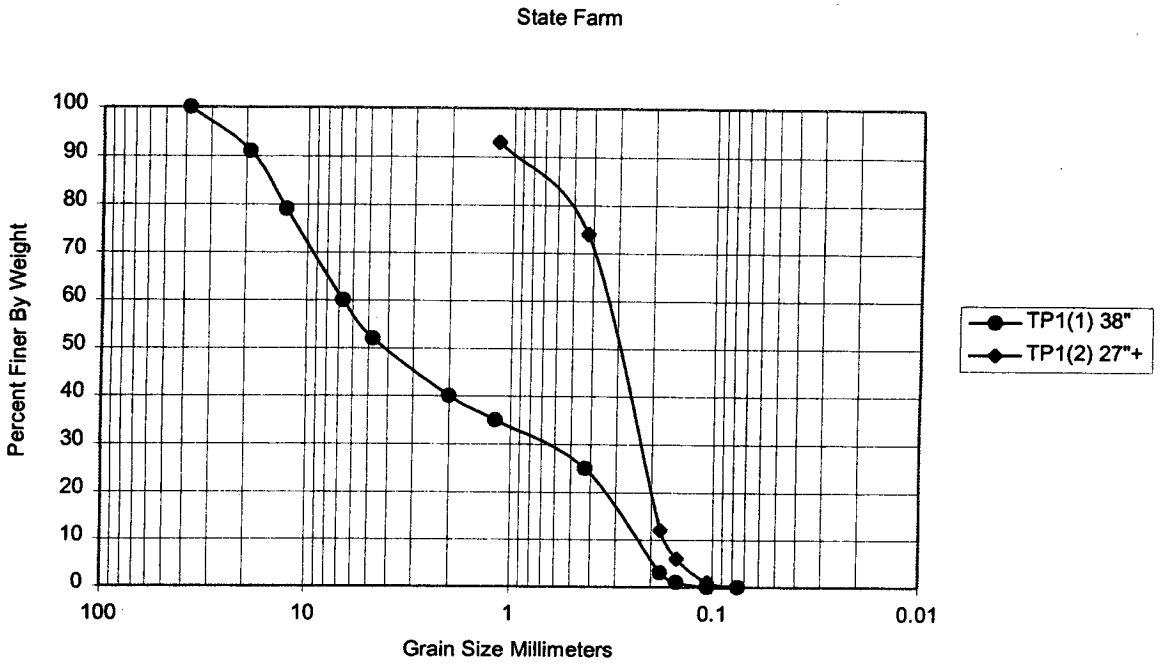

Figure C.24 – Grain size distribution for State Farm, Thurston County infiltration pond

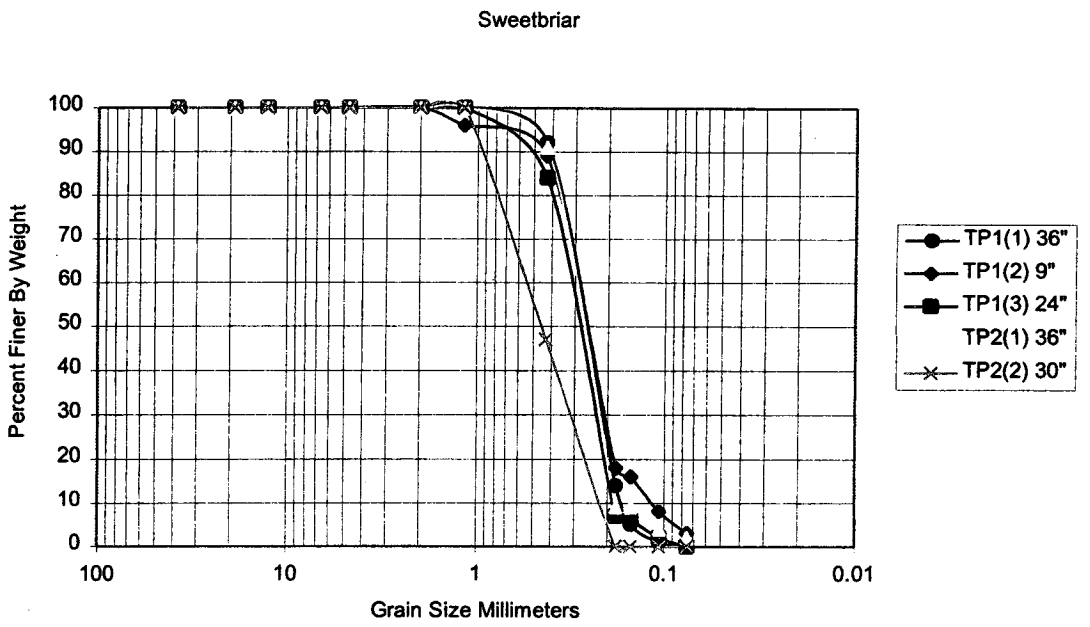

Figure C.25 – Grain size distribution for Sweetbriar, Thurston County infiltration pond

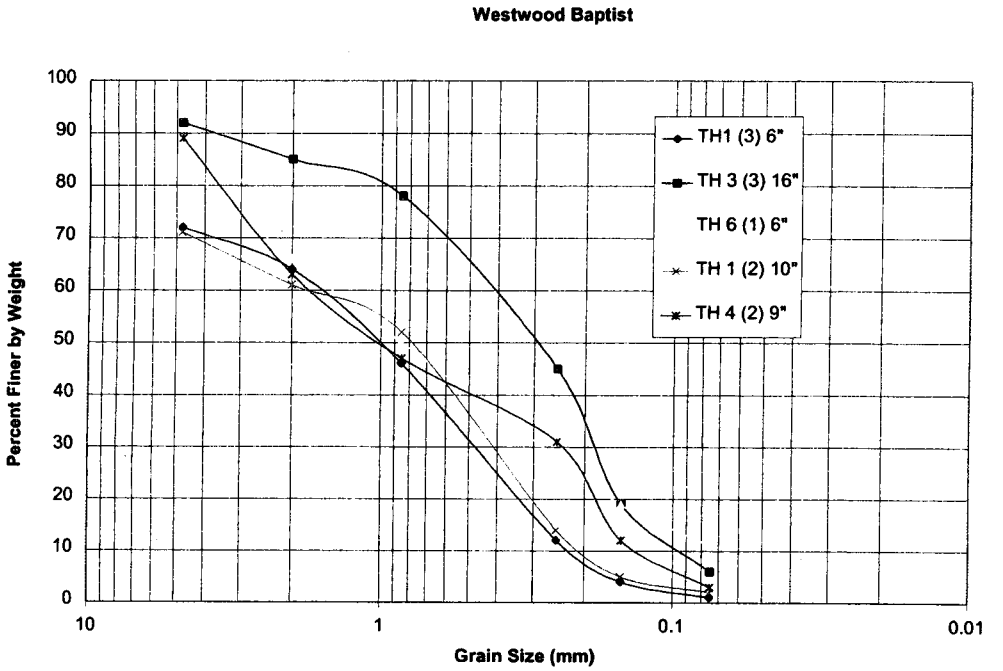

Figure C.26 – Grain size distribution for Westwood Baptist, Thurston County infiltration pond

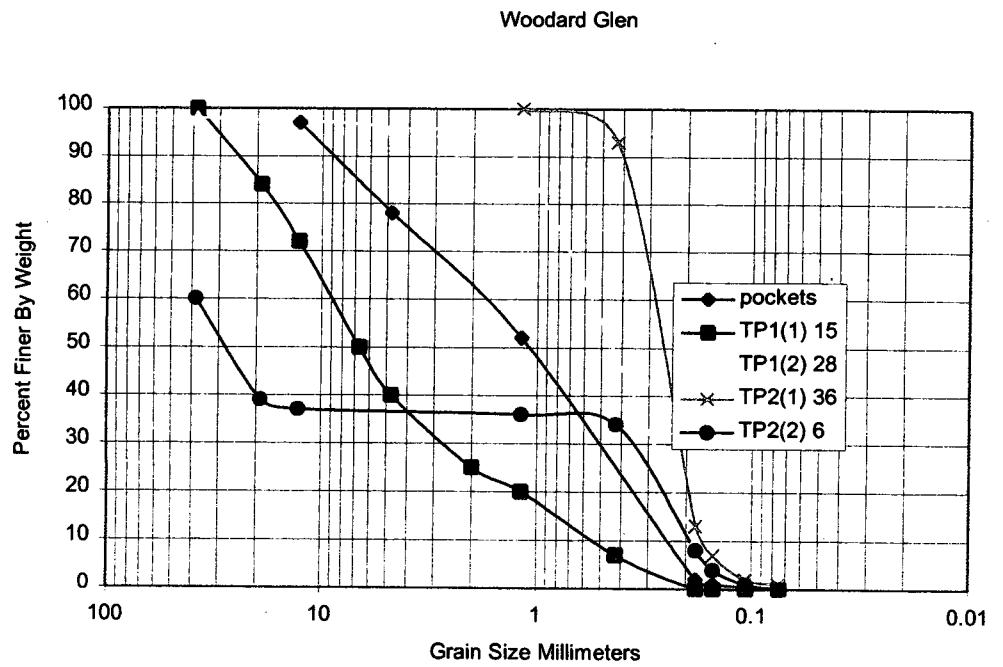

Figure C.27 – Grain size distribution for Woodward Glen, Thurston County infiltration pond

Appendix D—Description of Ponds Used in the Full-Scale Tests

Site Name	Site Address	Pond Age (years)	Pond Bottom Surface Area (ft^2)	Top Surface Area (ft^2)	Pond Volume (ft^3)	Pond Geometry
Clark Co.	Clark Co. 9616 NE 59th Av Vancouver, WA 98686	UNK	1,856	3,148	UNK	Rectangular
Beaverdam	King Co. SE Main St and 244th Av SE	UNK	~5,500	UNK	UNK	Trapezoidal
Balsum 7-11	Kitsap Co. Lund Av SE and Jackson Av Port Orchard, WA 98366	24	1,062	1,742	7200	Rectangular
Kirsta Firs,	Kitsap Co. K.C. Place and Cedar Rd E Port Orchard, WA 98366	23	1,030	2,078	3888	Rectangular
Airdustrial[1]	Thurston Co. Bonniewood Dr SW and 70th Ave Tumwater, WA	7	6,400	10,200	34,000	Rectangular
Bush Middle School[1]	Thurston Co. Kimmie St and 83rd Av Tumwater, WA	10	5,085	11,300	36,866	Triangular
Echo Glen[1]	Thurston Co.	10	7075	30,575	148,296 (wet pond + infiltration pond).	L-shaped.

Lacey Lid[1]	Thurston Co.[1] Yelm Hwy and Corporate Ctr Lacey, WA	10	17,100	53,840	248,276	Rectangular
Margaret McKenny[1]	Thurston Co. Morse-Merryman Rd SE and Quentin St Lacey, WA	10	6,720	19,590	72,352	Rectangular
Ridgeview[1]	Thurston Co. Steilacoom Rd and Sandra Lee Ct Lacey, WA	7	23,265	31,446	93,465	Rectangular
Springfield	Thurston Co. Lilly Rd NE and Maple View Dr Olympia, WA	N/A	1,104	UNK	UNK	Rectangular
State Farm[1]	Thurston Co. Evergreen Park Dr and Heritage Ct Olympia, WA	11	560	2,400	2,960	Small kidney shaped.
Sweetbriar [1]	Thurston Co. Boulevard Rd and 45th Av. SE Lacey, WA	8	15,000	25,800	92,123	Triangular
Westwood Baptist,	Thurston Co. Kaiser Rd and Everygreen Pkwy Olympia, WA	7	171,000	UNK	5,800,000	Baseball field
Woodard Glen[1]	Thurston Co Lister Rd NE and Cherry Blossom Olympia, WA	21	2,000	3,800	8,700	Small trapezoidal

[1] Sites given in the Thurston County Performance Study.

[2] Infiltration Rates calculated using hind-cast analysis.

Site Name	Observed Soil Type	Design Infiltration Rate and Testing Method	Full-scale Infiltration Rate (cm/hr)	Bottom Cover and Condition	Comments
Clark Co.	Loam/Silty loam	UNK		Mostly bare with patches of mixed grasses.	Biofilter
Beaverdam	Sand		5	Gravelly bottom. No vegetation.	Biofilter
Balsum 7-11	Silty Loam	UNK	6	Dense with tall grass. Color and wide leaf vegetation indicate moist/wet conditions.	No pre-treatment. Thick wetland vegetation covers the pond bottom.
Kirsta Firs	Sand	20+"/hr	1	Poor vegetation of mixed grasses, frequent bare area with granular exposed areas.	No pre-treatment.
Airdustrial	Loamy sand	2,84 in/hr.	2	Isolated tufts of grass, bare patches, little top soil, fine sediment coating. Pond bottom silt covered due to failing biofilter swale.	Biofilter swale. Reached groundwater at 5.5 ft in August.
Bush Middle School[1]	Loamy sand	15 in/hr. (infiltrometer)	[2] >25	Mixed grasses, poor vegetation, much bare area, highly granular exposed area.	Bio-filtration swale. Seasonally high groundwater at 2 to 3 ft from pond bottom.
Echo Glen[1]	Sand	6 in/hr.	[2] >34	Sod grass. Full cover/dense.	Wet pond pre-treatment
Lacey Lid[1]	Loamy medium sand	UNK	1	Mixed grasses and moss.	Wet pond pre-treatment. Groundwater reached at 6 ft in August.
Margaret	Gravely sandy	20 in/hr.	4	Scotch broom, hawkweed, mixed	Biofilter.

McKenny[1]	loam			grasses and mosses. Pond bottom had silt covering.	
Ridgeview[1]	Gravely sandy loam	6 in/hr.	[2] >10	Scotch broom and gravel.	Wet pond pre-treatment.
Springfield	Sandy loam, loamy sand	3 in/hr.	38-8, rate dropped as volumne of infiltrated water increased.	Patches of grass and moss.	No pre-treatment. Neighborhood known to have shallow groundwater table in winter.K48
State Farm[1]	Loamy medium sand	20 in/hr. 2 infiltrometer tests.	11	Mixed grasses. Thick vegetation.	No treatment. Water level at 11 to 12 ft.
Sweetbriar[1]	Fine sandy loam	4.8 in/hr.	1	Scotch broom, mixed grasses and moss. Grass with bare patches, little top soil and mossy areas.	No pre-treatment. Groundwater mounding beneath pond bottom.
Westwood Baptist	Loamy sand	6 in/hr.	1	Hard pan layers.	Biofilter. 8 ft to groundwater, 27 ft to till.
Woodard Glen[1]	Loamy sand	UNK	4	Mixed grasses and moss. Bare patches with little topsoil, mossy patches. Moss and fine sediment clogging pond bottom.	No-pretreatment.

Appendix E—Estimated Saturated Hydraulic Conductivity Values for Field Sites Based on Hazen Equation

Site	Layer	Thickness	d_{10}	Kw(cm/s)
Clark County (C=0.6)	TH1(1)	14"	3.0E-03	5.4E-06
	TH2(1)	10"	2.3E-03	3.2E-06
	TH3(1)	9"	5.0E-03	1.5E-05
	TH4(1)	6"	1.3E-03	1.0E-06
Beaverdam, King County (C=1)	TH1(1)	4"	7.0E-01	4.9E-01
	TH1(2)	6"	8.0E-02	6.4E-03
	TH1(3)	3"	6.2E-01	3.8E-01
	TH2(1)	4"	7.0E-01	4.9E-01
	TH2(2)	4"	8.0E-01	6.4E-01
	TH2(3)	4"	5.5E-01	3.0E-01
	TH3(1)	3"	7.0E-01	4.9E-01
	TH3(2)	12"	5.5E-01	3.0E-01
	TH4(1)	6"	7.0E-01	4.9E-01
	TH4(2)	8"	5.5E-01	3.0E-01
Average Kequivalent				
Balsam 7-11, Kitsap County (C=0.6)	TH1(1)	10"	2.0E-03	2.4E-06
	TH1(2)	18"	2.0E-03	2.4E-06
	TH2(1)	7"	3.0E-02	5.4E-04
	TH2(2)	24"	7.0E-03	2.9E-05
	TH2(3)	24"	8.0E-03	3.8E-05
Average Kequivalent				
Krista First, Kitsap County (C=1)	TH1(1)	13"	1.1E-01	1.2E-02
	TH1(2)	13"	4.0E-01	1.6E-01
	TH2(1)	27"	1.4E-01	2.0E-02
	TH2(2)	30"	1.8E-01	3.2E-02
	TH3(1)	10"	2.0E-01	4.0E-02
Average Kequivalent				
Airdustrial, Thurston County (C=0.6)	TH1(1)	67"	2.0E-01	2.4E-02
	TH2(1)	48"	1.3E-01	1.0E-02
Average Kequivalent				
Bush, Thurston County (C=1)	TH1(1)	20"	6.0E-01	3.6E-01
	TH1(2)	20"	5.0E-01	2.5E-01
	TH1(3)	35"	2.1E-01	4.4E-02

	TH2(1)	33"	4.4E-01	1.9E-01
	TH2(2)	30"	2.4E-01	5.8E-02
Average Kequivalent				
Echo Glen, Thurston County (C=1)	TH1(2)	7"	3.0E-01	9.0E-02
	TH1(3)	14"	9.0E-01	8.1E-01
	TH1(4)	12"	6.0E-01	3.6E-01
	TH1(5)	7"	1.3E+00	1.7E+00
Average Kequivalent				
Lacey Lid, Thurston County(C=0.8)	TH1(1)	69"	1.1E-01	9.7E-03
	TH2(1)	50"	1.6E-01	2.0E-02
Average Kequivalent				
Margaret McKenny, Thurston County (C=1)	TH1(1)	22"	3.4E-01	1.4E-01
	TH1(2)	20"	2.3E-01	6.3E-02
	TH1(3)	12"	1.1E-01	1.5E-02
Average Kequivalent				
Ridgeview, Thurston County (C=1.2)	TH1(1)	32"	2.4E+00	6.9E+00
	TH1(2)	5"	6.0E-01	4.3E-01
	TH1(3)	11"	2.2E+00	5.8E+00
	TH1(4)	15"	2.5E-01	7.5E-02
	TH2(1)	35"	1.4E+00	2.4E+00
	TH2(2)	14"	6.0E-01	4.3E-01
	TH2(3)	15"	2.0E+00	4.8E+00
	TH3(1)	60"	3.0E-01	1.1E-01
Average Kequivalent				
Springfield, Thurston County (C=1)	TH1(1)	13"	5.0E-02	2.5E-03
	TH1(2)	8"	8.0E-02	6.4E-03
	TH1(3)	10"	1.8E-01	3.2E-02
	TH2(1)	9"	9.0E-02	8.1E-03
	TH2(2)	6"	1.3E-01	1.7E-02
	TH2(3)	17"	9.0E-02	8.1E-03
	TH3(1)	14"	7.0E-02	4.9E-03
	TH3(2)	8"	5.4E-01	2.9E-01
	TH3(3)	7"	2.3E-01	5.3E-02
	TH4(1)	18"	6.0E-02	3.6E-03
	TH4(2)	8"	3.4E-01	1.2E-01
Average Kequivalent				
State Farm, Thurston County (C=1)	TH1(1)	38"	2.3E-01	5.3E-02
	TH1(2)	27"	1.6E-01	2.6E-02

Average Kequivalent				
Sweetbriar, Thurston County (C=0.8)	TH1(1)	36"	1.6E-01	2.0E-02
	TH1(2)	9"	1.1E-01	9.7E-03
	TH1(3)	24"	1.8E-01	2.6E-02
	TH2(1)	36"	1.8E-01	2.6E-02
	TH2(2)	30"	2.1E-01	3.5E-02
Average Kequivalent				
Westwood Baptist, Thurston County (C=1)	TH1(1)	11"	9.0E-02	
	TH1(2)	10"	2.1E-01	
	TH1(3)	6"	2.3E-01	
	TH2(1)	15"	9.0E-02	
	TH2(2)	6"	n/a	
	TH2(3)	5"	n/a	
	TH3(1)	6"	n/a	
	TH3(2)	6"	3.1E-01	
	TH3(3)	16"	9.0E-02	
	TH4(1)		n/a	
	TH4(2)		n/a	
	TH4(3)	31"	n/a	
	TH5(1)	4"	n/a	
	TH5(2)	14"	n/a	
	TH6(1)	6"	n/a	
Average Kequivalent				
Woodard Glen, Thurston County (C=.8)	TH1(1)	15"	5.5E-01	2.4E-01
	TH1(2)	28"	2.0E-01	3.2E-02
	TH2(1)	36"	1.8E-01	2.6E-02
	TH2(2)	6"	2.0E-01	3.2E-02
Average Kequivalent				